Quaternary Science Reviews 220 (2019) 372–400

Contents lists available at ScienceDirect

Quaternary Science Reviews

journal homepage: www.elsevier.com/locate/quascirev

High-frequency Holocene glacier fluctuations in the Himalayan-Tibetan orogen

Sourav Saha [a, b, *], Lewis A. Owen [c], Elizabeth N. Orr [d], Marc W. Caffee [e]

[a] Department of Earth, Planetary and Space Sciences, University of California, Los Angeles, CA 90095, USA
[b] Department of Physics, Geology, and Engineering Technology, Northern Kentucky University, KY 41099, USA
[c] Department of Marine, Earth, and Atmospheric Sciences, North Carolina State University, Raleigh, NC 27695, USA
[d] German Research Centre for Geosciences (GFZ), University of Potsdam, Institute for Geosciences, 14476 Potsdam, Germany
[e] Department of Physics, Department of Earth, Atmospheric and Planetary Sciences, Purdue University, West Lafayette, IN 47907, USA

ARTICLE INFO

Article history:
Received 28 February 2019
Received in revised form
16 June 2019
Accepted 12 July 2019
Available online 24 August 2019

Keywords:
Holocene
Glaciation
Central Asia
Cosmogenic isotopes
Paleoclimate modeling
Equilibrium-line altitudes

ABSTRACT

Holocene glacial chronostratigraphies in glaciated valleys spread throughout the Himalayan-Tibetan orogen, including the Himalaya, Tibet, Pamir, and Tian Shan, are developed using a landsystems approach, detailed geomorphic mapping, and new and published ^{10}Be surface exposure dating. New studies in the Kulti valley of Lahul and the Parkachik valley of the Nun Kun massif of the Himalaya of northern India define three glacier advances at ~14.7, 12.2, 0.5 ka, in addition to one historically dated late 19th Century advance in the Kulti valley, and one Late Holocene advance at ~0.2 ka in the Parkachik valley. Three major climatic groups (subdivided into five climatic zones) are defined across the orogen using Cluster Analysis (CA) and Principal Component Analysis (PCA) to identify glaciated regions with comparable climatic characteristics to evaluate the timing, and extent of Holocene glacier advances across these regions. Our regional analyses across the Himalayan-Tibetan orogen suggest at least one Lateglacial (~15.3–11.8 ka) and five Himalayan-Tibetan Holocene glacial stages (HTHS) at ~11.5–9.5, ~8.8–7.7, ~7.0–3.2, ~2.3–1.0, and <1 ka. The extent (amplitude) of glacier advances in 77 glaciated valleys is reconstructed and defined using equilibrium-line altitudes (ELAs). Modern glacier hypsometries are also assessed to help explain the intra-regional variations in glacier amplitudes during each regional glacier advance. A linear inverse glacier flow model is used to decipher the net changes in temperature (ΔT) between periods of reconstructed regional glacier advances in 66 glaciated valleys across different climatic regions throughout the orogen. The ^{10}Be, ELAs, and ΔT data suggest enhanced monsoonal and increased precipitation during the Early Holocene, followed by relative cooling and increased aridity during the Mid- and Late Holocene that influenced glaciation. The sublimation-dominated cold-based glaciers in the northern regions of Himalayan-Tibetan orogen are more affected during these shifts in climate than the temperate glaciers in the south.

1. Introduction

Studies of 20th and 21st Century glacier fluctuations throughout the Himalayan-Tibetan orogen indicate non-uniform retreat, and in some cases advance, of mountain glaciers due to warming and associated atmospheric changes (Bhambri et al., 2011, 2017; Bahuguna et al., 2014; Brun et al., 2017). Variable temporal and spatial responses of tropical-subtropical high-altitude glaciers to climate change present significant challenges for model predictions (Yan et al., 2018) and environmental risk assessment (Barker, 2007; Cogley et al., 2010; IPCC, 2014). Defining past spatial fluctuations of high-altitude mountain glaciers across a variety of climatic and orographic settings in the orogen on millennial and sub-millennial timescales highlights issues relevant to the nature of future environmental change in Central Asia (Bolch et al., 2012; Vaux Jr. et al., 2012; Owen, 2018; Rowan et al., 2018; Farinotti et al., 2019).

High-resolution glacial chronologies from glaciated valleys in the Himalayan-Tibetan orogen can be used to test the hypothesis that the long-term pattern of Himalayan glacier advances is either in phase or out of phase with glacier advances throughout the

* Corresponding author. 5641 Geology, University of California, Los Angeles, CA 90095, USA.
E-mail address: sahasv@ucla.edu (S. Saha).

https://doi.org/10.1016/j.quascirev.2019.07.021
0277-3791/

Northern Hemisphere, and elsewhere. Solomina et al. (2015, 2016) have proposed that the long-term pattern of Holocene glacier advances in the Himalayan-Tibetan orogen is not modulated by orbital forcing, but by regionally unique forcing factors. Recent studies by Saha et al. (2018), on the other hand, show that orbital forcing may play a significant role in driving Holocene glaciations in the northwestern part of the Himalayan-Tibetan orogen. Further research is required in other regions of the orogen to examine these conflicting views. Detailed glacial chronologies from other regions may further provide critical insights into the relative roles of climatic factors, which include: insolation driven movement of Earth's thermal equator; maritime influences; upper atmospheric circulation change and ocean heat transfer (Solomina et al., 2015; 2016; Saha et al., 2018); and non-climatic factors specific to each locality such as microclimate variability, topography, debris cover on glaciers, and glacier type (Barr and Lovell, 2014; Anderson et al., 2014). Previous studies (e.g., Dortch et al., 2013; Murari et al., 2014; Owen and Dortch, 2014; Heyman, 2014; Solomina et al., 2015, 2016) have compared Quaternary (mainly Pleistocene) glacial histories across the Himalayan-Tibetan orogen, but a clear delineation of the inter-regional variability in glacier responses to identical climatic perturbation, especially during the Holocene, is lacking.

Holocene glacial records are generally better-preserved, can be dated to a higher precision than those for the Pleistocene, and may have a better potential for examining detailed glacier successions (Blomdin et al., 2016; Saha et al., 2018). We therefore focus our study on Holocene glacial chronologies throughout the Himalayan-Tibetan orogen, including the Himalaya, Tibet, Pamir, and Tien Shan. Since we are specifically looking for variations in the timing and amplitude of glacier fluctuations between glacial events, we treat every catchment-specific event individually and assign them to a local glacial stage. Given the lack of preserved organic materials required for radiocarbon dating, but the abundance of quartz-rich boulders on moraines, we use cosmic-ray-produced (cosmogenic) ^{10}Be surface exposure dating of multiple boulders to determine the age of individual landforms. Limited optically stimulated luminescence (OSL) studies preclude us comparing glacial chronologies at the orogen-scale (cf. Bisht et al., 2017; Deswal et al., 2017). In this study, we have reconstructed Holocene glacial chronostratigraphies in two new study areas, as well as examining all previously published glaciated valleys throughout the orogen for which Holocene ^{10}Be ages are available (Fig. 1).

The two new study areas are located in the northwestern Himalaya and include the Kulti valley in the Lahul Himalaya and the Parkachik valley in Nun Kun massif (Fig. 1A). These study areas preserve a series of young moraines and contain relatively large glaciers (>10-km-long). These glaciers are arguably more erosive because they have formed broad glacial troughs, are melt-dominated, debris mantled, and located in a moderately wet microclimatic zone with annual precipitation of ~200–900 mm/a (Bookhagen and Burbank, 2006; Azam et al., 2014). These study areas are well suited to test the hypothesis of Saha et al. (2018) that smaller cold-based sub-polar glaciers located in the semiarid climate setting of the northwestern Himalaya tend to produce more scatter in the Holocene exposure ages. Additionally, glaciers in these two study areas are dominated by two prevailing climatic systems, the Indian summer monsoon (ISM) and the mid-latitude westerlies (Benn and Owen, 1998). The complex interplay of these systems influences both the present and late Quaternary glacier advances/retreats in the adjacent valleys (Lee et al., 2014; Owen et al., 1997, 2001). These study areas, therefore, may be key in evaluating the relative roles of the two dominant climate systems during Holocene glacier advances.

Sediments and landforms of different origins are distinguished and mapped using a landsystems approach (cf. Benn and Owen, 2002; Evans, 2003; Benn and Evans, 2010) in these areas. Comprehensive Holocene glacial chronologies are developed in both areas. We recalculated published ^{10}Be exposure ages from dated moraines in 77 valleys in 36 areas throughout the whole orogen (Fig. 1). We reconstruct the timing and amplitudes of Holocene glacial advances using these published exposure ages (n = 519) in conjunction with maps, equilibrium-line altitudes (ELAs), and ELA depressions (ΔELAs). Present-day glacier hypsometries are measured to explain variations in glacier amplitudes within a single climatic region. We also modeled the net change in past temperature for 66 glaciated valleys assuming a steady-state scenario and using a linear inverse glacier flow model based on the methods of Klok and Oerlemans (2003) and Oerlemans (2001, 2005).

Our approach provides a comprehensive framework to: i) examine the timing and spatial variability of Himalayan-Tibetan glacier fluctuations to Holocene climate change; ii) unravel the long-term and short-term forcings behind Holocene glacier fluctuations; and iii) understand the climatic sensitivity of the high-altitude mountain glaciers in Central Asia.

2. Physical setting

Continued crustal shortening, the result of the collision and partial subduction of the Indian and Eurasian continental lithospheric plates since the early Miocene, initiated the development of a series of foreland propagating thrust systems and uplifted mountain ranges in the Himalaya (Searle et al., 1997). These mountain ranges throughout the Himalaya extend from ~400 to >8000 m above sea level (asl; Fielding et al., 1994; Duncan et al., 2003). The Greater Himalayan and Zanskar ranges, bounded by the Main Central Thrust (MCT) to the south and the Indus-Tsangpo Suture Zone (ITSZ) to the north, constitute one of the highest mountain regions in the world (average elevation > 6000 m asl; Duncan et al., 2003). These mountains have had and continue to have a significant influence on past and present moisture supply; they are a barrier to incoming air masses (Owen et al., 1996; Burbank et al., 2012; Lee et al., 2014; Li et al., 2017).

Our two new study areas, the Kulti valley in Lahul and the Parkachik valley in Nun Kun massif (Fig. 1A), are located in northern India on the northwestern trending southwestern slopes of the Greater Himalaya and northern flanks of the Zanskar Range, respectively. The Kulti valley lies north of the Rohtang Pass (Fig. 2A) and consists mostly of Proterozoic black slate, phyllite, and fine-grained biotite-schist of the Batal Formation (Kumar et al., 1987; Rawat and Purohit, 1988; Bhargava, 2008), with occasional Neoproterozoic to Permian granite (Steck, 2003). Leucogranite dated to 24–18 Ma and gneiss and quartzite metamorphosed from Paleozoic-Mesozoic Tethyan sedimentary rocks are present in the Nun Kun massif (Vance and Harris, 1999). Both study areas have abundant glacial and fluvial landforms, including broad glacial troughs, moraines, debris flow and alluvial fans, talus slopes, glacially eroded bedrock, river terraces, lacustrine and outwash plains (Fig. 2).

The Kulti valley is in the rain shadow of the Pir Panjal Range. The valley presently receives most of its precipitation (>65%) from the ISM (Fig. 1A; Bookhagen and Burbank, 2006). Precipitation varies between ~200 and 900 mm/a from the valley floor to the higher reaches (Bookhagen and Burbank, 2006; Azam et al., 2014), producing a wet and cool transitional climate, conducive for the development of steep, high-activity, debris-mantled glaciers (Fig. 2A; Owen et al., 1996, 1997). Contemporary steady-state ELAs vary between ~4500 and 4800 m asl in the region (Owen et al., 1996, 1997; Chand et al., 2017) and glaciers are highly sensitive to changes in the ambient temperature (Bisht et al., 2017).

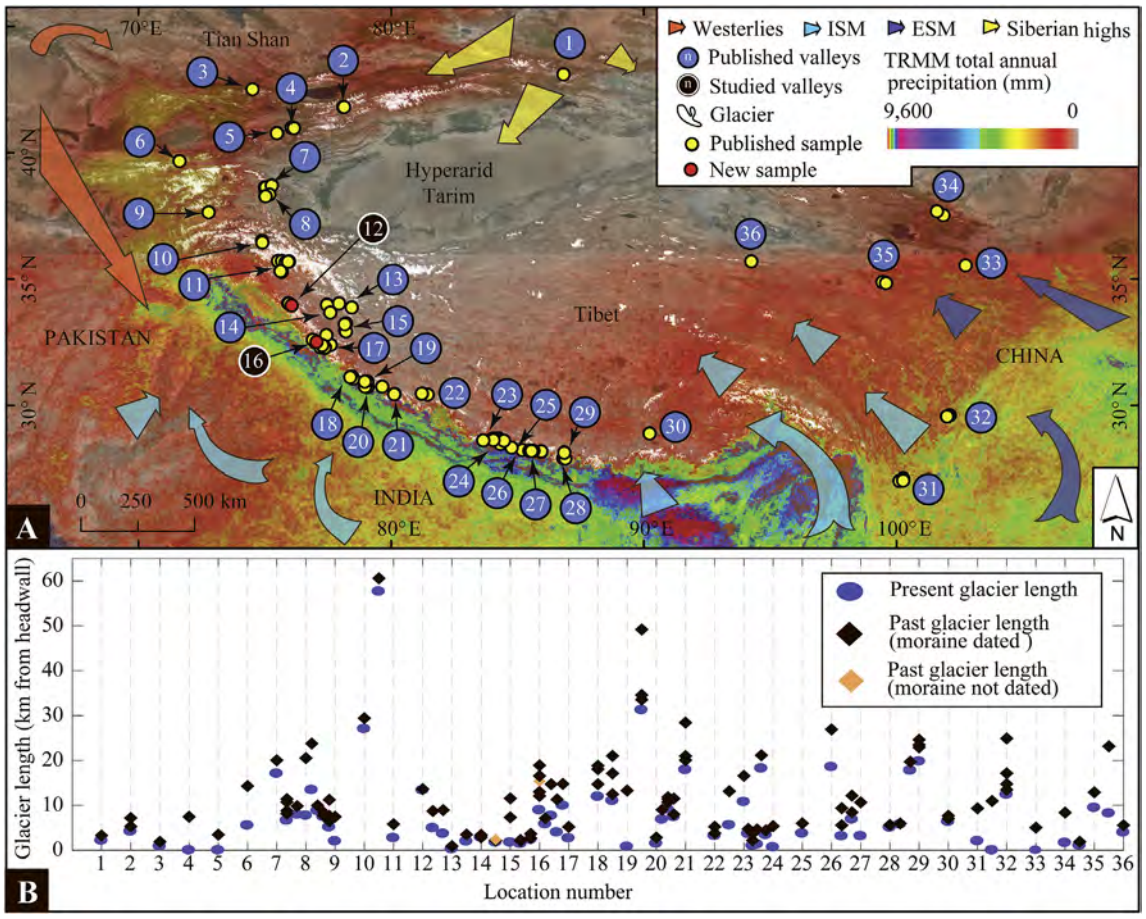

Fig. 1. Physical settings of the study areas. (A) TRMM and CRU CL 2.0 precipitation map, superimposed on hillshade map, showing the location of ^{10}Be dated (with ages <15 ka only) glaciated valleys across the Himalaya, the Tibet, the Pamir, and the Tian Shan. Two new (in black circles—this study) and 77 published (in blue circles) valleys are presented. Arrows indicate the propagating directions of the prevailing climate systems (ISM – Indian Summer Monsoon; ESM – East Asia Summer Monsoon). Valley locations are: (1) Daxi, Tian Shan, (2) Bordoo, Tian Shan, (3) Ala Archa, Tian Shan, (4) Aksai, Tian Shan, (5) Kitschi-Kurumdu, Tian Shan, (6) Koksu, Pamir, (7) Kongur Shan, Pamir, (8) Muztag Ata, Pamir, (9) Great Bogchigir, Karakoram, (10) Hunza valley, Karakoram, (11) Central Karakoram, (12) Parkachik, Sentic, Rantac, and Tarangoz, Nun Kun massif, (13) Chang and Pang, Ladakh, (14) Stok and Lato, Zanskar, (15) Puga and Karzok, Zanskar, (16) Kulti, Hamtah, and adjacent valleys, Lahul, (17) Yunam, Great Himalaya, (18) Tons, Garhwal, (19) Bhagirathi, Garhwal, (20) Bhillanganga and Dudhanga, Garhwal, (21) Nanda Devi, Garhwal, (22) Muguru, Gurla Mandhata, (23) Lete, Milarepa, Syaktan, Yak, Lyapche, Danfe and Dudh Khola, Annapurna, (24) Macha Khola, Gorkha Himal, (25) Mailun Khola, Ganesh Himal, (26) Langtang, Nepal, (27) Nyalam County, Southern Xixabangma, (28) Khumbu Himal, Nepal, (29) Rongbuk, N Mt. Everest, (30) Karola Pass, Mt. Kaluxung, (31) Renhe, Baishui, and Ganheba, Yulong and Ganheba mountains, (32) Hailuogou, Gonga Shan, (33) Dalijia Shan, NE Tibet, (34) Xiying He, Qilian Shan, (35) Anyemaqen mountains, (36) Kunlun Shan. (B) Diagram showing present (blue circle) and past (diamonds) lengths of glaciers from their respective headwall in each location. Each location often contains >1 valley and are represented near to their location number, e.g., adjacent valleys at location 7 are shown in between 7 and < 8. Reference sources for each of these areas are provided in the data supplement table (see Table 1 in Saha et al. Data in Brief). (For interpretation of the references to color in this figure legend, the reader is referred to the Web version of this article.)

The Parkachik valley, a tributary of Suru valley, is located on the north-facing slopes of the Nun Kun massif in the far west of the semiarid Zanskar Range (Figs. 1A and 2B). Topography strongly influences the precipitation gradient in the valley (Lee et al., 2014), with present-day precipitation varying between ~150 and 700 mm/a from the valley floor to the higher reaches (Bookhagen and Burbank, 2006). The massif has very steep slopes (>45°) rising to the high peaks of Nun at 7,135 and Kun at 7,077 m asl. Snow is delivered to the glaciers by avalanching and direct snowfall (Osmaston, 1994). In contrast to smaller sub-polar type glaciers elsewhere in Zanskar (Orr et al., 2017a,b, 2018; Saha et al., 2018), the Nun Kun massif has a few large glaciers, including the ~12-km-long Parkachik glacier (Fig. 2A). A thin layer of supraglacial debris mantles these glaciers (Fig. 2F). Currently, the mid-latitudinal westerlies contribute ~55–58% of the total annual precipitation to the region (Fig. 1; Lee et al., 2014). Regional ELAs vary between ~5000 and 5600 m asl (Damm, 2006).

Holocene glacial chronostratigraphies for both study areas are poorly defined (Owen and Dortch, 2014). Previous studies have attempted to reconstruct Pleistocene glacial chronostratigraphies in the Chandra and adjacent valleys using cosmogenic (Owen et al., 2001; Eugster et al., 2016; Saha et al., 2018) and luminescence dating (Deswal et al., 2017; Saini et al., 2016). These studies show complex but extensive glaciation during ~20–17 ka (~global last glacial maximum [LGM] or ~ chronozone 2 of Mix et al. (2001), although Clark et al. (2009) and Hughes and Gibbard (2015) define the LGM to ~26–19 and ~28–23 ka, respectively), ~16–14 ka (Lateglacial), and ~11.7–10 ka (~Early Holocene; Supplementary Material Fig. S1A). The oldest glacial stage in the Chandra valley, the Chandra glacial stage, as evidenced by ice-sculpted bedrock surfaces and bedrock benches at the altitude of 3150–4400 m asl, was not dated (Owen et al., 2001). Site-specific deglaciation, as recorded in polished bedrock and lodged boulders on drumlin surfaces, commenced between ~18 and 13 ka (Eugster et al., 2016; Saha et al., 2016). Our regional compilation, as shown in Fig. S1A, also illustrates a sub-millennial-scale site-specific glacial response

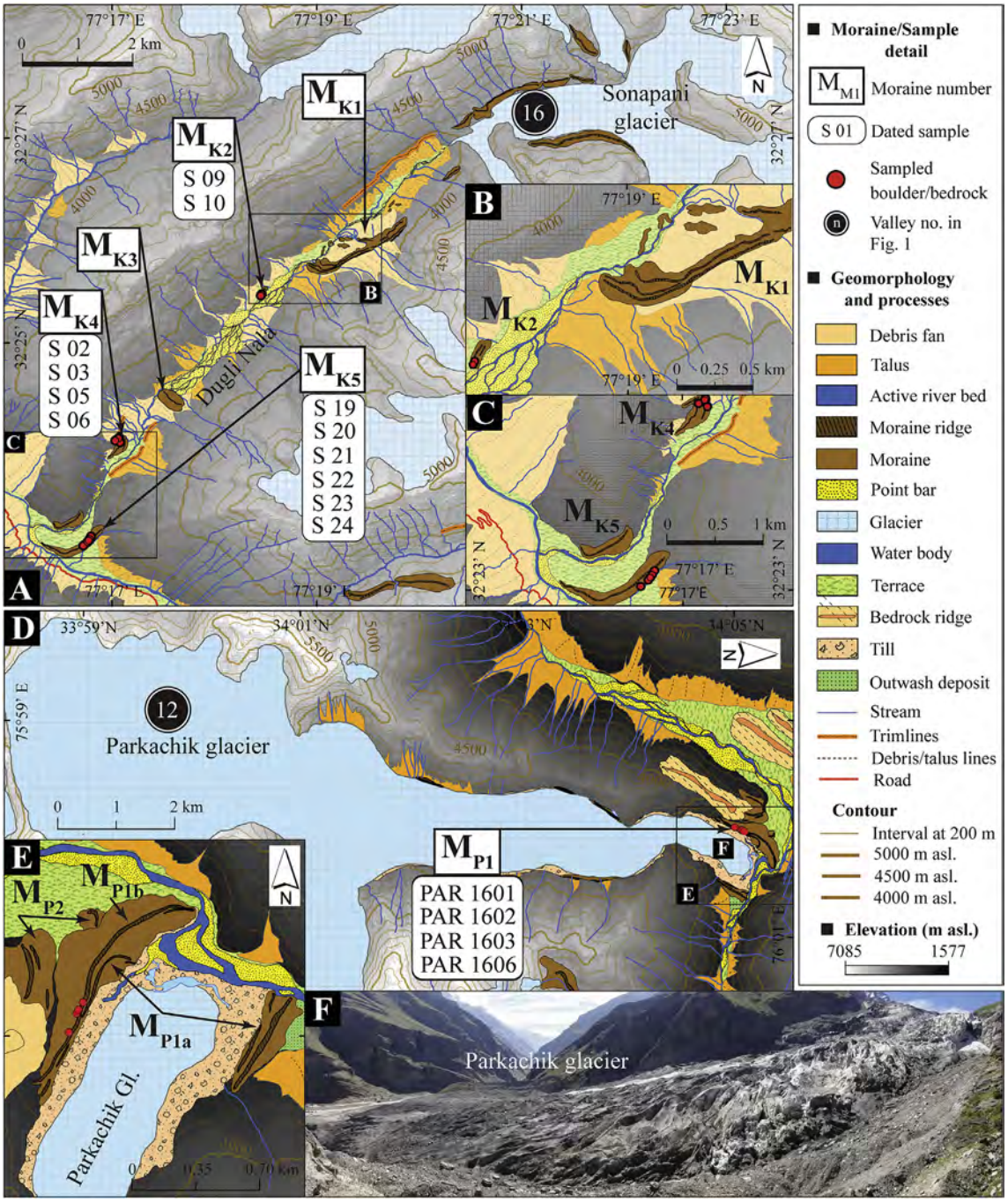

Fig. 2. Geomorphology of the study areas. (A) Kulti valley showing landforms and locations of moraine boulders. (B) Highlighted M_{K1} and M_{K2} moraine ridges. (C) Enlarged view of M_{K4} and M_{K5} moraines. (D) Sampling locations of M_{P1b} moraine and associated landforms in the Parkachik valley. (E) Highlighted M_{P1} moraine ridges. (F) View of Parkachik Glacier.

(advance/retreat) during ~18–13 ka. Besides, ^{10}Be dated glacier advances (recalculated in this study) at ~12.3 ± 0.6 ka (the Kulti glacial stage of Owen et al., 2001), at ~10.1 ± 0.4 ka (m_{H3} of Saha et al., 2018), at ~3.8 ± 0.1 ka (Sonapani I stage of Owen et al., 2001) and <0.2 ka (m_{H1} of Saha et al., 2018), are also proposed in the region. Historical photographs and trigonometrical maps of Geological Survey of India further indicate restricted glacier advances between the 18th and 19th centuries (Walker and Pascoe, 1907; Owen et al., 1996, 1997, 2001; Harcourt, 2010; Raina et al., 2015; Saini et al., 2016).

In the Nun Kun massif, the ^{10}Be dated glacial history (recalculated in this study) indicates an extensive glacier advance which predates (recalculated here) ~64.2–39.0 ka (Achambur glacial stage of Lee et al., 2014; Fig. S1B). Subsequent glacier advances are restricted and dated by Lee et al. (2014; all recalculated here) to ~21.2–17.0 (their Tongul glacial stage), ~17.0–15.0 and ~14.0–13.0 (their Amantick glacial stage), and ~0.7–0.5 ka (their Lomp glacial stage; Fig. S1B). The youngest set of lateral moraines which Lee et al. (2014) assigned to their Tanak glacial stage, were not previously dated in the massif. We have targeted this youngest set of moraines (M_{P1}) in this study.

3. Methods

3.1. Mapping and morphostratigraphy

Detailed geomorphic and surficial geologic maps were prepared using a hand-held GPS and digital mapping techniques in the field at the scale of 1:20,000 (±3 m; Fig. 2). Google Earth imagery, Advanced Spaceborne Thermal Emission and Reflection Radiometer (ASTER) global digital elevation models (GDEMs), and Landsat Enhanced Thematic Mapper Plus (ETM+) imagery were used to refine these maps. We used the scheme proposed by Owen and Derbyshire (1989), Owen et al. (1997), Hughes et al. (2005), and Hughes (2010) to define our morphostratigraphy and its nomenclature. The letter 'M' refers to a moraine, with the subscript letter 'K' for Kulti and 'P' for Parkachik valleys, respectively. We used subscript '1' for the (morphostratigraphically) youngest of all preserved sets of moraines and the subscript letter 'a' for the youngest ridge of a moraine set. A detailed account of these methods can be found in Orr et al. (2018) and Saha et al. (2018).

3.2. Geochronology

We carefully considered the morphostratigraphy, physical setting (e.g., stability, degradation, recent hillslope deposits), and surficial characteristics when choosing moraine boulders to sample. We avoided post-depositional surface deflation effects by choosing well-inset boulders on the crest of moraines (Fig. 3). The strong winds (5–15 km/h; Ramanathan, 2011) in this high-altitude environment likely preclude accumulation of snow and loess on boulders with heights of ≥1 m (except for a few samples; Table 1), minimizing the impact of shielding (<1%) on the cosmogenic nuclide inventory (Heyman et al., 2016). No sampled boulder showed any evidence of surface spallation, pitting, fracturing, and/or extensive weathering (see Fig. S2 for detailed characteristics). Approximately 500 g of rock to a depth of ≤5 cm from the top of each boulder was collected using a hammer and chisel (Table 1). We used compass and inclinometer to measure shielding from the boulder surface to the horizon at 10° azimuths. A detailed account of our field sampling procedures is provided in Orr et al. (2018) and Saha et al. (2018).

We performed quartz extraction and ^{10}Be sample preparation at the Quaternary Geochronology Laboratories in the University of Cincinnati following the methods outlined in Kohl and Nishiizumi (1992), and Nishiizumi et al. (1994). AMS measurements were performed at the Purdue Rare Isotope Measurement (PRIME) Laboratory at Purdue University (Sharma et al., 2000). See supplementary material S3 and Saha et al. (2018) for more details.

Beryllium-10 exposure ages were calculated, and published ages were recalculated, using the community standard Cosmic Ray Exposure program (CREp) of Martin et al. (2017) and CRONUS-Earth V3 of Balco et al. (2008; see Table 1 in Saha et al. Data in Brief). For Lifton-Sato-Dunai (*LSD*) and time-dependent Lal and Stone (*Lm*) scaling schemes, a global ^{10}Be production rate at sea level of 4.11 ± 0.26 and 4.13 ± 0.20 atoms/g SiO_2/a, respectively was used (Borchers et al., 2016; Martin et al., 2017). The relative differences among different age calculators are outlined in Saha et al. (2018). Exposure ages were calculated using the scaling schemes of *LSD* (Lifton et al., 2014), *Lm* (Balco et al., 2008), and time-independent Lal and Stone (*St*; Lal, 1991; Stone, 2000), but we only reported the CREp *LSD* ages in the text below. Saha et al. (2018) showed that the differences among different scaling schemes for Holocene ^{10}Be age are <10%. We assume zero-erosion rates and report all the ages in thousands of years (ka) before AD 2016 (Table 1; supplementary material S3, see Table 1 in Saha et al. Data in Brief).

In our two new study areas, multiple boulders (2–6) were sampled from each moraine to define the exposure age of the moraine, and hence the minimum age of a glacier advance (Gosse, 2005; Ivy-Ochs et al., 2007; Putkonen et al., 2008). For moraine ages from the literature, we only used data if ≥2 concordant boulder ages were measured. We applied reduced chi-squared (χ^2) statistics to assess the distribution of ages (Applegate et al., 2010, 2012; Kaplan et al., 2013; Putnam et al., 2013b). Any age population with $\chi^2 > 1$ likely had outliers, and further statistical treatment was performed (cf. Saha et al., 2018). Chauvenet's criterion (Taylor, 1997; Dunai, 2010; Putnam et al., 2013b) was used to detect outliers. Outliers for our new study areas were only removed if convincing field evidence supported our statistical results (e.g., possible recent hillslope deposits, shallow burial, and/or toppling). We relied on statistical treatment and the author's recommendations for the previous studies (see Table 1 in Saha et al. Data in Brief)

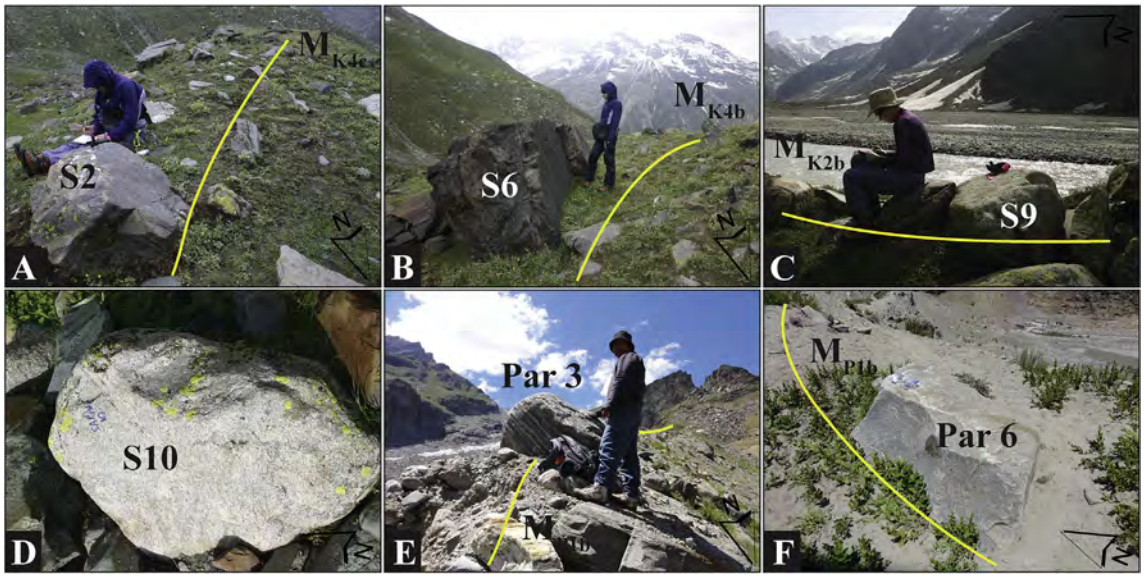

Fig. 3. Examples of sampled boulders for ^{10}Be exposure dating. Boulders inset into M_{K4C} (A) and M_{K4b} (B) lateral rides in the Kulti valley. (C and D) Relative to M_{K4} moraine, subdued boulders are present on the young M_{K2b} lateral ridge in the valley. (E and F) Boulders are large, fresh, and well inset into the crest of the M_{P1b} lateral ridge in the Parkachik valley.

Table 1
Holocene moraine surface-exposure sample details and ^{10}Be ages (in thousands of years before AD 2016; labeled 'ka'±1σ) for the Kulti valley of the Lahul Himalaya and Parkachik valley of the Nun Kun.

Moraine morpho-stratigraphy	Sample ID	Latitude (°N)	Longitude (°E)	Elevation (m asl)	Boulder size (Length x width x height in cm)	Sample thickness (cm)	Shielding correction	Quartz weight (g)	^{9}Be Carrier added (g)	^{10}Be/^{9}Be ± 1σ (10^{-14})	[^{10}Be] ± 1σ (10^{4} atoms g^{-1})	LSD Age ± 1σ (ka)[h]	Lm Age ± 1σ (ka)[i]
Kulti valley, Lahul													
M_{K5}	S19	32.3833	77.2783	3255	300 × 290 x 90	2.0	1.000	31.090	1.0107[b]	21.20 ± 0.64[d]	22.80 ± 0.69	8.92 ± 0.63	8.33 ± 0.46
M_{K5}	S20[a]	32.3833	77.2783	3258	240 × 190 x 50	2.0	1.000	27.090	0.9400[b]	4.12 ± 0.39[d]	4.73 ± 0.45	2.11 ± 0.25	1.95 ± 0.22
M_{K5}	S21	32.3833	77.2783	3256	330 × 290 x 130	2.0	1.000	10.521	0.4221[b]	9.48 ± 0.34[e]	32.03 ± 1.14	13.19 ± 0.78	12.54 ± 0.72
M_{K5}	S22	32.3833	77.2783	3268	140 × 60 x 90	2.0	1.000	24.678	0.9505[b]	35.20 ± 1.40[e]	44.85 ± 1.78	16.11 ± 1.01	15.33 ± 0.86
M_{K5}	S23[a]	32.3833	77.2783	3272	160 × 80 x 30	2.0	1.000	30.900	0.9912[b]	2.98 ± 0.28[d]	3.16 ± 0.30	1.28 ± 0.14	1.20 ± 0.13
M_{K5}	S24[a]	32.3833	77.2783	3274	150 × 130 x 40	3.0	1.000	29.690	0.9855[b]	2.79 ± 3.58[d]	3.06 ± 3.93	1.25 ± 1.60	1.16 ± 1.49
M_{K4}	S2	32.4000	77.2850	3522	130 × 80 x 60	2.0	0.913	29.717	0.9440[b]	34.87 ± 1.83[e]	36.64 ± 1.92	11.96 ± 0.86	11.42 ± 0.71
M_{K4}	S3	32.4000	77.2850	3527	135 × 120 x 160	2.0	0.915	29.220	0.9990[b]	35.05 ± 1.49[d]	39.64 ± 1.69	12.90 ± 0.85	12.29 ± 0.76
M_{K4}	S5	32.4000	77.2850	3526	260 × 160 x 120	2.0	0.915	29.240	0.9820[b]	29.39 ± 1.49[d]	32.65 ± 1.65	10.86 ± 0.65	10.33 ± 0.63
M_{K4}	S6	32.4000	77.2850	3528	140 × 130 x 70	2.0	0.915	26.440	1.0140[b]	31.53 ± 0.67[d]	39.99 ± 0.85	12.99 ± 0.72	12.40 ± 0.63
M_{K2}	S9	32.4233	77.3067	3676	60 × 30 x 35	2.0	0.917	28.900	0.9635[b]	1.15 ± 0.42[d]	1.27 ± 0.46	0.40 ± 0.15	0.37 ± 0.14
M_{K2}	S10	32.4233	77.3067	3678	75 × 35 × 30	2.0	0.913	32.592	0.9560[b]	2.01 ± 0.20[e]	1.95 ± 0.19	0.62 ± 0.08	0.59 ± 0.07
Parkachik valley, Nun Kun													
M_{P1}	PAR 1601	34.0835	75.9998	3700	500 × 400 × 150	2.0	0.968	21.065	0.3548[c]	0.48 ± 0.05[f]	0.56 ± 0.06	0.15 ± 0.02	0.14 ± 0.02
M_{P1}	PAR 1602	34.0844	76.0001	3687	100 × 60 × 100	3.0	0.973	13.654	0.3502[c]	0.18 ± 0.04[f]	0.33 ± 0.08	0.09 ± 0.02	0.08 ± 0.02
M_{P1}	PAR 1603	34.0846	76.0002	3678	180 × 50 × 80	3.5	0.974	9.665	0.3536[c]	0.28 ± 0.02[g]	0.71 ± 0.05	0.19 ± 0.02	0.19 ± 0.02
M_{P1}	PAR 1606	34.0850	76.0004	3667	210 × 115 × 70	2.0	0.969	7.905	0.3531[c]	0.24 ± 0.04[g]	0.74 ± 0.12	0.21 ± 0.04	0.19 ± 0.04

Note: Density value of 2.7 g cm^{-3}, the erosion rate of 0.00 cm a^{-1}, and AMS standard of 07KNSTD were used for all samples to calculate surface exposure ages; weathering is limited to none.
[a] Outliers are identified and removed.
[b] Carrier ^{9}Be concentration is 495 ppm.
[c] Carrier ^{9}Be concentration is 1045.9 ppm.
[d] Ratios are corrected from background ^{10}Be: 5.72 ± 0.48 × 10^{-14} (^{10}Be/^{9}Be ± 1σ).
[e] Ratios are corrected from background ^{10}Be: 3.13 ± 0.21 × 10^{-14} (^{10}Be/^{9}Be ± 1σ).
[f] Ratios are corrected from background ^{10}Be: 0.12 ± 0.05 × 10^{-14} (^{10}Be/^{9}Be ± 1σ).
[g] Ratios are corrected from background ^{10}Be: 0.08 ± 0.03 × 10^{-14} (^{10}Be/^{9}Be ± 1σ).
[h] Lifton-Sato-Dunai (LSD) scaling model using CREp online calculator.
[i] Lal and Stone time-dependent (Lm) scaling model using CREp online calculator.

to detect and remove outliers. The simple arithmetic means ± 1σ were used to define the mean moraine ages and the age uncertainties.

Each morphostratigraphically distinct mean moraine age in a valley are reported here as a *local glacial stage* (cf. Owen and Dortch, 2014; Saha et al., 2018). Probabilistic models suggest that each valley likely has ~30% probability (as recorded in moraines) to preserves its repeated advances from the same source (Gibbons et al., 1984; Kirkbride and Brazier, 1998; Kirkbride and Winkler, 2012). We, therefore, first defined climate regions (see section 'Climate Zonation'), i.e., regions with similar climatic characteristics and then compiled all *local glacial stages* for each climatic region (~10^{4-6} km^2) to reconstruct a complete regional glacial history. Using a combination of radial plotter, finite mixture model, and probability density function (kernel density or '*ksdensity*' fit in MATLAB), discrete population/Gaussians of local glacial stages are first identified (Galbraith et al., 1999; Dortch et al., 2013). Student's t-test analysis is then applied to verify whether these selected population/Gaussians are statistically significant (≥95% confidence) and defined as *regional glacial stages* (~10^{4-5} km^2; cf. Dortch et al., 2013; Murari et al., 2014). Age overdispersion (OD) values are also estimated for the regional age population to assess further whether they are part of a single Gaussian or multiple (Galbraith et al., 1999). OD of ≤20% is considered reliable to estimate the mean of a regional glacial stage (Guérin et al., 2015). We followed the formal Holocene stratigraphic subdivision approved by the International Commission on Stratigraphy (ICS: www.stratigraphy.org/index.php/ics-news-and-meetings/125-formal-subdivision-of-the-holocene-series-epoch, last accessed July 1, 2019; Walker et al., 2012) to help evaluate our *regional stages*. According to the ICS (all reference to before AD 2000 [b2k]), the Early Holocene spans 11.7–8.3 ka, the Mid-Holocene spans 8.3–4.2 ka, and the Late Holocene is from 4.2 ka to b2k. Additionally, we used the word *Himalayan-Tibetan Holocene stages* or *HTHS* to define our orogen-wide inter-regional glacial stages.

3.3. Equilibrium-line altitudes

Former ELAs are determined assuming a simplistic steady-state scenario (Sugden and John, 1976) and using area-altitude (AA), area accumulation ratio (AAR), and toe-headwall accumulation ratio (THAR) methods for each glacier advance (Table 2; Benn et al., 2005; Osmaston, 2005). The modern maximum elevations of lateral moraines (MELM; Nesje and Dahl, 1992) are established to calculate present ELAs (Table 2). We obtained the AARs and THARs from the published literature for our climatic regions (see section 5.2.1 and Table S4). Different combinations of AARs (e.g., ranging from 0.45 to 0.80) and THARs (e.g., varies from 0.3 to 0.6) were used depending on the glacier setting, physical characteristics, and climate. See Table 2 in Saha et al. (Data in Brief) for detailed ratios used for our different climatic regions in this study. Herein we report the (arithmetic) mean ELA and ΔELA with ± 1σ uncertainty, obtained from multiple indices and ratios (Table 2; see Table 2 in Saha et al. Data in Brief).

We also evaluated the spatiotemporal distribution of ΔELAs across the orogen to provide insight into the relative strength of precipitation and temperature as major forcing factors for glacier oscillations (cf., Saha et al., 2018). Yan et al. (2018) in their Parallel Ice Sheet Model (PISM) of LGM glaciation across the orogen showed that glaciers in western and southern Himalaya and Tibet are the most sensitive to climate perturbations relative to those in the interior. We therefore expect precipitation-sensitive cold-based sub-polar types of Himalayan-Tibetan glaciers (Fig. 4) to likely have significant ΔELAs during periods of increased precipitation and greater cloud albedo (diffusion radiation). Enhanced cloud albedo favors a decrease in incoming shortwave radiation and in conjunction with evaporative/sublimation cooling (latent heat transfer) foster negative energy balance, i.e., cooling by a dynamic response (Rupper and Roe, 2008; Rupper et al., 2009). Relative to cold-based glaciers, temperature-sensitive wet-temperate glaciers (Fig. 4) likely have greater ΔELAs during cold-dry climatic relapses (Bisht et al., 2017).

3.4. Glacier hypsometry

Modern glacier hypsometry was generated using ASTER GDEM (Fig. S5) for 68 of the 77 glaciated valleys in which glaciers still exist, and where ^{10}Be ages are available. Glaciated areas were normalized using z-scores (Mahmood, 2016) for comparison because glaciers vary greatly in size throughout the orogen. Z-score normalization is performed by subtracting the variable from the population mean and dividing by the standard deviation of the population.

3.5. Climate zonation

A primary climatic group map was reconstructed using >42,500 mapped Central Asian glaciers extracted from the Randolph Glacier

Table 2
A summary of ELAs and ΔELAs in our study areas.

Glacial	Mean	Glacier	Mean	Mean	Head	Toe	MELM	Area-	Area-Accumulation ratio			Toe-Headwall altitude ratio			Mean	ΔELA
Stage	moraine age (ka)	area (~km^2)	slope (~°)	aspect	(m asl)	(m asl)	(m asl)	Altitude (m asl)	AAR (0.45)	AAR (0.55)	AAR (0.65)	THAR (0.40)	THAR (0.50)	THAR (0.60)	ELA (m asl)	(m)
Kulti valley, Lahul																
Present	–	17.7	17	W	5465	3901	4640	4815	4929	4819	4719	4533	4690	4846	4749 ± 127	–
M_{K1}	~0.12 ± 0.01 (Historical)	22.9	18	W, SW	5478	3601	–	4727	4879	4759	4590	4403	4585	4766	4673 ± 157	92 ± 31
M_{K2}	0.51 ± 0.16	23.4	18	W, SW	5478	3662	–	4704	4859	4739	4569	4397	4580	4762	4659 ± 154	106 ± 30
M_{K3}	N/A?	24.4	17	W, SW	5498	3631	–	4662	4839	4709	4529	4387	4575	4762	4638 ± 153	127 ± 38
M_{K4}	12.18 ± 0.99	24.9	17	W, SW	5498	3432	–	4641	4829	4699	4500	4255	4460	4664	4578 ± 188	186 ± 62
M_{K5}	15.30 ± 0.60	25.7	17	W, SW	5498	3151	–	4598	4809	4659	4469	4099	4335	4570	4506 ± 232	259 ± 109
Parkachik valley, Nun Kun																
Present	–	47.5	19	N	7014	3592	5251	5437	5510	5419	5339	4967	5310	5652	5361 ± 202	
M_{P1}	0.16 ± 0.05	48.6	19	N	7014	3556	–	5401	5499	5409	5319	4943	5290	5636	5357 ± 216	20 ± 9
M_{P2}	N/A?	–	–	–	–	–	–	–	–	–	–	–	–	–	–	–

Note: The present here refers to the year 2016 AD.
m asl is a meter above sea level.
N/A? Indicates numerical dates are not available.

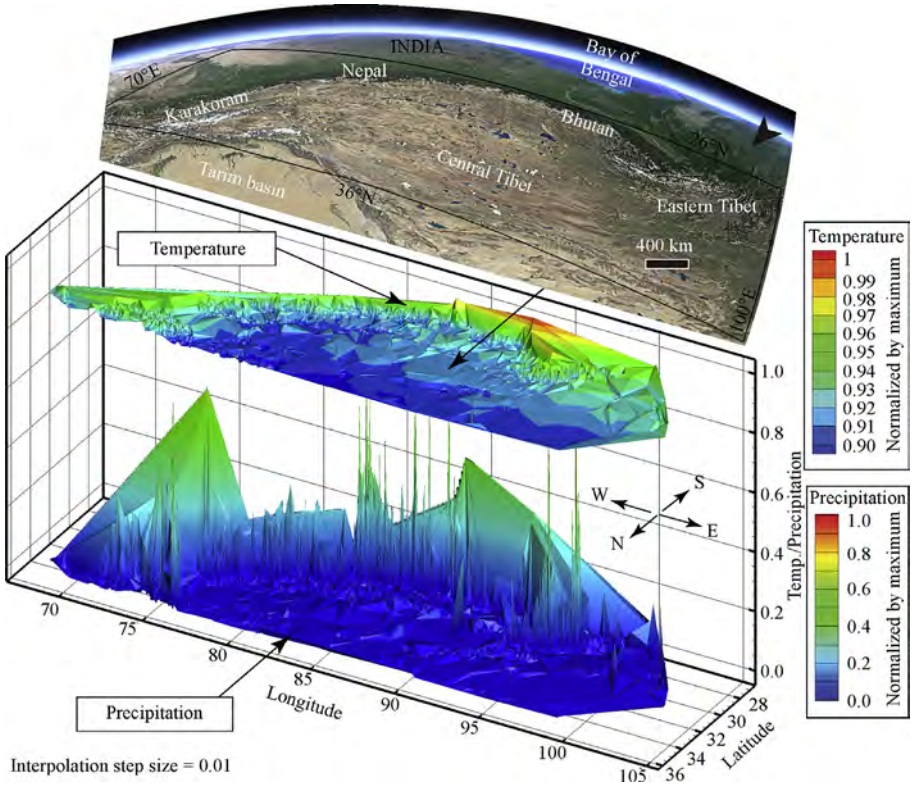

Fig. 4. 3D Distribution of annual mean temperature (source: CRU CL. 2.0) and precipitation (source: TRMM) across the Himalayan-Tibetan orogen showing the strong N-S climatic gradient. Note that the map is inverted for the ease of viewing, i.e., the view is looking southwestward; Google Earth map for reference. The height and the color scheme on the maps represent the normalized values (1–0) of mean annual temperature and precipitation on each glacier. Normalization is achieved by dividing the climate variables by their maximum value (cf. Sagredo and Lowell, 2012); i.e., 1 represents the highest temperature/precipitation value(s) among all the point clouds/glaciers and 0 is the lowest. Each glacier is used as a point to extract the climate variables and their height is interpolated to create the 3D maps (see Saha et al. MethodsX for more details). The southern Himalayan glaciers, in general, shows high precipitation and higher temperature, i.e., wet-temperate types, whereas the glaciers further north in the Transhimalaya and Tibetan Plateau experience significantly low temperature/precipitation, i.e., cold-dry sub-polar types. Note also that the TRMM derived mean annual precipitation values have more extreme values (or spikes) in the transitional zones (between the high and low precipitation regions) compared to the reanalysis temperature data. (For interpretation of the references to color in this figure legend, the reader is referred to the Web version of this article.)

Inventory (RGI 6.0; RGI Consortium, 2017), and climate data of New et al. (2002; Fig. 4) to better compare the relative influence of the prevailing climate systems on glaciers and for inter-regional variances in the Himalayan-Tibetan orogen.

Monthly surface temperature maps were generated using the CRU CL 2.0 (at 10′ of latitude and longitude) reanalysis dataset for the period 1961–1990 (New et al., 2002). Due to poor resolution of the reanalysis data (New et al., 2002), we generated monthly precipitation maps from the Tropical Rainfall Measuring Mission (TRMM) data (4-km-horizontal x 250-m-vertical) for the period 1998–2009 (Bookhagen and Burbank, 2006). Nine climate parameters including annual mean temperature, annual temperature range, annual total precipitation, annual precipitation range, total summer monsoon precipitation, total winter precipitation, seasonality concentration index (SCI), dimensionless seasonality index (DSI), and relative entropy (RE), were derived from the monthly temperature and precipitation data (see Saha et al. MethodsX for definitions of these indices).

Sample glaciers used in our study covers ~27–35° N and ~67–103°E coordinates (Fig. 5A and S6), that is the focus of our study. The climate data of the ^{10}Be dated sample glaciers that fall north of latitude ~35° N, i.e., valley locations 1–10 of Fig. 1, are extracted separately from the CRU CL 2.0 dataset, largely because the gridded TRMM data is only generated up to 36° N (Bookhagen and Burbank, 2006). They are then included in the analysis.

Glaciers with identical climate were grouped using Cluster Analysis (CA; Zuming and Maohuan, 1989) and refined by Principal Component Analysis (PCA; Sagredo and Lowell, 2012; Seaby and Henderson, 2014) in the R statistical package (The R Core Team, 2018). These groups are defined herein as climatic regions. We produced a cluster dendrogram (see Saha et al. MethodsX) by grouping the most analogous samples (glaciers) using the Euclidean distance and the unweighted pair-group method with arithmetic averaging (UPGMA; Romesburg, 2004). To test the significance of our clusters (groups), we calculated the cophenetic distance between two samples (glaciers) in the cluster dendrogram and performed a Pearson's product-moment correlation between the sample Euclidean and cophenetic distances (Seaby and Henderson, 2014; see Saha et al. MethodsX). Also, we performed an analysis of similarities (ANOSIM), which in R is based on the difference of mean ranks between groups and within groups (The R Core Team, 2018). The function *anosim* is directly applied to the dissimilarity function *dist* in R, which is then used to determine the compositional dissimilarities between and within the groups. The aim is to test whether the samples (glaciers) within groups are more similar than would be expected by random chance (see Saha et al. MethodsX).

3.6. Modeling past temperature

We reconstructed the Holocene (relative to present) temperature changes (T in Kelvins [K]) for 66 of the 77 high-altitude Himalayan-Tibetan glaciated valleys using the medial length, average slope, and annual total precipitation of the respective glacier. Past

atmospheric temperatures (T) were not reconstructed for the remainder 11 study areas because essential parameters, e.g., existing glacier ice cover, well-defined laterofrontal and/or end moraines to reconstruct glacier geometry, moraine (^{10}Be) ages, and availability of reliable (contemporary) climate variables, were not met.

We used a linear inverse glacier flow model of Klok and Oerlemans (2003) and Oerlemans (2001, 2005). This flow model is based on the first-order glacier dynamics (Oerlemans, 2001, 2005) and successfully applied to 169 globally distributed glaciers since AD 1700 (Oerlemans, 2001, 2005). Unlike more explicit numerical glacier/ice sheet models, that require many complex geologic, climatic, and energy balance variables (cf. Azam et al., 2014; Roe and Baker, 2014; Rounce et al., 2015) and are often catchment specific (cf. Carr et al., 2010; Eaves et al., 2016; Pellitero et al., 2016; Putnam et al., 2013a,b), the current model requires a limited number of variables and hence it is easy to reconstruct for a wide range of Himalayan glaciers and widely different climatic regions throughout the orogen. Although the model has its limitations for site-specific applications and should be used cautiously (Oerlemans, 2005), we argue that we are more interested in capturing the inter-regional pattern of net temperature (ΔT) change during Holocene glacier advances rather than absolute values throughout the orogen and hence, is suitable for average broadscale spatiotemporal analysis.

Also, the linear flow model considers climate sensitivity (c) and response time (τ) of the glacier to estimate the lag time (see Saha et al. MethodsX for more details about c and τ). If ambient temperature primarily drives glacier fluctuations on a continental scale, climate sensitivity (c), therefore, can be defined as the decrease in equilibrium glacier length per K increase in temperature (Oerlemans, 2005). A simple linear response equation is, therefore, proposed (Oerlemans, 2005):

$$\frac{dL(t)}{dt} = -\frac{1}{\tau}\left[cT(t) + L(t)\right] \quad (1)$$

Here, T is a temperature perturbation (e.g., annual mean), t is time, L is the medial glacier length with respect to present snout position. Assuming a simple glacier advance scenario, we measured respective mean moraine age and distance from the snout to calculate t and L, respectively. dL is the linear interpolation over ten years (dt) interval. c and τ were determined from a first-order glacier dynamics theory (see Saha et al. MethodsX for details) and explicitly explained in Schmeits and Oerlemans (1997), Oerlemans (1997, 2001), and Oerlemans et al. (1998). We individually calculated c and τ for each glacier, and hence, distinct for cold-based/polythermal/temperate glaciers.

The inverse model to solve for T, thus, can be stated as:

$$T(t) = -\frac{1}{c}\left[L(t) + \tau\frac{dL(t)}{dt}\right] \quad (2)$$

This linear inverse glacier flow model uses present annual precipitation to estimate c and τ of the individual sample glacier (see Saha et al. MethodsX to measure c and τ). Past change in annual precipitation would, therefore, likely result in changes in c and τ. Proxy and model studies based on lake shorelines and δ^{18}O also showed that precipitation increase in the western and interior Tibet was ~55–200% higher than present during the Early Holocene (Huth et al., 2015; Li et al., 2017; Shi et al., 2017). Since it is challenging to quantify the spatiotemporal evolution of past precipitation, we added ±30% uncertainties to c and τ to account for this unknown uncertainty of the model. Additional limitations of the model are also presented in Oerlemans (2005). Further estimates of uncertainties were made by combing T for sample glaciers in each region and measuring a mean and $\pm 1\sigma$ from the data (see Saha et al. MethodsX). We only present net temperature (ΔT) change in the text following the recommendation of Putnam et al. (2013a,b).

4. Detailed study areas

4.1. Kulti valley

Kulti valley is occupied by the <10-km-long Sonapani glacier in its upper reaches (>4000 m asl). This debris-mantled glacier, covering and area of ~32.5 km^2, consists of five hanging glaciers that merge into a valley glacier that tapers into a narrow icefall at ~3860 m asl and created a V-shaped gorge above the icefall (Figs. 2A, 5A, S7A, B). Five sets of morphostratigraphically distinct moraines were identified and mapped in the valley (Fig. 2A and S2). These five sets of moraines (M_{K1}, M_{K2}, M_{K3}, M_{K4}, M_{K5}) in the Kulti valley are traversed by the ~9-km-long Dugli Nala meltwater stream (Fig. 2A, S7C, D, I, J).

M_{K1}, located at ~3700–4000 m asl, is a ~1.8-km-long discontinuous southeast trending laterofrontal moraine set on the south side of the valley (Fig. S7A). The farthest laterofrontal ridge of the moraine is ~2.9 km from the glacier snout (Fig. 2A). Glacial trimlines are present in the north side of the valley (Fig. 2A and S7A). Inset within the moraine are several <5-m-high northeast-southwest trending ~100-m-long hummocks (Fig. S7B). No suitable boulders were found to sample for dating. Fig. S2 presents detailed moraine and boulder characteristics.

Two subdued northeast trending ~5-m-high and ~150-m-long rounded lateral moraine ridges (M_{K2a}, M_{K2b}) are present ~0.9 km from M_{K1}, at altitudes of ~3669–3676 m asl (Figs. S2, S7C, D). Two boulders were sampled from the M_{K2b} ridge (Figs. 2A and B; 3C, D).

A northwest-trending terminal moraine ridge, M_{K3}, is present ~2.1 km from M_{K2}, at an altitude of ~3638–3640 m asl (Fig. 2A and S7E). This ~30-m-high and ~450-m-long moraine ridge is referred to as the Rataskal terminal moraine by Raina et al. (2015). No samples for dating were collected from M_{K3} since post-depositional hillslope deposits have partially buried the original terminal moraine (Figs. S2, S7E, F). A broad braided channel with lacustrine deposits is present upstream of M_{K3}, likely formed by damming of the moraine (Raina et al., 2015).

M_{K4} moraine set, ~0.9 km from M_{K3} at an altitude of ~3426–3500 m asl consists of three northeast trending rounded lateral ridges (Figs. S7G and H). Four boulder samples were collected from M_{K4b} and M_{K4c} lateral ridges (Figs. 2A, C, 3A, B, S2). These ridges are ~20-m-high and ~500-m-long and mainly preserved in the northwest of Dugli Nala. A subdued lateral moraine ridge to the southeast is mostly buried under hillslope deposits (Fig. 2C).

A sharp-crested laterofrontal moraine set, M_{K5}, ~1.3 km from M_{K4}, is at an altitude of ~3164–3270 m asl. The moraine set trends northeast with a sharp bend to the west at its frontal part (Fig. S7I). While the northwest ridge is ~0.5-km-long and does not contain any large boulders, the SE ridge is ~1.1-km-long and contains several larger boulders (Figs. S2 and S7J). We sampled six boulders from this grass-covered ridge (Fig. 2A, C). We suspect recent hillslope deposits on the moraine surface because of the narrow valley mouth (Fig. S7I). The moraine morphology and presence of lacustrine sediments capped with fluvial and debris flow sediments to the east of the moraine, likely indicate blocking of the main Chandra valley by the glacier (Owen et al., 1997).

4.2. Parkachik Valley

A large accumulation area (74%) and high steep peaks of Nun and Kun feed Parkachik glacier in the Parkachik Valley, the largest

glacier in the Nun Kun massif (Fig. 2D and S7K). This glacier is unique in the Zanskar Range due to its large size and extent (Lee et al., 2014). The glacier extends into four tributaries in the higher reaches (Fig. 2D). There are three other cirque glaciers on the northern flanks of the Nun Kun massif, and from west to east these include Tarangoz, Rantac, and Sentick glaciers. The moraines of these glaciers were previously dated by Lee et al. (2014) using ^{10}Be. Two moraine sets, M_{P1}, and M_{P2}, of Parkachik glacier, were mapped based on morphostratigraphy.

M_{P1} is the youngest laterofrontal moraine set with two ice contact ridges at an elevation of ~3595–3730 m asl (Fig. 2D, E, S7K, L). M_{P1a} is closest to the glacier and presently unstable (Fig. S7L). The ~0.6-km-long sharp-crested west lateral ridge of M_{P1b} was sampled for ^{10}Be dating (Figs. 2D, E, 3E, F, S2). This moraine ridge is well preserved, but the moraine flank, facing the glacier, is currently undergoing base erosion by the meltwater stream (Fig. S7L). We sampled four stable tabular boulders from this ridge (Fig. 3E and F). The eastern lateral ridges are ~1.3 km long with no suitable boulders for sampling.

M_{P2} moraine set, located outside of M_{P1} to the east, consists of four grass-covered rounded ridges (Fig. S7K and M). These are steep (20–30°), ~30-m-high, <0.35-km-long and discontinuous, and more of bedrock-cored ridges than moraines. One of the outer bedrock-cored ridges supports up-valley section of the west lateral ridge of M_{P1} (Fig. S7K). The bedrock-cored ridges contain thin veneers of matrix-supported pebbly diamicton that overlay the polished and weathered bedrock surfaces. We did not collect any samples from this moraine due to the lack of suitable boulders for dating (Fig. S2).

5. Results

5.1. Local glacial analyses

5.1.1. Dating results: Kulti valley

The oldest M_{K5} laterofrontal moraine ridges were previously assigned to the Kulti glacial stage by Owen et al. (1996, 1997, 2001) based on their morphostratigraphic position and relative dating. Their Kulti glacial stage was dated, using ^{10}Be (recalculated here), elsewhere in Lahul to ~12.3 ± 0.6 or 13.7 ± 1.3 ka by Eugster et al. (2016). We have dated six boulders from the SE moraine ridge (Fig. 5A). Our ^{10}Be ages range from ~16.1 to 1.2 ka (Table 1; see also Table 1 in Saha et al. Data in Brief) showing large scatter ($\chi^2 = 464$) and possible influence of recent hillslope deposits. We discarded four young ages (samples S19, S20, S23, and S24) from further analysis. The remaining two ages yield a tentative mean age of 14.7 ± 2.1 ka. However, if the sample S19 (~9 ka) is included (not statistically recommended), a mean age of 12.7 ± 3.6 ka is expected.

Four sampled boulders on the M_{K4} moraine present an age clustering with a χ^2 of 2.0 (see Table 1 in Saha et al. Data in Brief). Ages in the distant moraine ridges (M_{K4b} and M_{K4c}) range from ~13.0 to 10.9 ka (Table 1), with a mean age of 12.2 ± 1.0 ka (Fig. 5A).

No ages are available for our M_{K3} terminal moraine (Fig. 5A), which Owen et al. (1996, 1997, 2001) previously assigned to the Sonapani I glacial stage using relative dating.

Two boulders on the young M_{K2} moraine have ages of ~0.6 to 0.4 ka (Table 1; S 4) with a tentative mean age of 0.5 ± 0.2 ka (Fig. 5A).

The formation of the M_{K1} moraine complex predates AD 1906 (Fig. 4A) based on the photograph taken by Walker and Pascoe (1907 in Raina et al., 2015). According to their description, the glacier snout was at ~3,711 m in AD 1906, only a few hundred meters up-valley from the lowest moraine ridges of M_{K1} moraine complex (see Fig. 15, page 38 of Owen et al., 1996). Owen et al. (1996, 1997, 2001) assigned this moraine to their Sonapani II glacial stage, a late 19th Century advance.

5.1.2. Dating results: Parkachik valley

Ages for the ice-contact M_{P1} moraine form a tight cluster that ranges from ~0.2 to 0.1 ka (Table 1; see Table 1 in Saha et al. Data in Brief) with a χ^2 of 5.4 (acceptable at 95% confidence interval). We calculate a mean age of ~0.2 ± 0.1 ka for this lateral moraine (Fig. 5B). Lee et al. (2014) could not date the youngest ice-contact moraine (TG4) adjacent to Parkachik glacier in the Tarangoz valley of the Nun Kun massif (Fig. 2D). Their youngest dated moraine, TG3, is dated to ~0.6 ± 0.1 ka (see Table 1 in Saha et al. Data in Brief). We suggest that the M_{P1} moraine likely represents the youngest local glacial advance in the massif.

Röthlisberger and Geyh (1985a, b) used ^{14}C dating of humic acid to date the Parkachik moraine to 5055 ± 381 cal yr BP (recalibrated using CALIB 7.1 of Stuiver et al., 2018). In the absence of any photographic evidence and precise coordinate systems, we were unable to find their sample location or any organic materials in both M_{P1} and M_{P2} moraine sets to verify these ^{14}C ages.

5.1.3. Reconstructed ELAs and net temperature change

Sonapani glacier in the Kulti valley extended ~10 km from its present position (Fig. 1B) at ~14.7 ka with a ΔELA of 259 ± 109 m (Table 2; Fig. 5A). A subsequent ~7.6 km advance (Fig. 1B) at ~12.2 ka represents a ΔELA of 186 ± 62 m (Table 2; Fig. 5A) in the valley and comparable to the Early Holocene glacier advance (ΔELA ~182 ± 57 m at ~10.5 ka) in Hamtah valley on the southern side of the Chandra valley (Saha et al., 2018). The inverse glacier flow model produces a net temperature increase of 2.7 ± 0.2 °C (58.7% of the total increase) for ~14.7–12.2 ka (note: for the ease of interpretation, ΔT K is expressed as ΔT °C). Our undated Rataskal terminal moraine (M_{k3}), located ~6.5 km (Figs. 1B and 5A) from the present snout, had a ΔELA of 127 ± 38 m.

Sonapani glacier also advanced ~4 and ~3 km (Fig. 1B) from the present snout during the Late Holocene at ~0.5 ka and late 19th Century, having ΔELAs of 106 ± 30 and 92 ± 31 m, respectively. We modeled a net ambient temperature increase of ~0.9 ± 0.2 (19.6% to total change) and 1.0 ± 0.2 °C (21.7%) for ~12.2–0.5 ka and ~0.5–0.1 ka, respectively. Since the ~0.1 ka advance, there has been a net temperature increase of ~0.5 °C based on the linear flow model.

The glacier only extended ~0.3 km (Fig. 1B) from its present snout at ~0.2 ka with a ΔELA of 20 ± 9 m in the Parkachik valley (Table 2; Fig. 5B). Based on the linear flow model, we calculated a net temperature increase of 0.5 ± 0.1 °C since ~0.2 ka.

5.2. Regional analyses

5.2.1. Climate groups and zones

Previous studies have shown a latitudinal gradient of contemporary snowlines (Benn and Owen, 1998; Owen and Benn, 2005; Yao et al., 2012; Heyman, 2014), and longitudinal and latitudinal variations of prevailing climatic systems (Vaux Jr. et al., 2012) across the Himalaya and Tibet. While the winter mid-latitude westerlies significantly influence the western end of the Himalaya and Tibet (Mölg et al., 2014), the ISM and East Asian Summer Monsoon (ESM) largely dominate the southern and eastern (maritime) regions, and to a limited extent the interior (continental) portions of the orogen (Fig. 1A; Jin et al., 2014). Additionally, the Siberian high-pressure system dominates the Tian Shan during the winter (Fig. 1A; Cohen et al., 2001). Three broad types of glaciers have been proposed, which include wet-temperate glaciers, sub-polar (cold) arid-semiarid glaciers, and polythermal transitional glaciers (Fig. 4; Derbyshire et al., 1991; Yang et al., 2009a,b; Shangzhe et al., 2010; Yao et al., 2012; Zhu et al., 2013). The temperate glaciers are mostly melt-dominated, thick debris-mantled and have low-altitude snowlines (Fig. 4; Derbyshire et al., 1991; Yang et al., 2009a,b; Shangzhe et al., 2010; Yao et al., 2012; Zhu et al., 2013). They are

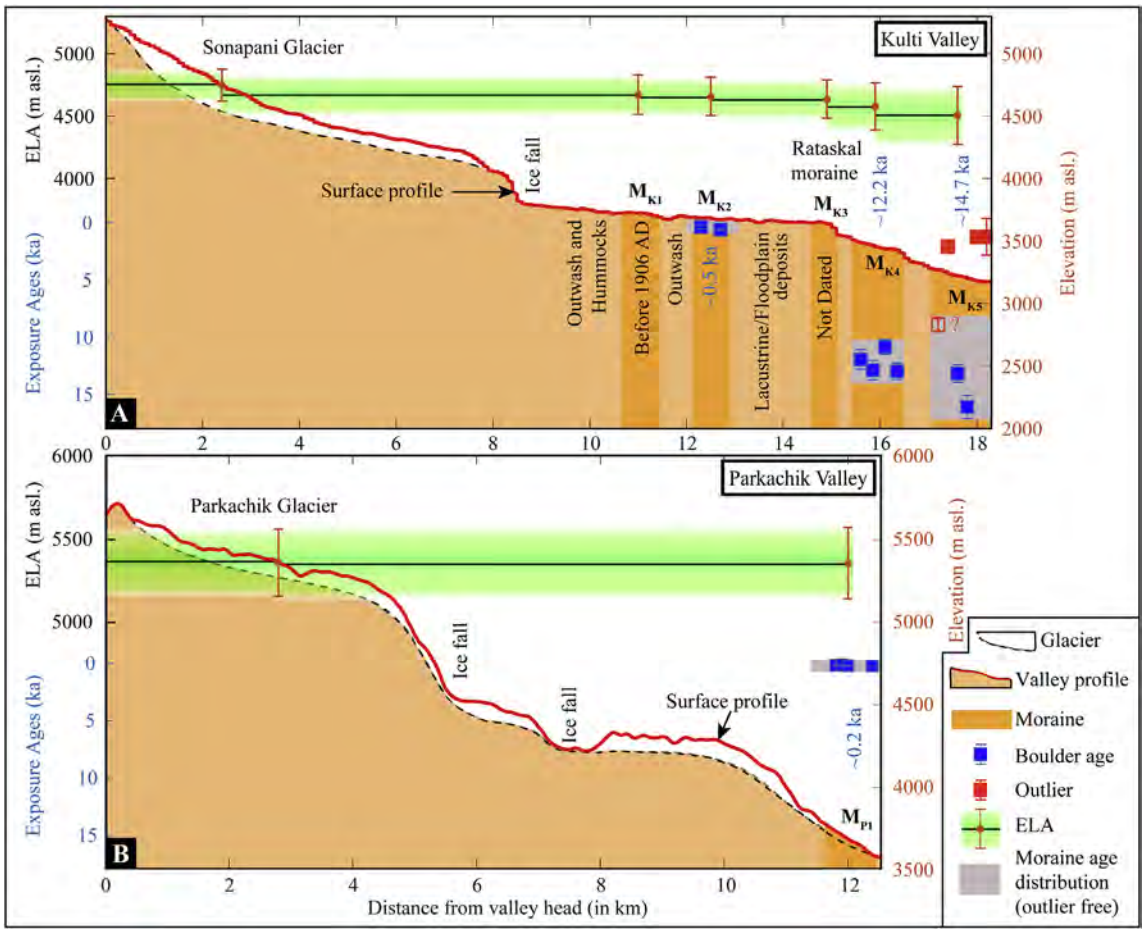

Fig. 5. Cross-valley profiles (red lines) showing topography, major landforms, reconstructed ELAs, and ^{10}Be moraine chronologies for the Kulti (A) and the Parkachik (B) valleys in the NW Himalaya of northern India. The mean moraine ages with 1σ uncertainties that are morphostratigraphically distinct represent the local glacial stages in respective valleys. Both valleys show typical stair-case topography with steep ice falls. (For interpretation of the references to color in this figure legend, the reader is referred to the Web version of this article.)

more susceptible to changes in temperature. The cold arid-semiarid glaciers, in contrast, are sublimation dominated, usually debris-free, and located at higher altitudes (Fig. 4; Derbyshire et al., 1991; Yang et al., 2009a,b; Shangzhe et al., 2010; Yao et al., 2012; Zhu et al., 2013). These types of glacier are more sensitive to changes in precipitation. Polythermal transitional glaciers are intermediate between cold and temperate glaciers.

While local altitude, relief, aspect, hypsometry, microclimate, pre-existing topography, debris cover, and slope deposits play a crucial role in determining individual glacier dynamics at the catchment-scale (Roe, 2011; Barr and Lovell, 2014), climate likely plays a first-order role in defining glacier characteristics at the scale of $>10^3$ km (cf. Sagredo and Lowell, 2012). We capture these glacier-types using a comprehensive climate group map (Fig. 6).

Our CA dendrogram shows five major climate groups of glaciers (Fig. 6A). These include:

- *Climate Group 1* includes mostly sub-polar cold arid-semiarid glaciers, spread across the northwest Himalaya, the western, interior continental, and northeast Tibet, and parts of Pamir and Tian Shan (Fig. 6B). Nearly 59.6% of sample glaciers fall in this group.
- *Climate Group 2* glaciers are transitional between arid-semiarid and wet-temperate glaciers and distributed across the Karakoram, the Great Himalaya, and edges of the south, east and northeast (maritime) Tibet (Fig. 6B) and include 32.9% of the sample glaciers.
- *Climate Group 3* consists typically of wet-temperate glaciers, spread across the southern edges of *Climate Group 2*, i.e., along the Lesser Himalaya, southeast Tibet, and in sporadic pockets of high precipitation. This includes ~3.4% of sample glaciers, and the glaciers in this group are directly influenced by maritime changes (Fig. 6B).
- *Climate Group 4* are mainly a humid transitional type and located in the further south and pockets of very high precipitation (Fig. 6B) and include 3.5% of the sample glaciers.
- *Climate Group 5* is likely the wettest and temperate type of glacier (0.6% of sampled glaciers), is maritime climate dominated, and distinctly located along the southern Nepalese Himalaya and in some small loci of regionally high-peaks (Fig. 6B).

A strong positive correlation (0.69 at 95% confidence level) exists between Euclidian and cophenetic distances in the dendrogram, further supporting the CA clustering (Fig. 6A). An ANOSIM test also yielded a high R-value (0.73) at 99% confidence level which supports the hypothesis that the samples within climate groups are more similar than by random chance.

We have also refined our CA groups by running PCA (Table 3; Fig. 6C). Our first three principal components (PCs) explain ~88% of

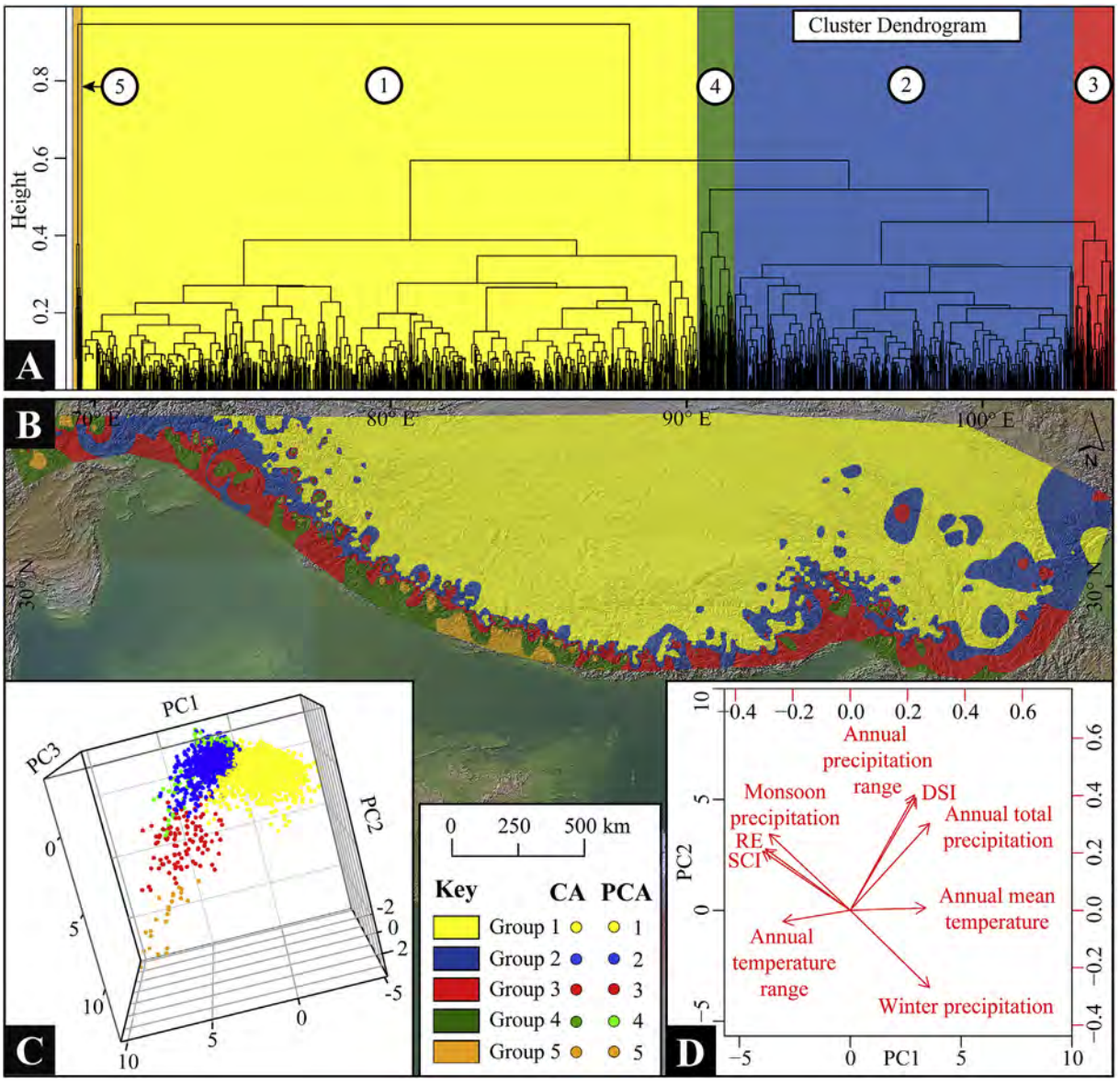

Fig. 6. Cluster and Principal Component Analyses of Himalayan-Tibetan glaciers to identify identical climate groups. (A) The dendrogram (hierarchical tree) representing groups of most similar glaciers based on the climate parameters. Each terminal of the hierarchical tree represents a single glacier (n = 42,511). Each vertical line joins the groups at a certain level of similarity. Five major climate groups are identified. (B) Each glacier point, based on its cluster, is interpolated over the region to generate a climate zone map and superimposed over a hillshade map. Because our gridded TRMM data is only generated up to 36° N lat.; for study areas beyond 36° N see explanation in section 3.5. (C) PCA results are shown in three dimensions (PC1, PC2, PC3). These three axes explain 88% of the total variance (PC1 53%, PC2 26% and PC3 9%). The groups derived in CA and PCA methods are identical (see the key). (D) Biplot is showing the magnitude and sign of each parameter's contribution to the PC1 and PC2 (Table 3).

Table 3
Principal component (PC) loading for all the variables used in this study.

Variables	PC1	PC2	PC3	PC4	PC5	PC6	PC7	PC8	PC9
Annual mean temperature	0.33	0.01	0.52	−0.26	−0.74	−0.03	0.01	0.00	−0.02
Annual temperature range	−0.29	−0.05	−0.73	−0.13	−0.60	0.06	0.02	0.01	−0.01
Annual total precipitation	0.35	0.38	−0.24	0.06	−0.01	−0.77	−0.23	−0.16	0.03
Annual precipitation range	0.29	0.49	−0.14	−0.08	0.03	0.50	0.02	−0.43	0.46
Total summer monsoon precipitation	−0.35	0.33	0.18	0.43	−0.18	0.02	−0.38	0.45	0.42
Total winter precipitation	0.35	−0.34	−0.18	−0.47	0.17	0.05	−0.40	0.44	0.36
SCI	−0.38	0.26	0.14	−0.47	0.09	0.09	−0.59	−0.23	−0.36
RE	−0.37	0.27	0.12	−0.53	0.11	−0.29	0.52	0.17	0.33
DSI	0.28	0.50	−0.14	−0.05	0.05	0.23	0.17	0.57	−0.49

the total variance in the sample glaciers. We infer that PC1 (53% of the total variance) corresponds strongly and positively to annual total precipitation, annual precipitation range, and DSI (Fig. 6D, Table 3). The influence of temperature parameters is only partial and limited (Fig. 6D). Similarly, PC2 (26%) agrees more closely and negatively to summer monsoonal precipitation, RE, and SCI and positively to winter precipitation from the mid-latitude westerlies (Fig. 6D, Table 3). PC1 appears to track the climate at the glacier locations, whereas PC2 reflects the seasonal variability. Based on the sensitivity analysis, the climate groups at the regional-scale are more susceptible to changes in precipitation parameters.

The PCA yielded similar results to the CA (see Fig. 6), suggesting robustness in the analysis. The first three principal components (Fig. 5C; Table 3) also suggest that the climate groups are distinct from each other except for climate group 4. Climate group 4 (humid transitional climate) overlaps closely with climate group 2 (Fig. 6C). Similarly, climate group 5 only encloses a few (0.6%) wettest southern glaciers, possibly representing end members. For the purpose of this study, we, therefore, discount climate group 4 and 5 and focus on latitudinally distinct climate groups 1–3 for the rest of the analysis.

Our statistical treatment does not capture the longitudinal climate zonation, i.e., maritime versus continental. The glaciers located in the northeast and southeast of the orogen are more sensitive to tropical maritime changes than the glaciers in the northwest. Similarly, glaciers in the southern central part receive more moisture than glaciers in the northwest part of the orogen. The Sutlej river basin is considered the maximum extent of the mid-latitudinal westerlies (Vaux Jr. et al., 2012). Since the longitudinal climatic gradient is crucial for our inter-regional analysis, additional climate variables, such as annual snowfall and $\delta^{18}O$ distribution, may be required to refine our initial climate groups.

Similarly, the published and new ^{10}Be dated moraines used in this study are limited (0.002% of the total 42,511 glaciers) and disproportionately distributed with large longitudinal gaps (i.e., sample glaciers) across the orogen (Figs. 1A and 6B). For example, a large longitudinal hiatus exists between northwestern and western Himalayan sampled glaciers. The longitudinal gap is also prominent between western and central Himalayan glaciers. We, therefore, did not group, e.g., all the arid and semiarid glaciers of the northwestern and northeastern part of the orogen into a single category, but further subdivided the climate groups 1–3 to additional climatic zones to accomplish the objective of the analysis; that is to compare Holocene glacier advances inter-regionally. Hence, our latitudinal climatic groups are subdivided into longitudinal climatic zones based on the approximate spatial extent of the prevailing climate systems (cf. Vaux Jr. et al., 2012) and the distribution of ^{10}Be dated samples. The following framework (five climatic zones) is proposed and used from here on:

- *Climate Group 1*: Arid and semiarid colder climatic region including climatic zone 1a (Transhimalaya, northwestern Tibet, Pamir, and Tian Shan), and climatic zone 1b (southern and northeastern Tibet).
- *Climate Group 2*: Transitional climatic region including climatic zone 2a (western Himalaya), climatic zone 2b (central and eastern Himalaya).
- *Climate Group 3*: Wet and temperate climatic region including climatic zone 3 (central and eastern Himalaya; since no moraines in the western Himalaya are ^{10}Be dated).

5.2.2. Regional glacial stages, ELAs, and hypsometries

Within a broad zone, variability in reconstructed past and contemporary ELAs at the catchment-scale may be attributed to variable glacier hypsometries and corresponding (altitudinal) temperature gradients (Blomdin et al., 2016). Since glacier hypsometry is arguably influenced by a variety of factors including relief and terrain conditions, and microclimate, we further evaluated the intra-regional variability of glacier extents by assessing the average glacier hypsometries and ELAs (Table 4; Fig. S5).

Climatic zone 1a: Arid and semiarid colder climatic region—*Transhimalaya, northwestern Tibet, Pamir, and Tian Shan.*

We identified four distinct subgroups of glaciers based on average hypsometry and contemporary ELA distributions of the sampled (^{10}Be dated) glaciers in this zone (Table 4; Fig. S5). These include the Muztag Ata massif of the northwestern Tibet, the Pamir and the Tian Shan, the Karakoram, and the Ladakh and the Zanskar ranges; the major orographic barriers. These wide-ranging glacier hypsometries and ELAs likely play a crucial role in determining variable glacier responses and amplitudes to identical climatic perturbations.

Two tentative and five major regional stages of glacier advances are identified using 47 local glacial stages from 15.0 to 0.2 ka (Table 5; Fig. 7). A distinct (7.5% age OD) regional glacier advance occurred during the Lateglacial (15.2–11.7 ka; Figs. S8A and S9A); a tentative ($n = 2$) one in the Early Holocene (10.3–9.7 ka with 0% age OD; Table 5; Figs. S8A and S9B); a well clustered (0% age OD) one in the early Mid-Holocene at 8.0–7.7 ka (Table 5; Figs. S8B and S9C); in the latter part of the Mid-Holocene and into the Late Holocene at 6.6–3.5 ka (23% age OD; Table 5; Fig. S8B); and three during the Late Holocene at 2.3–1.3, ~1 (tentative), and <1 ka (28–39% age OD; Table 5; Figs. S8C, D, S9E). For the <1 ka regional advance, we argue that multiple overlapping local glacier advances at the century-timescale are probable (Fig. S8D). We are unable to distinguish further regional sub-stages for this period (Fig. 7).

Extensive ΔELAs are recorded in the Lateglacial (~300 ± 200 m) and Early Holocene (~670 ± 160 m; see Table 2 in Saha et al. Data in Brief; Fig. 7). Subsequent ΔELAs are progressively restricted over time (i.e., ~355 ± 235 m at 8.0–7.7 ka, ~270 ± 140 m at 6.6–3.5 ka, ~100 ± 65 m at 2.3–1.3 ka, ~40 ± 30 m at ~1 ka, and ~100 ± 95 m at <1 ka; see Table 2 in Saha et al. Data in Brief; Fig. 7).

Regional Holocene glacier chronostratigraphies (or Himalayan Holocene stages [HHs]) are previously developed by Saha et al. (2018) for the northwestern Himalaya and Tibet. Their HHs

Table 4
Average hypsometric and contemporary ELAs across five climatic zones.

Glacier subgroups	Toe (m asl)	Cirque head (m asl)	Present ELAs (m asl)
Climatic Zone 1a: Arid and semiarid colder climatic region— Transhimalaya, northwestern Tibet, Pamir, and Tian Shan.			
Muztag Ata, NW Tibet	~4500	~7000	~4017–5749
Pamir and the Tian Shan	~3550	~4500	~3963–4144
Karakoram[a]	~3930	~6000	~4713–5057
Ladakh and Zanskar	~5450	~6210	~5489–5870
Climatic Zone 1b: Arid and semiarid colder climatic region—southern and northeastern Tibet			
Southern and northeastern Tibet	~4500	~6590	~4407–5259
Climatic Zone 2a: Transitional climatic region—western Himalaya			
Garhwal Himalaya	~3740	~6020	~4611–5062
Nun Kun, Lahul, and Gurla Mandhata	~4000	~6780	~4500–6152
Climatic Zone 2b: Transitional climatic region—central and eastern Himalaya			
Central Himalaya	~4880	~6780	~5390–5809
Eastern Himalaya	~2980	~7000	–
Climatic Zone 3: Wet-temperate climatic region—central and eastern Himalaya			
Central and Eastern Himalaya[b]	~3930	~6590	~4440–5584

[a] Batura and Hunza glaciers are the largest (~57 km-long) and extending from ~2600 to 7540 m asl.
[b] Some smaller cirque glaciers (e.g., Syaktan, Yak Upper, Danfe, Macha Khola, and Mailun Khola) have an altitudinal range from snout-to-cirque between ~4690 and 5450 m asl.

Table 5
A summary of Lateglacial and Holocene local and regional stages of glacial advances based on recalculated cosmogenic ^{10}Be surface exposure age data.

Location number as shown in Fig. 1	Local glacial stage	Local stage age (ka)[a]	Regional stage age range (ka)	Number of samples used (outlier free)	χ^2 value[b]	Gaussian peak (ka)[c]	Kernel density fit (ka)[d]	P $_{(sigma^2\text{-tailed})}$ between stages
Climatic Zone 1a. Arid and semiarid Transhimalaya, northwest Tibet, Pamir, and Tian Shan								
5	Kitschi-Kurumdu-M2 (Zech, 2012)	15.16 ± 3.03	15.2–11.7	4	17.74	13.9 ± 0.1	14.0 ± 0.9	0
11	Mungo 2 stage-m_{1I} (Seong et al., 2007)	14.98 ± 0.29		5	0.17			
11	Mungo 2 stage-m_{1D} (Seong et al., 2007)	14.62 ± 0.32		3	0.19			
10	Batura stage-t6 (Owen et al., 2002)	14.30 ± 0.01		2				
11	Mungo 2 stage-m_{1I} (Seong et al., 2007)	14.08 ± 0.23		3	0.11			
6	AV (Abramowski et al., 2006)	14.02 ± 0.16		3	0.04			
11	Mungo 2 stage-m_{1G} (Seong et al., 2007)	13.77 ± 0.53		10	0.56			
11	Mungo 2 stage-m_{1F} (Seong et al., 2007)	13.44 ± 0.19		3	0.08			
9	BO8 stage (Röhringer et al., 2012)	13.18 ± 0.64		2	0.65			
2	BOR 2 stage (Blomdin et al. (2016))	13.08 ± 2.13		3	10.59			
11	Mungo 2 stage-m_{3I} (Seong et al., 2007)	13.06 ± 0.40		3	0.33			
7	Olimde 2 stage-m_{3H} (Seong et al., 2009)	13.01 ± 0.14		3	0.04			
10	Batura stage-t6 (Owen et al., 2002)	12.49 ± 1.05		2				
11	Mungo 2 stage-m_{1E} (Seong et al., 2007)	12.41 ± 0.33		2	0.25			
8	Olimde 2 stage-m_{5C} (Seong et al., 2009)	11.71 ± 0.40		2	0.46			
8	Olimde 3 stage-m_{3F} (Seong et al., 2009)	10.25 ± 0.16	10.3–9.7 (tentative)	6	0.1	10.3 ± 0.1	10.2 ± 0.3	0
8	Olimde 3 stage-$m_{3F'}$ (Seong et al., 2009)	9.69 ± 0.34		8	0.43			
7	Olimde 4 Stage-m_{4H} (Seong et al., 2009)	7.98 ± 0.10	8.0–7.7	6	0.06	7.4 ± 0.1	8.0 ± 0.2	0
8	Olimde 4 Stage-m_{6A} (Seong et al., 2009)	7.80 ± 0.29		5	0.48			
8	Olimde 4 Stage-m_{5A} (Seong et al., 2009)	7.74 ± 0.27		6	0.41			
11	Mungo 2 stage-m_{2G} (Seong et al., 2007)	6.64 ± 0.35	6.6–3.5	4	0.68	4.4 ± 0.1	5.7 ± 0.8	0
11	Askole 2 stage-m_{2b} (Seong et al., 2007)	5.98 ± 0.69		4	0.92			
3	Aksai (Koppes et al., 2008)	5.70 ± 0.16		2				
8	Olimde 5 stage-$m_{6C'}$ (Seong et al., 2009)	5.05 ± 0.14		3	0.33			
15	KM-4 stage/mG2 (Hedrick et al., 2011)	4.66 ± 1.17		6	13.12			
7	Olimde 6 stage-m_{5H} (Seong et al., 2009)	4.32 ± 0.11		3	0.19			
7	Olimde 6 stage-m_{6H} (Seong et al., 2009)	3.97 ± 0.30		3	2.17			
15	PM-2 stage (Hedrick et al., 2011; Saha et al., 2018)	3.50 ± 0.87		3	17.79			
13	Ladakh Chang La cirque (Dortch et al., 2013)	2.29 ± 0.28	2.3–1.3	4	2.02	2.1 ± 0.0	2.2 ± 0.4	0
15	m_{G1} (Saha et al., 2018)	2.25 ± 0.42		3	9.37			
8	Olimde 7 stage-m7A (Seong et al., 2009)	2.20 ± 0.07		6	0.19			
7	Olimde 7 stage-m7H (Seong et al., 2009)	1.66 ± 0.17		3	0.75			
14	m_{S2} (Orr et al., 2017a, b; Saha et al., 2018)	1.42 ± 0.48		6	21.83			
7	Olimde 7 stage-m_{3I} (Seong et al., 2009)	1.39 ± 0.42		4	4.58			
15	m_{G1} (Orr et al., 2017a, b)	1.33 ± 0.12		1	–			
11	Askole 3 stage-m_{1H} (Seong et al., 2007)	1.03 ± 0.28	~1.0 (tentative)	5	0.82	1.0 ± 0.0	1.0 ± 0.1	0
15	m_{M2} (Saha et al., 2018)	1.00 ± 0.08		4	0.9			
8	Olimde 8 stage-m_{8A} (Seong et al., 2009)	0.69 ± 0.27	<1.0	3	10.19	?	0.6 ± 0.1	0
15	m_{M1} (Saha et al., 2018)	0.64 ± 0.09		3	1.47			
2	BOR 1 (Blomdin et al., 2016)	0.64 ± 0.23		3	10.96			
13	Pangong high cirque (Dortch et al., 2013)	0.54 ± 0.11		3	0.63			

(*continued on next page*)

Table 5 (*continued*)

Location number as shown in Fig. 1	Local glacial stage	Local stage age (ka)[a]	Regional stage age range (ka)	Number of samples used (outlier free)	χ^2 value[b]	Gaussian peak (ka)[c]	Kernel density fit (ka)[d]	P $_{(sigma^2\text{-tailed})}$ between stages
14	m_{A2c} (Saha et al., 2018)	0.52 ± 0.20		3	24.25			
8	Olimde 8 stage-m_{6C} (Seong et al., 2009)	0.51 ± 0.15		4	4.19			
3	Ala Archa (Koppes et al., 2008)	0.49 ± 0.25		2				
1	Daxi (Li et al., 2014)	0.33 ± 0.02		4	0.49			
15	PM-3 stage (Hedrick et al., 2011)	0.28 ± 0.05		3	2.22			
14	m_{A1} (Saha et al., 2018)	0.26 ± 0.08		3	6.78			
Climatic Zone 1b. Arid and semiarid southern and northeastern Tibet								
33	Group D moraines (Wang et al., 2013)	13.45 ± 0.25	13.5–12.9	2			13.2 ± 0.7	0
34	LLL (Lasserre et al., 2002)	13.16 ± 1.05		6	1.66			
35	Halong glacial stage (Owen et al., 2003a)	12.89 ± 1.26		6	4.68			
32	PR (Owen et al., 2005)	11.47 ± 0.70	11.5–9.5	4	1.56		10.8 ± 1.0	0
35	Holocene moraine (Owen et al., 2003b)	10.08 ± 0.53		1	–			
35	Halong glacial stage (Owen et al., 2003a)	9.48 ± 1.70		2				
36	M2 moraines (Owen et al., 2006)	8.04 ± 0.74	~8.0 (tentative)	2		8.0 ± 0.7	?	
32	Youngest (Owen et al., 2005)	3.28 ± 0.74	~3.3 (tentative)	3	6.2	3.3 ± 0.7	?	
Climatic Zone 2a. Transitional western Himalaya								
22	M5 (Owen et al., 2010)	15.30 ± 0.60	15.3–11.8	3	0.54	14.0 ± 0.2	13.7 ± 1.2	0
16	M_{k5} (This study)	14.65 ± 2.06		2				
16	Kulti glacial stage (Owen et al., 2001)	14.45 ± 0.70		1	–			
18	Tons Valley-location C (Scherler et al., 2010)	14.06 ± 0.10		2				
16	Kulti glacial stage (Owen et al., 2001)	14.03 ± 0.16		2	0.05			
16	Kulti glacial stage (Owen et al., 2001)	13.95 ± 0.88		2	1.11			
21	Moraine m2 (Barnard et al., 2004b)	13.71 ± 0.69		1	–			
20	mm1 (Murari et al., 2014)	13.62 ± 0.66		4	0.67			
12	Anantick stage-ST-3 (Lee et al., 2014)	13.55 ± 0.88		2				
16	M_{k4} (This study)	12.18 ± 0.99		4	2.06			
16	Kulti glacial stage (Owen et al., 2001)	11.76 ± 0.59		2	0.54			
18	Tons Valley-location D (Scherler et al., 2010)	11.09 ± 0.50	11.1–10.3	1	–	10.6 ± 0.2	10.8 ± 0.5	0
16	m_{H3} (Saha et al., 2018)	10.48 ± 0.48		3	0.48			
18	Tons Valley-location F' (Scherler et al., 2010)	10.26 ± 0.35		2				
20	mk1 (Murari et al., 2014)	10.25 ± 0.83		5	0.64			
22	M7 (Owen et al., 2010)	8.75 ± 0.55	8.8–8.3	2		7.8 ± 0.2	8.4 ± 0.5	0
19	Kedar glacial stage (Barnard et al., 2004a)	8.28 ± 0.45	(tentative)	2				
18	Tons Valley-Location F (Scherler et al., 2010)	6.09 ± 0.54	6.1–5.0	4	4	5.5 ± 0.1	5.5 ± 0.2	0
19	Shivling glacial stage (Srivastava, 2012; Sci. report)	5.22 ± 0.27		7	0.63			
22	M8 (Owen et al., 2010)	5.01 ± 0.88		2				
19	Gangotri glacial stage (Srivastava, 2012; Sci. report)	2.16 ± 0.35	~2.2 (tentative)	2		2.2 ± 0.4	?	
18	Tons Valley-Location G (Scherler et al., 2010)	0.66 ± 0.34	<1	2		?	0.3 ± 0.1	0
17	Yn (Saha et al., 2016)	0.62 ± 0.15		2	2.13			
21	Moraine m4 (Barnard et al., 2004b)	0.60 ± 0.28		2				
19	Gangotri stage (Barnard et al., 2004a; Srivastava, 2012)	0.56 ± 0.30		5	4.45			
12	Lonp stage-TG-3 (Lee et al., 2014)	0.53 ± 0.13		2	12.53			
16	M_{k2} (This study)	0.51 ± 0.16		2				
22	M9 (Owen et al., 2010)	0.46 ± 0.10		4	2.57			
20	mk2 (Murari et al. (2014))	0.31 ± 0.17		3	19.33			
16	m_{H1a} (Saha et al., 2018)	0.26 ± 0.13		3	8.55			
18	Tons Valley-Location E (Scherler et al., 2010)	0.26 ± 0.08		2				
22	M10 (Owen et al., 2010)	0.24 ± 0.15		3	10.04			
19	Bhujbas glacial stage (Srivastava, 2012; Sci. report)	0.21 ± 0.02		1	–			
20	mbd1 (Murari et al., 2014)	0.21 ± 0.02		3	0.61			
20	mbd2 (Murari et al., 2014)	0.16 ± 0.15		5	103.54			
20	mbd3 (Murari et al., 2014)	0.15 ± 0.10		3	71.63			

Table 5 (*continued*)

Location number as shown in Fig. 1	Local glacial stage	Local stage age (ka)[a]	Regional stage age range (ka)	Number of samples used (outlier free)	χ^2 value[b]	Gaussian peak (ka)[c]	Kernel density fit (ka)[d]	P $_{(sigma^2\text{-tailed})}$ between stages
20	mbd4 (Murari et al., 2014)	0.13 ± 0.11		2				
Climatic Zone 2b. Transitional central and eastern Himalaya								
27	Puluo 2 moraine (Schaefer et al., 2008)	13.47 ± 0.58	~13.5 (tentative)	4	0.41		?	
28	Chhukung glacial stage (Finkel et al., 2003)	11.52 ± 0.11	11.5–10.1	3	0.04		9.8 ± 0.7 and 11.3 ± 0.7	0
28	Chhukung glacial stage (Finkel et al., 2003)	10.97 ± 0.03		2				
30	Local LGM moraines (Owen et al., 2005)	10.10 ± 0.73		5	0.89			
30	Recessional moraine (Owen et al., 2005)	6.03 ± 1.97	6.0–3.2	2			4.6 ± 0.7	0
28	Thuklha glacial stage (Finkel et al., 2003)	4.43 ± 0.32		3	1.08			
29	T5c (Owen et al., 2009)	3.18 ± 0.23		5	1.18			
29	T6 (Owen et al., 2009)	2.08 ± 0.09	~2.1–1.0	3	0.51	2.1 ± 0.1	1.0 ± 0.2 and	0
30	Neoglacial moraines (Owen et al., 2005)	1.04 ± 0.10	(tentative)	4	0.31		2.1 ± 0.2	
30	Little Ice Age moraines (Owen et al., 2005)	0.46 ± 0.06	<1	2			0.5 ± 0.2	0
29	T7 (Owen et al., 2009)	0.33 ± 0.19		3	12.31			
Climatic Zone 3. Wet-temperate central and eastern Himalaya								
31	Ganhaizi (Kong et al., 2009)	12.97 ± 1.41	13.0–10.9	2			12.0 ± 1.0	0
31	Ganheba (Kong et al., 2009)	11.96 ± 1.94		2				
31	Yulong (Kong et al., 2009)	?		0				
23	Yak Glacier lower (Pratt-Sitaula, 2005)	11.66 ± 1.29		2				
23	Lyapche Glacier (Pratt-Sitaula, 2005)	11.54 ± 0.80		3	2.02			
24	LT3: Langtang Stage (Abramowski, 2004)	10.90 ± 0.43		3	0.55			
23	Syaktan Glacier (Pratt-Sitaula et al., 2011)	9.48 ± 0.91	9.5–8.7	4	3.38		8.9 ± 0.5	0
23	Danfe Glacier (Pratt-Sitaula et al., 2011)	8.87 ± 0.36		7	0.53			
23	Yak upper (Pratt-Sitaula, 2005)	8.72 ± 0.40		5	0.75			
25	M3 (Gayer et al., 2006)	7.04 ± 0.64	7.0–4.4	2			4.6 ± 0.6 and	0
23	Lete (Zech et al., 2009)	6.36 ± 1.21		1			6.2 ± 0.5	
26	Langtang glacial stage (Barnard et al., 2006)	5.47 ± 0.40		2				
26	MK4: LIA (Abramowski, 2004)	4.99 ± 0.92		4	2.83			
26	Langtang glacial stage (Barnard et al., 2006)	4.60 ± 0.33		1				
26	LT6 (Abramowski, 2004)	4.42 ± 0.15		2				
23	Neoglacial (Zech et al., 2009)	1.70 ± 0.50	~1.7 (tentative)	2		1.7 ± 0.5	?	
26	Yala I glacial stage (Barnard et al., 2006)	0.76 ± 0.20	<1 (tentative)	6	0.61	?	0.7 ± 0.1	0
23	E moraine crest (Heimsath and McGlynn, 2008)	0.55 ± 0.16		5	5.54			

[a] All local stage age uncertainties are reported in 1σ.
[b] Corrected Chi-squared values are from outlier free distribution.
[c] All regional stage age uncertainties are reported in 1σ.
[d] Kernel Density fit is performed using ksdensity function in MATLAB and using the PDF model after Dortch et al. (2013) and Murari et al. (2014).

reconstruction included our climatic zone 1a plus the Lahul and Nun Kun areas of the zone 2a, which together constitute ~52% of the total ^{10}Be ages of this study (Table 5). Due to a large number of local glacial stages, they statistically identified seven prominent *HHs*. However, in our study, we distinguished climatic zone 1a from zone 2a, and zone 1a constitutes only ~45% of the total ^{10}Be ages (Table 5). We, therefore, identified four prominent and two tentative Holocene regional glacier advances for this zone (Fig. 7). This suggests that our statistical treatment is sensitive to the number of data, especially whether the stages are prominent or tentative and/or further subdivision of regional stages may be possible if indeed they are climatically perturbed.

Climatic zone 1b: Arid and semiarid colder climatic region—southern and northeastern Tibet. The sample glaciers in this region, from the toe-to-cirque head, have a hypsometric distribution between ~4500 and 6590 m asl (Fig. S5) and ELA distribution between ~4407 and 5259 m asl (see Table 2 in Saha et al. Data in Brief).

Two prominent and two tentative regional stages are reconstructed based on only eight local glacial stages (Fig. 7). Regional glacier advances are recorded during the Lateglacial (13.5–12.9 ka; Fig. S8K), Early Holocene (11.5–9.5 ka; Fig. S8K), Mid-Holocene (~8.0 ka; Fig. S8L), and Late Holocene (~3.3 ka; Fig. S8L). The ~8.0 and ~3.3 ka regional glacial stages are tentative (n = 1; Table 5), indicating limited to insignificant glaciations during the Mid- and Late Holocene in this climatic zone.

Extensive ΔELAs are recorded in the Lateglacial (~590 ± 200 m), followed by progressively restricted glacier advances in the Holocene (ΔELAs: ~160 ± 35 m at 11.5–9.5 ka, ~170 ± 70 m at ~8.0 ka, and ~80 ± 70 m at ~3.3 ka; see Table 2 in Saha et al. Data in Brief;

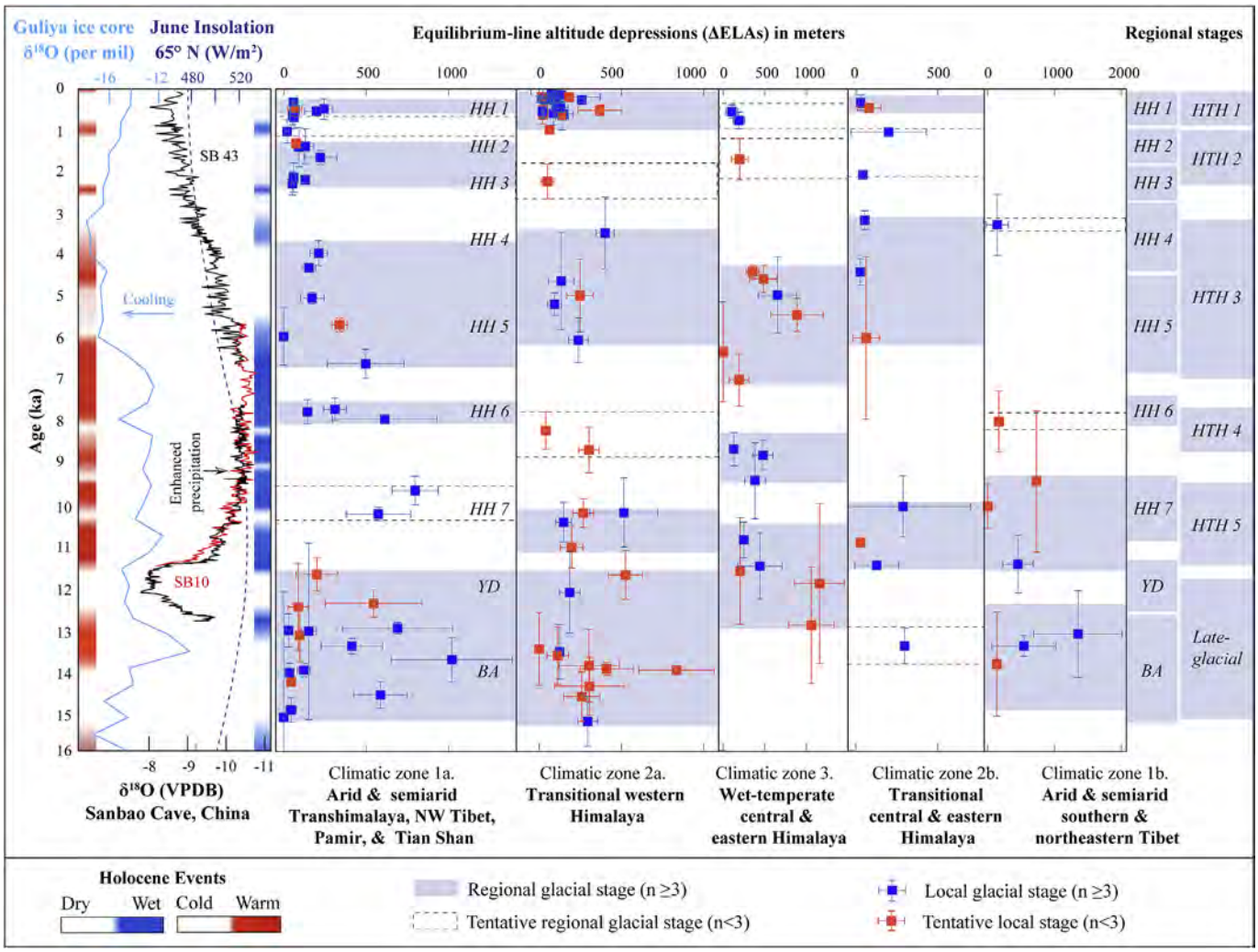

Fig. 7. Timing and amplitude of Lateglacial and Holocene regional glacier advances across the Himalayan-Tibetan orogen compared with continuous proxy records. Five climatic zones (Climate Groups 1–3) are used (see section *5.2.1*) for inter-regional comparisons. Local glacial stages (mean ^{10}Be ages in x-axis) for each region are combined (see Table 1 in Saha et al. Data in Brief) and compared against the corresponding ΔELA (in y-axis; see Table 2 in Saha et al. Data in Brief). Uncertainty bars are ±1σ. Regional Himalayan-Tibetan Holocene stages (HTHS) for the whole orogen (this study) are compared against Himalayan Holocene stages (*HHs*) reconstructed for the NW Himalaya and Tibet in Saha et al. (2018). A simplified summary of major Lateglacial-Holocene climatic events is shown by shaded blue and red bars, representing significant dry-wet and cold-warm periods, respectively. These periods are reconstructed after Demske et al. (2009), Wünnemann et al. (2010), Berkelhammer et al. (2012), Rawat et al. (2015a, 2015b), Srivastava et al. (2017). The color scheme for the red and blue bars only represents the time range and not the magnitude of the change. Reconstructed orbital trend at 65°N latitude (after Berger, 1978), oxygen isotopes from speleothems (Sanbao cave, China after Dong et al., 2010), and from Guliya ice cores (Guliya ice core, Tibet after Thompson et al., 1997) are shown at the bottom for climatic interpretation. The Sanbao cave speleothem SB10 data is shown as red and SB43 speleothem data as black. (For interpretation of the references to color in this figure legend, the reader is referred to the Web version of this article.)

Fig. 7).

Climatic zone 2a: Transitional climatic region—*western Himalaya.* We have identified two distinct hypsometric subgroups of glaciers in this region based on their average toe-to-cirque head distribution (Table 4; Fig. S5) and ELAs (see Table 2 in Saha et al. Data in Brief). There are more monsoon-influenced glaciers in the Garhwal Himalaya and transitional glaciers in the Nun Kun, Lahul, and Gurla Mandhata (Table 4; Fig. S5).

Two tentative and four major stages of regional glacier advances are identified based on 37 local advances during the Lateglacial and Holocene (Fig. 7; Table 5). Glaciers advanced extensively between 15.3 and 11.8 ka (ΔELAs 335 ± 215 m; Table 2 in Saha et al. Data in Brief; Fig. 7, S8E, S9J), becoming progressively restricted during the Early Holocene at 11.1–10.3 (ΔELAs 285 ± 165 m; Table 2 in Saha et al. Data in Brief; Fig. 7, S8E, S9K) and 8.8–8.3 ka (ΔELAs 170 ± 185 m; Table 2 in Saha et al. Data in Brief; Fig. 7 and S8F), the Mid-Holocene at 6.1–5.0 ka (ΔELAs 190 ± 85 m; Table 2 in Saha et al. Data in Brief; Fig. 7), and the Late Holocene at ~2.2 and < 1 ka in the region (ΔELAs 30 ± 10 m; Table 5; Table 2 in Saha et al. Data in Brief).

The ~2.2 ka glacier advance is tentative (local stage = 1) and hence, is not considered further (Fig. 7). The 16 local glacier advances during <1 ka, however, are highly scattered (79% OD) and bimodal (Fig. S8G). We refrain from assigning any peak stage/substages for the last 1 ka due to the possibility of a high degree of inheritance and highly scattered local glacial stages.

Climatic zone 2b: Transitional climatic region—central and eastern Himalaya. Two subgroups of glaciers are evident based on their general hypsometries (Table 4; Fig. S5) and ELAs (see Table 2 in Saha et al. Data in Brief). They include the Central Himalayan transitional glaciers (e.g., Nyalam, Khumbu, and Rongbuk) and the Eastern Himalayan transitional glaciers, e.g., Renhe, Baishui, Ganheba, and Hailuogou glaciers.

The number of reconstructed local glacial stages for this region

is limited (n = 11; Table 5). Based on the available ^{10}Be ages, three tentative (~13.5, ~2.1–1.0, and <1 ka) and two prominent (11.5–10.1 and 6.0–3.2 ka) regional glacial stages are recognized (Table 5; Fig. 7 and S8J).

The estimated ΔELAs are ~145 ± 180 m at 6.0–3.2 ka and only ~65 ± 55 m during the last 1 ka (Fig. 7). The ΔELAs during the rest of the regional stages are highly speculative and tentative (see Table 2 in Saha et al. Data in Brief).

Climatic zone 3: Wet and temperate climatic region—central and eastern Himalaya. All sample glaciers in the region have average hypsometric distribution from ~3930 to 6590 m asl (toe-to-cirque head) and ELAs of ~4440–5584 m asl (see Table 2 in Saha et al. Data in Brief), except the glacier hypsometries for a few smaller cirque glaciers (Table 4).

Two tentative and three major regional stages of glacier advances are reconstructed between the Lateglacial and the Late Holocene using 18 local glacier stages (Table 5; Fig. 7). Extensive local glacier advances are reconstructed during the Lateglacial-Early Holocene transition at 13.0–10.9 ka (ΔELAs ~625 ± 455 m; Table 2 in Saha et al. Data in Brief; Fig. 7 and S8H), followed by restricted glacier advances in the Early Holocene at 9.5–8.7 ka (6.3% age OD; ΔELAs ~330 ± 180 m; Table 2 in Saha et al. Data in Brief; Fig. 7, S8H, S9S). However, the Mid-Holocene glacier advances at 7.0–4.4 ka (age OD 9.2%; Figs. S8I, S9T) are significantly more extensive (ΔELAs ~515 ± 270 m; Table 2 in Saha et al. Data in Brief; Fig. 7) than the two tentative Late Holocene glacier advances at ~1.7 (local stage = 1) and <1 ka (local stage = 2) (ΔELAs ~150 ± 65 m; Table 5; Table 2 in Saha et al. Data in Brief; Fig. 7 and S8I) in this zone.

The overlapping Lateglacial-Early Holocene regional glacier advances (13.0–10.9 ka) could likely be a result of limited data and/or signify distinct hypsometric influences in local glacier advances to the same climatic perturbation (cf. Pratt-Sitaula et al., 2011). Late Holocene glacier advances are also poorly reconstructed for this zone, and it is, therefore, difficult to infer any climatic significance to them.

5.2.3. Past atmospheric temperature changes

The modeled past temperature change based on glacier flow modeling is better defined for ages <9.5 ka for all climate groups 1–3 (Fig. 8). For ages >9.5 ka, the number of glaciers used is very small (1–5), except for the transitional (climate group 2) and humid (climate group 3) climatic regions (Fig. 8), providing lower confidence in our model results for Lateglacial advances. Due to enhanced precipitation during the Early to Mid-Holocene relative to today (Fig. 7), we also argue that c and τ calculated using a (+) 30% increase in precipitation is probably a better representative scenario for the modeled T.

Climatic zone 1a: Arid and semiarid colder climatic region—Transhimalaya, northwest Tibet, Pamir, and Tian Shan. The reconstructed regional atmospheric temperature (a total of 24 valleys) for this zone indicates a net temperature (ΔT) change of −3.1 ± 0.1, +1.7 ± 0.2, −1.1 ± 0.2, and −2.1 ± 0.5 °C (ΔT K is expressed as ΔT °C) during 14.0–12.7, 12.7–11.7, 11.7–9.7, and 9.7–7.7 ka, respectively (Fig. 8). Our model results are tentative because there are very few suitable older local glacial stages (only 2–4 valleys) that can be used to estimate regional T for these times.

We estimated a significant ΔT increase ranging from ~1.9 (±1.1) to 6.0 (±0.7) °C for regional glacial advances between the early Mid- (8.0–7.7 ka) and Mid-to early Late Holocene (6.6–3.5 ka) (Fig. 8). During the subsequent Late Holocene regional glacial stages, i.e., ~3.5 to 2.3–1.3 ka and 2.3–1.3 to 1.0 ka, the ΔT increase is estimated to be ~1.0 ± 1.3 and ~0.5 ± 0.3 °C, respectively (Fig. 8). During the latest 1.0 to 0.2 ka regional glacial stage, however, the ΔT rise is significant in this zone (~1.4 ± 0.9 °C; Fig. 8).

Climatic zone 1b: Arid and semiarid colder climatic region—southern and northeastern Tibet. Only four glacial valleys were suitable for reconstructing regional past temperature change in this zone (Fig. 8). The best approximation of regional ΔT decrease of 0.9 ± 0.1 °C is estimated for the Early and Mid-Holocene regional glacier advances, i.e., between 10.0 and 9.5 and ~8.0 ka, respectively (Fig. 8). However, a ΔT rise ranging from ~1.9 (±1.1) to 2.7 (±0.7) °C is reconstructed between the Mid- (~8.0 ka) and Late Holocene (~3.3 ka) regional glacier advances (Fig. 8).

Climatic zone 2a: Transitional climatic region—western Himalaya. We modeled the past temperature change in this zone based on 20 glaciated valleys. The ΔT increase is estimated to be ~0.7 ± 2.9 °C between the Younger Dryas (12.7–11.8 ka) and Early Holocene (11.1–10.3 ka; Fig. 8). The ΔT increase is estimated to ~1.6 ± 0.0 °C during the two Early Holocene advances (11.1–10.3 to 8.8–8.3 ka; Fig. 8). The ΔT increase during the Early (8.8–8.3 ka) to Mid-Holocene (6.1–5.0 ka) glacier advances was ~1.2 ± 0.0 °C (Fig. 8). The ΔT rise is estimated to ~1.9 ± 0.0, ~0.7 ± 1.5, and ~0.8 ± 0.4 °C, during the three Late Holocene glacier advances in this zone at 6.1–5.0 to ~2.2 ka, ~2.2 to ~1.0 ka, and ~1.0 to 0.13 ka, respectively (Fig. 8).

Climatic zone 2b: Transitional climatic region—central and eastern Himalaya. We used seven local glacier advances to estimate the past temperature change in this zone. During the Lateglacial (~13.0 ka) and Early Holocene (11.5–10.1 ka) regional glacier advances, a ΔT increase of ~2.9 ± 2.2 °C is calculated, which is relatively higher than the ΔT increase in the transitional western Himalaya (i.e., ~1.8 ± 1.0 °C; Fig. 8). Since only 1–2 local glacial stages are used for ages >10.1 ka, the sharp fluctuation in temperature during 11.5–10.1 ka, is likely due to limited data and/or extreme scenario (Fig. 8).

The ΔT increase range from ~1.3 ± 1.3 to 2.5 ± 1.9 °C from Early (11.5–10.1 ka) to Mid-Holocene (6.0–3.2 ka) in this zone (Fig. 8). The ΔT increase is modeled to be ~0.6 ± 1.6, ~0.6 ± 0.9, and ~0.7 ± 00 °C for the subsequent three Late Holocene advances at ~3 to ~2.1, ~2.1 to ~1, and ~1 to 0.14 ka, respectively (Fig. 8).

Climatic zone 3: Wet and temperate climatic region—central and eastern Himalaya. The reconstructed temperature profile for the last 11.4 ka for this zone is based on eleven valleys. A ΔT increase of ~1.6 ± 0.0 °C is modeled between the two Early Holocene advances (11.4–10.9 and 9.5–8.7 ka) in the zone (Fig. 8). A similar ΔT increase of ~1.5 ± 0.2 °C is also estimated from the Early (9.5–8.7 ka) to Mid-Holocene (7.0–4.4 ka; Fig. 8). The ΔT increase is estimated to ~1.5 ± 0.1 °C between the Mid- (7.0–4.4 ka) and Late Holocene (~1.7 ka; Fig. 8). The ΔT increase is ~0.8 ± 0.7 °C during the last ~1.0 to 0.2 ka in this climatic zone (Fig. 8).

6. Discussion

6.1. Dating uncertainties

We rejected 125 ^{10}Be age outliers from a total age population of 519 ages in our study based on the criteria highlighted above. A large scatter in our young ages (<15 ka) is evident from the high χ^2 values (Fig. 9A). Nearly 21% of our data have $\chi^2 \leq 1$, which indicates that the limited scatter is largely a result of laboratory analytical uncertainties. The rest of the data with $\chi^2 > 1$ have a high age scattering and could be explained by geomorphic process-uncertainties (Applegate et al., 2012, 2010; Owen and Dortch, 2014). Nearly 51% of our data (Fig. 9A) display positive skewness, convex upward cumulative probability distribution, and older age tails that are likely influenced by inherited ^{10}Be (cf. Applegate et al., 2012). Recent studies on Late Holocene moraine boulders in the NW Himalaya have emphasized the problem of inherited ^{10}Be (cf. Saha et al., 2018). There are two possible ways prior exposure, often

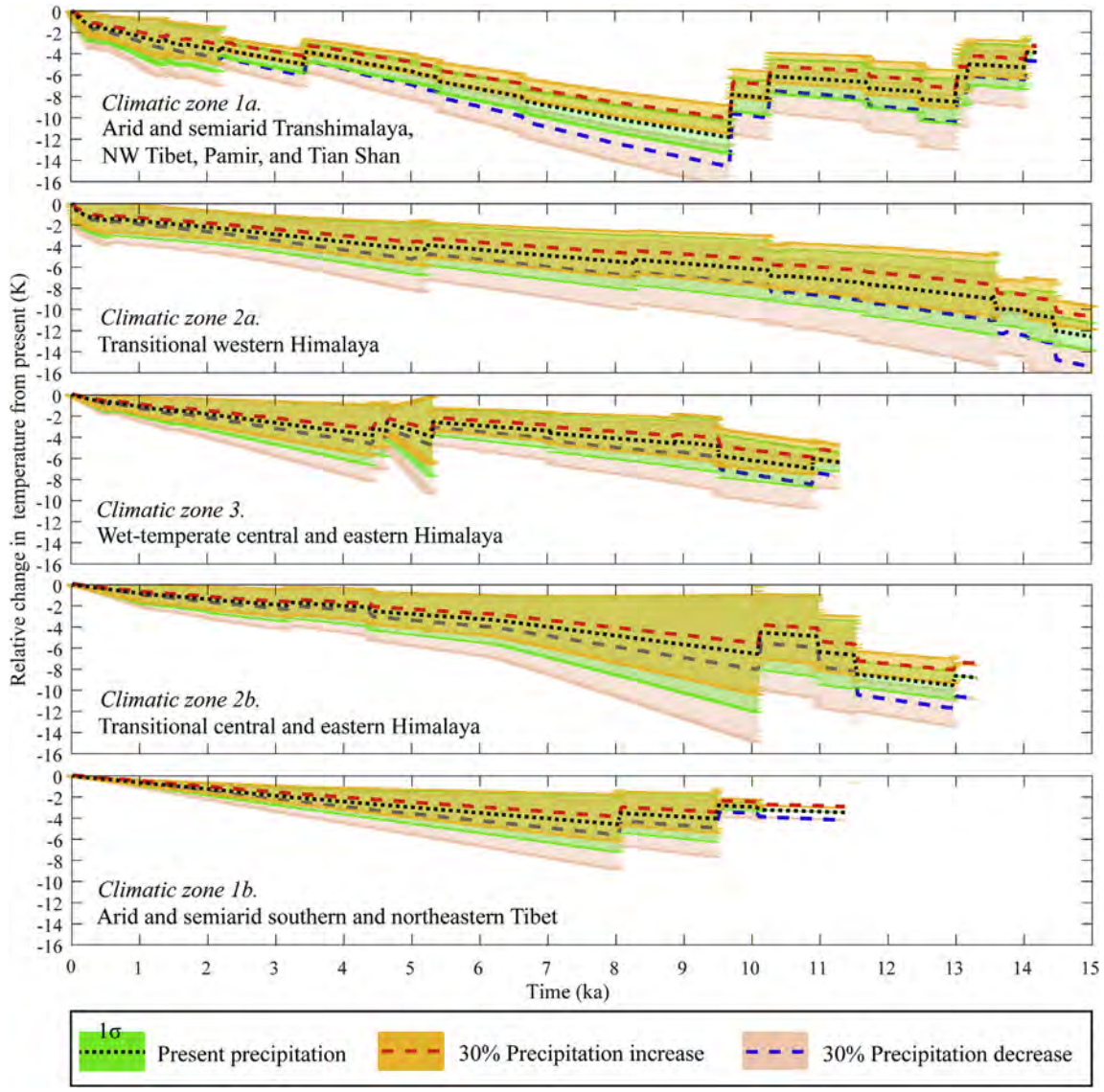

Fig. 8. Reconstructed past temperatures in different climatic zones (*1a, 1b, 2a, 2b, and 3*) using the inverse linear flow model (after Oerlemans, 2001, 2005) based on glacial records in 66 local glaciated valleys. Ages >9.5 ka have overall lower confidence due to a limited number of glaciers used. We added ±30% precipitation uncertainties to account for the errors associated with c and τ. The sharp jumps are associated with the number of data available. A large reduction in the number of modeled local glacier *T* results in a larger regional shift. Regional net temperatures (*ΔT*) are estimated after theses modeled temperature graphs. Only glacier advances are recorded using the moraine positions, and hence, the modeled *T* does not capture relative cooling. Glaciers, broadly, were more extensive in the Early Holocene and progressively more restricted over time, which also explains the gradual rise in modeled *T* profiles.

referred to as inheritance, are possible: 1) as a part of the bedrock slope system before incorporation into the glacier system (Heimsath and McGlynn, 2008); and 2) the ^{10}Be production in boulders *en transit* to deposition through the supraglacial system (Shroder et al., 2000; Ward and Anderson, 2011; Lukas et al., 2012; Gibson et al., 2017; Scherler and Egholm, 2017). Bedrock inheritance depends on several factors including, but not limited to catchment erosion rates, the stochastic rockfalls, and avalanche debris, and periglacial weathering rates (cf. Dühnforth et al., 2010; Ward and Anderson, 2011).

Inherited ages as high as 0.7–6.3 ka may be possible depending on the microclimate, tectonic and geomorphic regimes, and glacier dynamics (cf. Heimsath and McGlynn, 2008). Additional complexity may be imposed by reworking of older glacial deposits and/or rock glacier deposits especially in cold-based semiarid and arid glacier settings with low erosion rates (cf. Shroder et al., 2000; Çiner et al., 2017). Studies that use both ^{10}Be and ^{26}Al on moraines boulders in the central and eastern Tibet (Scäfer et al., 2002; Tschudi et al., 2003), Karakoram (Owen et al., 2002), and Lahul (Owen et al., 2001) have average ^{26}Al/^{10}Be ratios between ~5.5 and ~6.0:1, i.e., slightly lower than expected 6.75:1 (Balco and Shuster, 2009), and may suggest the less erosive power of cold-based glaciers. Hence, supraglacial exposure may overestimate boulder ages by as much as ~0.3–0.1 ka in cold-based glaciers in the NW Himalaya (cf. Shroder et al., 2000; Çiner et al., 2017) and ~0.9–0.05 ka in the humid glaciers in the central and eastern Himalaya (Heimsath and McGlynn, 2008; Murari et al., 2014). Alternatively, instability in young moraines, including post-depositional boulder toppling, may be responsible for a deficit in ^{10}Be concentration, often referred to as incomplete exposure (28% of the total 121 moraines; Fig. 9A), yielding apparent ages younger than the true age of the landform. Unlike LGM or older moraine boulders, this

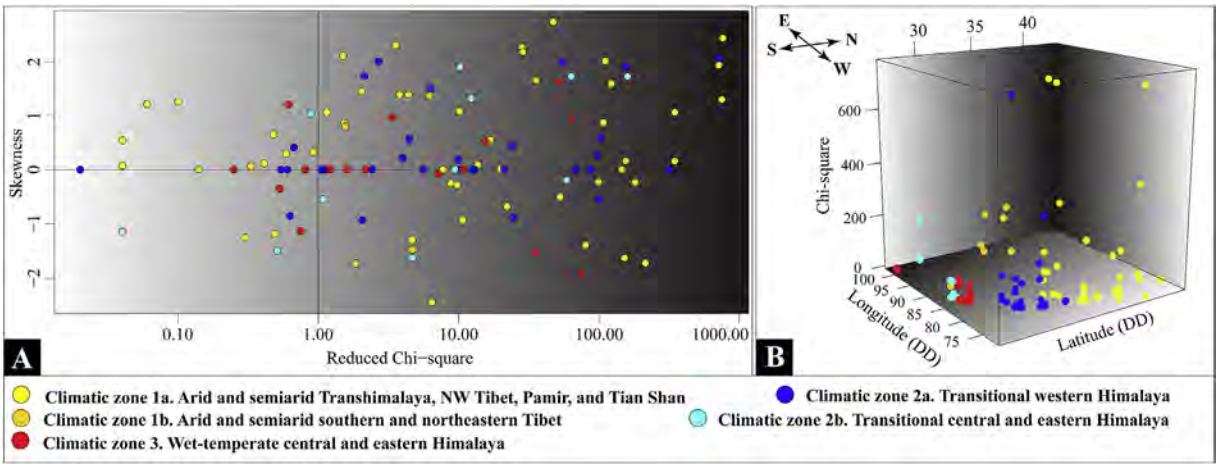

Fig. 9. Scatter diagrams showing reduced χ^2 values. A. Scatter diagram showing χ^2 and skewness distribution. Positive skewness with $\chi^2 > 1$ indicates older tail distribution (e.g., likely inheritance) and vice-versa. B. Latitudinal and longitudinal distribution of χ^2 values of 121 local glacial stages in the Himalayan-Tibetan orogen from Lateglacial to Late Holocene. More erosive glaciers in the wet-temperate and transitional central and eastern Himalaya show overall low χ^2 values compared to less erosive glaciers in the arid and semiarid regions.

undetectable perturbation on the ^{10}Be inventory can be substantial for young Holocene boulders, which systematically contributes to the high degree of scattering (Fig. 9). Any Holocene ^{10}Be chronological comparisons, therefore, should be made with extreme caution.

Additionally, inter-regional comparisons of the χ^2-values (Table 5) also suggest that more erosive temperate glaciers in the humid and transitional central and eastern Himalaya have less scatter relative to less-erosive glaciers in the arid and semiarid interior and western Tibetan Plateau, Transhimalaya, and northwestern Himalaya (Fig. 9B). Our ^{10}Be results from larger polythermal-to-temperate broad valley glaciers in the northwestern Himalaya largely indicate tight age clustering (except recent hillslope deposits on M_{K5}), and χ^2-values are within the 95% confidence interval (see Table 1 in Saha et al. Data in Brief). We, thus, argue that high-resolution Holocene chronostratigraphies may be better defined in more erosive glacier settings where geological uncertainties contributing towards inheritance are comparatively limited.

6.2. Local glacier advances

We obtained chronologies for three new ^{10}Be dated local glacier advances in the Kulti valley and one new local glacier advance in the Parkachik valley of the NW Himalaya (Fig. 5). The oldest and most extensive (ΔELA of 259 ± 109 m) local glacier advance in the Kulti valley is dated to ~14.7 ± 2.1 ka or ~12.7 ± 3.6 ka if the ~9 ka outlier is included during the Lateglacial (Fig. 5A). Coeval Lateglacial local glacier advances with similar ΔELAs (e.g., ~340 ± 61 m) are also defined in the adjacent glaciated valleys of the upper Chandra (Fig. S1A; Owen et al., 2001; Eugster et al., 2016) and the upper Yunam catchments (Saha et al., 2016), indicating catchment-wide glaciation during this period. Additionally, a few overlapping drumlins and polished bedrock (^{10}Be) ages also suggest site-specific glacier retreat during this time in the upper Chandra catchment (Fig. S1A). Glacier advances during the Lateglacial are widespread throughout the Himalayan-Tibetan orogen, and stronger summer monsoons are recorded in several glacial proxy records (Figs. 7 and 10; Owen et al., 2001, 2002; Lasserre et al., 2002; Barnard et al., 2004a; Abramowski et al., 2006; Seong et al., 2007, 2009; Schaefer et al., 2008; Röhringer et al., 2012; Wang et al., 2013; Murari et al., 2014).

A subsequent glacier advance at ~12.2 ± 1.0 ka is also recorded in the Kulti valley, which overlaps with the oldest preserved moraine (M_{K5}) age at ±1σ if the ~9 ka outlier is considered. This may likely suggest that M_{K4} is either a result of: i) a subsequent readvance (if ~9 ka is an outlier) with Sonapani glacier changed its direction, resulting in the survival of the moraine on the upslope; or ii) a recessional moraine formed during the stillstand or retreat of the glacier after the M_{K5} advance (Fig. 2A, C). We are unable to resolve this conundrum at this point with the information available to us. However, one should note that similar Early Holocene (~12.3–10.4 ka) glacier advances, with identical ΔELAs of ~180 m, are also reported in the two other valleys of the upper Chandra catchment (Figs. 5, 7 and 10; Owen et al., 2001; Saha et al., 2018). In addition, recent OSL dating of lacustrine sediments, inset within the moraines in the Miyar Valley, ~100 km downstream of the Kulti valley, indicate a glacier advance that predates ~10–8 ka (Deswal et al., 2017). An OSL dated (~9 ka) outwash terrace also indicate an Early Holocene glacier advance in the adjacent Yunam catchment (Sharma et al., 2016). Early Holocene local glacier advances/readvances are, therefore, regionally widespread and similar in amplitude and may provide more credence to the glacier readvance theory in the Lahul region (Fig. S1A). The 2.7 ± 0.2 °C ΔT increase between the Lateglacial and Early Holocene in the Kulti valley is greater (58% of the total increase) than subsequent local glacier advances. This warming may be linked to the initiation of peat accumulation near the adjacent Chandra Tal (Lake) at ~12.9 ± 0.2 ka (Owen et al., 1997, Rawat et al., 2015a, 2015b) and suggest wetter conditions. Sharma et al. (2016) proposed stronger Early Holocene monsoons as the major driving force for these widespread local glacier advances of equal amplitudes in the region.

We could not date the Rataskal terminal moraine (~6.5 km from the snout; Fig. 5A) of the Kulti valley but based on the ages of other moraines we speculate that it may have formed during the Early to Mid-Holocene.

The late Holocene glacier advance in the Kulti valley was limited in extent (ΔELA: ~106 ± 30 m; Fig. 5A) suggesting a significant change in the forcing factors from Early to Late Holocene. This is equivalent to several restricted local glacier advances at ~0.5 ± 0.2 ka in the Lahul (ΔELAs: ~57–167 m) and elsewhere in the Himalayan-Tibetan orogen (ΔELAs: ~1–370 m; Figs. 7 and 10; Saha et al., 2018 and references therein). Historical data from the Geological Survey of India (Walker and Pascoe, 1907; Owen et al.,

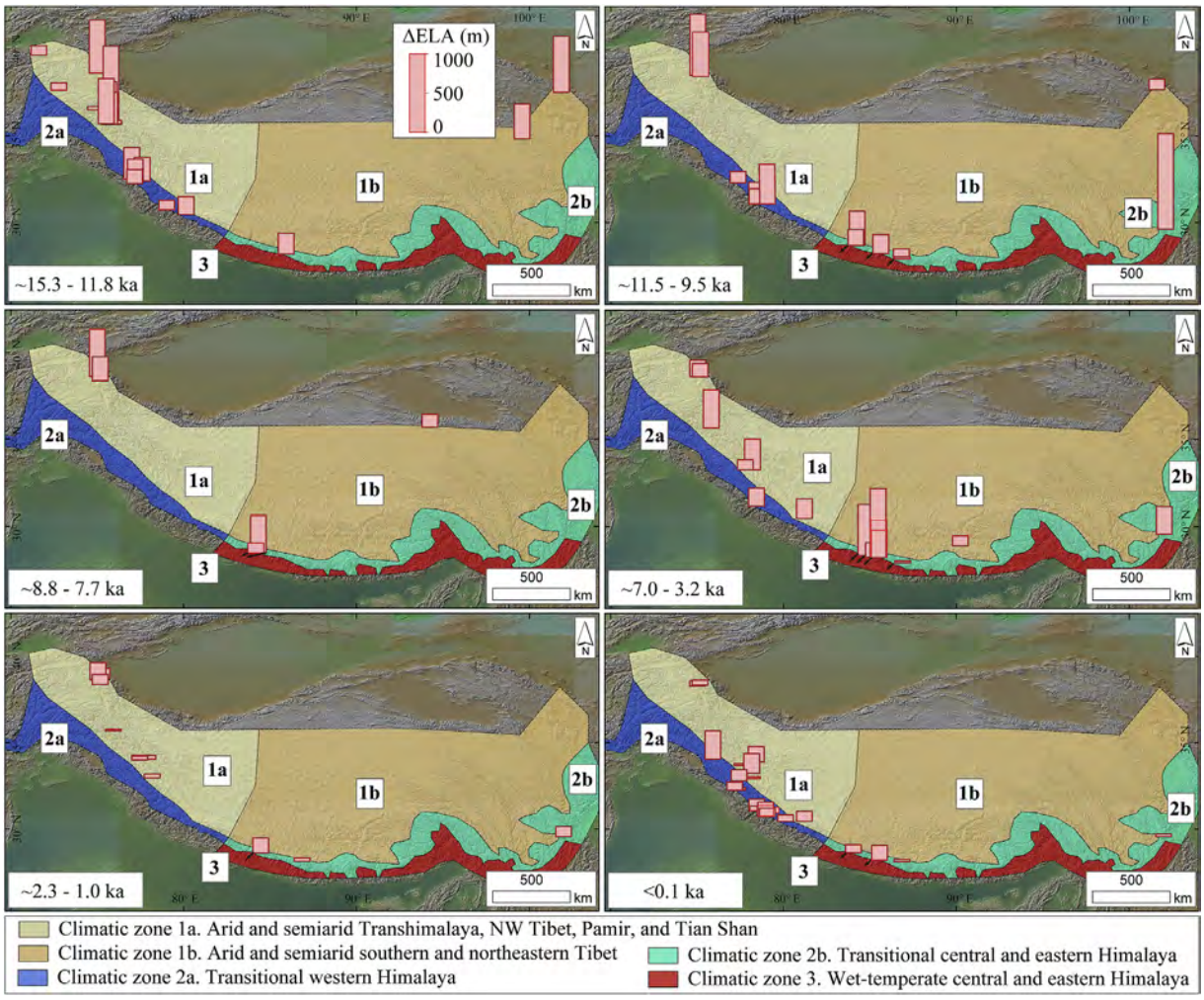

Fig. 10. Spatial distribution of ΔELAs throughout the Himalayan-Tibetan orogen during coeval regional glacier advances from Lateglacial to Late Holocene. Five climatic zones are superimposed on a hillshade map; the hillshade map is sourced from www.geomapapp.org.

1996, 1997, 2001; Raina et al., 2015) further indicates a glacier still-stand and the formation of subdued hummocky moraine complex (M_{K1}) in the Kulti valley during the late 19th Century, ~3 km from the snout of Sonapani glacier (Fig. 5A). Our dated moraine (M_{P1}) in the Parkachik valley of the Nun Kun massif also has a mean age of ~0.2 ± 0.1 ka (Fig. 5B). The Late Holocene glacier advance in the Parkachik valley, however, is relatively restricted with a ΔELA of ~20 m as compared to the Kulti valley with a ΔELA of ~95 m. This may indicate a further decline in the strength of the forcing factors northwestward. Equivalent Late Holocene glacier advances/still-stands are also historically (mapped) recorded in the Miyar valley (Harcourt, 2010; Saini et al., 2016), the upper Bhagirathi valley (Raina et al., 2015 and references therein), and dated in the adjacent Hamtah valley (Saha et al., 2018; Fig. S1). There is additional research based on ice cores, tree rings, lake sediments, and historical documents elsewhere in the orogen which further supports glacier advances during the ~18th–19th centuries (Yang et al., 2009a,b, Xu and Yi, 2014; Liang et al., 2015). We argue that the late 19th Century advance/still-stand in the region were widespread and may be distinct from the ~0.5 ka advances. Since the relative uncertainties for the dated <1 ka moraines are high and preclude from identifying regional-scale century or decadal glacier fluctuations, extensive historical evidence of a ~18th–19th century advance in the region is particularly noteworthy.

6.3. Regional glacier advances

Three major groups of glaciers (climatic groups 1–3) are identified for inter-regional Holocene chronostratigraphical comparisons (Fig. 6), which remarkably capture the orographically influenced latitudinal climatic gradient (cf. Li et al., 2017). We are unable to capture the longitudinal climatic gradient because we only used temperature and precipitation, which are largely affected by the latitudinal distribution of topography (Fig. 4). These climatic groups are, therefore, further subdivided into climatic zones 1a, 1b, 2a, 2b, and 3 for inter-regional analysis based on the available ^{10}Be-defined Holocene local glacial chronologies and influence of prevailing climatic systems.

Our modeled *T* profiles are reconstructed for a wide variety of glaciers across the entire orogen and regionally averaged to account for the limitations associated with the individual catchments (cf. Pratt-Sitaula et al., 2011). However, the model is probably not well defined for the past mass-balance effect (c and τ) of individual glaciers, because *P* increase in some areas of the western and interior Tibet was much higher (~55–200%) during the Early Holocene than present (Huth et al., 2015; Li et al., 2017; Shi et al., 2017). The actual *P* increase, therefore, may exceed our assumed ±30% change in *P* in the semi-arid and arid regions and probably suggest that the actual *T* increase was much less than our modeled

T from the Early to Mid-Holocene (Fig. 8). We also assumed a simplistic glacier advance scenario (cf. Putnam et al., 2013b) where glaciers become progressively more restricted over time, or in other words, continuous rise in *T*. The detailed geologic records of glacier fluctuations (advances and retreats) are not available for this study and hence, the model does not capture relative cooling. Additional limitations of the model include: 1) simplified energy and mass-balance relationship; 2) the influence of meteorological variables other than *T* and *P* are not considered; 3) the number of glacier length records and degree of spatiotemporal coverage varies across all the climate zones; and 4) our assumption is violated for the Mid-Holocene when *P* decrease in the semi-arid regions (climatic zone 1a) was substantial than *T*.

The model *T*, therefore, may not accurately capture the exact (absolute) changes in ambient temperature, but the sense of change (ΔT) is significant, especially when compared inter-regionally. We thus interpret the results from glacial chronologies, ΔELAs, and model *T* results to show that the long-term changes in glacier geometries have taken place differently across discrete climatic zones (1a, 1b, 2a, 2b, 3) of the orogen and likely modulated by changes in *P* during the Early to Mid-Holocene, and changes in *T* from Mid-to Late Holocene. In contrast, at the catchment scale, individual glacier hypsometries may determine the relative change in their glacier geometries during the Holocene (cf. Pratt-Sitaula et al., 2011).

Regional glacial stages across all the zones of the orogen are further simplified, and synchronous regional advances are discussed below. Based on 121 local glacial stages, we have reconstructed five inter-regional Holocene glacial stages across the orogen, that we call Himalayan-Tibetan Holocene stages (HTHS), plus a Lateglacial stage. We include the Lateglacial advance as a comparison with Holocene glacial stages below.

6.3.1. Lateglacial advance (~15.3–11.8 ka)

Extensive regional glacier advances are recorded during this time throughout the Himalayan-Tibetan orogen (Figs. 7 and 10) with regional mean ΔELAs ranging from 270 to 600 m (Figs. 7 and 10). The ΔELA uncertainties are also very high at the catchment-scale in these areas (ΔELAs 30–1020 m) due to widely variable glacier hypsometries and corresponding temperature gradient in the Transhimalaya, northwestern Tibet, Pamir, and Tian Shan (climatic zone 1a; Fig. S5). However, in general, regional glacier advances are more extensive (ΔELAs are ~100–400 m lower) in the colder arid and semiarid regions (climatic zones 1a and 1b) during this stage relative to the transitional climatic regions (climatic zones 2a and 2b; Fig. 10). We suggest that locally variable but relatively enhanced moisture supply and corresponding radiative cooling likely favored extensive Lateglacial glaciations among the arid and semiarid glaciers relative to the southerly transitional temperate glaciers. While Saha et al. (2018) identified two discrete glacial advances at this time in the northwestern Himalaya and Tibet, e.g., ~15.4–12.7 and ~12.6–11.4 ka, such distinction is not clear in the arid and semiarid northeastern Tibet (climatic zone 1a), transitional (climatic zone 2b) and wet-temperate (*zone 3*) central and eastern Himalaya due to limited robust local glacial stages (Fig. 10).

The regional glacier advances during this time likely coincide with the climatic changes associated with warm-wet Bølling-Allerød Interstadial and cold-dry Younger Dryas Stadial (Chiang et al., 2014; Denton and Broecker, 2008; Marcott et al., 2019) throughout the orogen. Evidence of widespread cooling is detected in lake records in Lahul (Rawat et al., 2015a, 2015b), Zanskar (Demske et al., 2009), the northeastern Tibet (Ji et al., 2005a; Thomas et al., 2016), and the southeastern Tibet (Kramer et al., 2010a) and further corroborate our results.

6.3.2. HTHS 5 (~11.5–9.5 ka)

Extensive Early Holocene HTHS are identified in all zones (Fig. 7). We estimated the greatest glacier extent among the moisture-sensitive glaciers of the arid and semiarid Transhimalaya, northwestern Tibet, Pamir, and Tian Shan (climatic zone 1a; Fig. 7) with an average ΔELA of ~300–400 m lower than the transitional western Himalaya (climatic zone 2a) and the wet-temperate central and eastern Himalaya (climatic zone 3). The average ΔELA is estimated to be ~400–600 m lower in the arid and semiarid Transhimalaya, northwestern Tibet, Pamir, and Tian Shan (climatic zone 1a) as compared to the transitional central Himalaya (climatic zone 2b), and the arid and semiarid northeastern Tibet (climatic zone 1b; Fig. 10). Enhanced moisture supply to the northwest of the orogen and corresponding radiative cooling possibly explain such spatial pattern of glaciation and ΔELAs (Rupper and Roe, 2008; Rupper et al., 2009). However, HTHS 5 (equivalent to HH 7 in Saha et al., 2018) consist of several tentative local glacial stages in climatic zones 1a, 1b, 2b, and 3 (Fig. 7) and require significant future improvement with additional chronologies.

Early Holocene wetter-warmer climate associated with strong summer monsoon is widely evident in several continuous proxy records in the orogen (Dong et al., 2010; Dykoski et al., 2005; Fleitmann et al., 2007, 2003; Gasse et al., 1996; Herzschuh et al., 2006; Hu et al., 2008; Hudson et al., 2016; Thompson et al., 1997; Wang et al., 2005). Sediment core records from the Arabian Sea also support wetter-colder phase during this time (Rawat et al., 2015a, 2015b; Azharuddin et al., 2017).

Our linear flow model results also indicate that the net temperature increase between the Lateglacial and HTHS 5 in the transitional central and eastern Himalaya (climatic zone 2b) is ~1.8 ± 1.0 °C higher than that of transitional western Himalaya (climatic zone 2a; Fig. 8). Comparatively greater Early Holocene warming in climatic zone 2b, therefore, is likely responsible for this restricted glaciation.

Colder but drier Early Holocene climate is evident from several lake records of the central (Ji et al., 2005a; Yanhong et al., 2006; Yu et al., 2006), eastern (Mischke and Zhang, 2010), and northeastern Tibet (Ji et al., 2005a). This relative dryness may be responsible for the subdued Early Holocene glacier advances in the arid and semiarid northeastern Tibet (climatic zone 1a; Figs. 7 and 10).

6.3.3. HTHS 4 (~8.8–7.7 ka)

Prominent regional glacier advances during this Early to Mid-Holocene transition are evident in two (climatic zones 1a and 3) and tentatively in two (climatic zones 1b and 2a) climatic regions of the orogen (Table 5; Fig. 7). This stage coincides with the ~8.2 ka abrupt climate cooling in the North Atlantic (Matero et al., 2017). Glaciers in the more westerlies-dominated arid and semiarid northwestern Tibet (climatic zone 1a) advanced extensively during this time leading to mean ΔELA ~50–400 m lower than the glaciers in the distant arid and semiarid northeastern Tibet (climatic zone 1b; Figs. 7 and 10). More moisture and colder climate teleconnected via the mid-latitudinal westerlies (Mölg et al., 2013) possibly favored high glacier activity in climatic zone 1a. Whereas, aridity in the east may be responsible for the muted glacier response in climatic zone 1b. Although our model results indicate net temperature decrease (e.g., ~2.1 ± 0.5 and ~0.9 ± 0.1 °C, respectively) in both the arid and semiarid regions between HTHS 5 and 4, given the limited data set, we are unable to confirm this cooling in the Early Holocene.

Similarly, in the more temperature-sensitive wet-temperate central Himalaya (climatic zone 3), extensive regional glaciation is recorded with average ΔELA ~90–200 m lower than the transitional western Himalaya (climatic zone 2a; Fig. 10), a pattern anticipated during large-scale ambient cooling. However, since our

HTHS 4 is tentative to absent in most of the zones, additional chronologies are needed to evaluate our results.

Lacustrine and pollen (proxy) records indicate a widespread cold-wet spell during this phase in the northwest (Wünnemann et al., 2010) and western Himalaya (Phadtare, 2000), and in the southern Tibet (Hudson et al., 2016). Similarly a cold-dry (aridity) spell prevailed in the central (Dong et al., 2010), northeast (Ji et al., 2005a, Ji et al., 2005b; Mischke and Zhang, 2010), and southeast Tibet (Kramer et al., 2010a) during this stage, which further supports our initial inferences.

6.3.4. HTHS 3 (~7.0–3.2 ka)

The glacial records in the orogen show extensive glaciation during this HTHS in the more temperature-sensitive wet-temperate central and eastern Himalayan glaciers (climatic zone 3; Fig. 10). In climatic zone 3, the mean ΔELA is 60–400 m lower than the arid and semiarid NW Tibet (climatic zone 1a) and 100–400 m lower than the transitional western (climatic zone 2a) and central and eastern Himalaya (climatic zone 2b; Fig. 7). The least glacier activities occurred in the arid and semiarid northeastern Tibet with ΔELA of only ~81 ± 71 m (climatic zone 1b; Fig. 10). Enhanced cooling, as also recorded in other proxy records (Bisht et al., 2017; Azharuddin et al., 2017; Srivastava et al., 2017), is suggested to explain such spatial pattern of glaciation across all climate zones. However, HTHS 3, in general, shows age overdispersion of 9–23% with poor chronologies for climatic zones 2b and 3. Further subdivisions (e.g., HH 5 and 4 of Saha et al., 2018 for the northwestern Himalaya; Table 5, Fig. 7), of HTHS3 across the orogen are quite possible upon additional chronological reconstructions.

The majority of the proxy records in the orogen indicate intensified warming and stronger monsoon at ~7.0–6.0 ka, followed by a decline in monsoonal strength (Phadtare, 2000; Ji et al., 2005a, Ji et al., 2005b; Wünnemann et al., 2010; Srivastava et al., 2017). An abrupt shift is detected during ~5.5–4.8 ka towards colder and drier climate over the orogen (cf. Srivastava et al., 2017). A decline in the monsoon intensity and strengthening of the mid-latitudinal westerlies associated with North Atlantic cooling are proposed for this shift (Clift et al., 2012; Leipe et al., 2014). From Early to Mid-Holocene, our model results indicate a significant ΔT increase of ~1.9–6.0 °C in climatic zone 1a (Fig. 8), whereas the ΔT rise in other regions are comparable (e.g., climatic zone 1b: ~1.9–2.7 °C, climatic zone 2b: ~1.3–2.5 °C, and climatic zone 2a: ~1.2–1.5 K; Fig. 8). This significant temperature increase modeled after glacier length in climatic zone 1a is not supported by proxy data. We speculate that part of the intensive glacier retreat since ~8 ka in climatic zone 1a (or muted response in climatic zone 1b) is associated with extreme aridity (Ji et al., 2005a, Ji et al., 2005b; Herzschuh et al., 2006; Zhu et al., 2009; Kramer et al., 2010a,b; Mischke and Zhang, 2010; Wünnemann et al., 2010; Berkelhammer et al., 2012; Huang et al., 2016; Shi et al., 2017). This also suggests that our model assumption that ambient temperature primarily drives glacier fluctuations on a continental scale is not always true at the 10^{3-4} years timescale.

6.3.5. HTHS 2 (~2.3–1.0 ka)

Mostly tentative and restricted glacier advances (ΔELAs of 21–222 m) occurred during 2.3–1.0 ka in the orogen. Saha et al. (2018) recently proposed two glacial stages (their HH 3 and 2) in the northwestern Himalaya, which encompass HTHS 2. We speculate that orogen-wide two substages (~2.3–1.7 and ~1 ka) are possible, but given the systematic inheritance for ages <2 ka and high age overdispersion, we cannot verify these individual substages. For instance, neither lake proxy records (cf. Huang et al., 2016) nor any glacier records are detected during HTHS 2 in the arid and semiarid northeastern Tibet (climatic zone 1b). Detailed Late Holocene chronological reconstructions are required to evaluate HTHS 2 and assess whether glaciers advances during this HHTS are associated with climate/non-climatic factor(s)/intrinsic climatic variability (Ji et al., 2005a; Ji et al., 2005b; Phadtare, 2000; Srivastava et al., 2017; Wünnemann et al., 2010).

6.3.6. HTHS 1 (<1 ka)

Approximately 30 local glacier stages (25%) have exposure ages <1.0 ka. We are unable to define any substages for this period due to high age overdispersion (18–79%) likely due to inheritance. Individual glacier advances including the Little Ice Age (LIA) can be reconstructed at the catchment-scale (see section 6.2), but at the regional-scale large uncertainties preclude from further analysis.

The extent of glaciation for HTHS 1 is generally very restricted across all climate zones (average ΔELA ~100–150 m; Fig. 10). High-glacier amplitudes are evident in the wet-temperate central Himalaya (climatic zone 3) with mean ΔELAs of ~40–100, ~50–100, and ~90–150 m and are lower than the transitional western Himalaya (climatic zone 2a), the arid and semiarid Transhimalaya, northwestern Tibet, Pamir, and Tian Shan (climatic zone 1a), and the transitional central and eastern Himalaya, respectively (climatic zone 2b; Fig. 10).

ΔT increase is approximately identical (~0.8 °C) in all zones of the orogen (Fig. 8) from ~1.0 to 0.2 ka, except in *zone 1a* where the ΔT rise is ~1.4 ± 0.9 °C (Fig. 8).

We suggest possible cold-dry climate in the arid and semiarid northwestern Tibet, and cold-wet climate in the Transhimalaya and transitional western Himalaya based on the spatial distribution of ΔELAs and ΔT for this period. Proxy records also corroborate this spatially distinct general climate pattern (Liu and Thompson, 1998; Phadtare, 2000; Srivastava et al., 2017; Thompson et al., 1997; Wünnemann et al., 2010; Singh et al., 2019).

7. Global Holocene glacial signal

Our regional glacial chronostratigraphical reconstruction indicates one Lateglacial, and at least five synchronous HTHSs. Additional substages may also be possible for some regions where ^{10}Be glacial chronologies are sufficient and widespread (cf. Saha et al., 2018). We herein add to initial Holocene glacial chronostratigraphical reconstructions of Saha et al. (2018) and provide a detailed orogen-wide inter-regional pattern of Holocene glaciation. Detailed studies of ΔELA suggest overall high glacial amplitude in the Lateglacial and Early Holocene, which coincide with the northerly shift of Earth's thermal equator (ITCZ) and increased monsoonal precipitation (Dykoski et al., 2005; Jennerjahn et al., 2004; Lea et al., 2003; Severinghaus et al., 2009; Wang et al., 2001, 2004), as well as abrupt North Atlantic cooling during the Younger Dryas Stadial and at ~8.2 ka (Denton and Broecker, 2008; Matero et al., 2017). Corresponding Early Holocene (~11.5–9.5 and ~8.8–7.7 ka) extensive glacier advances are also identified in the glacial records of the European Alps (Moran et al., 2016, 2015; Schimmelpfennig et al., 2014, 2012; Schindelwig et al., 2012), Greenland (O'Hara et al., 2017), Arctic Canada (Young et al., 2012), Svalbard (Van der Bilt et al., 2015), tropical Andes, Africa, and Southern Hemispheric extratropical regions (Solomina et al., 2015; 2016 and references therein).

Progressively restricted glacier advances over time are evident in subsequent glacier advances in the orogen (Figs. 7–9). A considerable Mid-Holocene regional glacier retreat is apparent in the arid and semiarid regions and supports a major shift towards extreme aridity in the orogen (Fig. 8). Subsequent Late Holocene glacier advances, including during the LIA, were accordingly restricted (Fig. 9). These changes are attributed to reduced northern hemisphere insolation and corresponding north Atlantic cooling

(Chiang et al., 2014; Denton and Broecker, 2008; Lund et al., 2006). The enhanced mid-latitude westerly winds likely teleconnected the Late Holocene cooling events in the Himalayan-Tibetan orogen (Mölg et al., 2014; Srivastava et al., 2017; Yancheva et al., 2007).

Overall, our study reinforces the view of Saha et al. (2018) that the orbital forcing primarily modulates the long-term pattern of Holocene glaciation in the Himalayan-Tibetan orogen. The relative strength/weakness of both summer monsoon and mid-latitude westerlies, that are teleconnected to the north Atlantic oceanic-atmospheric changes (Ivanochko et al., 2005; Goswami et al., 2006; Rajeevan and Sridhar, 2008; Deplazes et al., 2014; He et al., 2017; Kakade and Kulkarni, 2017), on the other hand, determine the amplitude of short-term Holocene glacier advances in different regions of the orogen as highlighted by the HTHSs. Precipitation changes played a major role in forcing glaciation throughout the Holocene and will likely contribute significantly to future cryospheric changes in this alpine environment.

8. Conclusions

Our geomorphic mapping, cosmogenic ^{10}Be surface exposure dating, ELAs, glacial hypsometry, and inverse linear flow model approach yielded the following conclusions:

i. The Kulti valley in the Lahul Himalaya and the Parkachik valley in Nun Kun massif, located in the transitional northwestern Himalaya, had relatively large (>10-km-long) and broad polythermal-to-temperate valley glaciers that produced a series of young moraines during the late Quaternary. Three sets of morphostratigraphically distinct moraines in the Kulti valley are dated to ~14.7 or ~12.7 (M_{K5}), ~12.2 (M_{K4}), and ~0.5 ka (M_{K2}), whereas the youngest moraine complex (M_{K1}) is historically dated to the late 19th Century. The ΔELA was 259 ± 109 m during the Lateglacial in the Kulti valley. The glacier cover became progressively less throughout the Holocene. The modeled ΔT increase in the valley is maximum (58% of the total increase) between the Lateglacial and Early Holocene.

ii. Parkachik glacier in the Parkachik valley of the Nun Kun massif advanced at ~0.2 ka (M_{P1}) with restricted ΔELA of $\sim 92 \pm 31$ m. Based on our analysis and dating results, it is evident that high-resolution Holocene chronostratigraphies may be better reconstructed in more erosive glacier settings where geological uncertainties are comparatively limited.

iii. Initially, five climate groups (1–5) of glaciers with comparable climatic characteristics are identified in our study using CA. Further refinement by PCA indicates climate groups 4 and 5 are either overlapping or are small end members and hence are not considered for further comparisons. Three major climate groups (1–3), however, are used for inter-regional comparisons. These climate groups include: 1) climatic zone 1a - arid and semiarid Transhimalaya, northwestern Tibet, Pamir, and Tian Shan, and climatic zone 1b - arid and semiarid southern and northeastern Tibet; 2) climatic zone 2a - transitional western Himalaya, and climatic zone 2b - transitional central and eastern Himalaya; and 3) climatic zone 3 - wet-temperate central and eastern Himalaya.

Our PCA vectors and sensitivity analyses confirm that most of the Himalayan-Tibetan glaciers are highly susceptible to changes in precipitation at the regional scale. The pronounced north-south and east-west climatic transacts, mainly for precipitation, therefore, probably control the large-scale variability of contemporary and Holocene glacial extents across the orogen. In contrast, at the catchment-scale, glacial hypsometries likely play a crucial role. This observation must be reconciled with future glacier-climate models to quantify variable glacier responses to identical climatic perturbation.

iv. Building on the work of Saha et al. (2018) who identified seven prominent Himalayan Holocene stages (HHs) for the NW Himalaya and Tibet and using 121 local glacial stages, we reconstructed regional glacial stages from the Lateglacial to Late Holocene in five discrete zones (1a,b, 2a,b, and 3) across the orogen (Fig. 10). These are assigned to: 15.2–11.7, 10.3–9.7, 8.0–7.7, 6.6–3.5, 2.3–1.3, ~1, and <1 ka in climatic zone 1a; 13.5–12.9, 11.5–9.5, ~8.0 and ~3.3 ka in climatic zone 1b; 15.3–11.8, 11.1–10.3, 8.8–8.3, 6.1–5.0, ~2.2 and < 1 ka in climatic zone 2a; ~13.5, 11.5–10.1, 6.0–3.2, ~2.1–1.0, and <1 ka in climatic zone 2b; and ~13.0–10.9, 9.5–8.7, 7.0–4.4, ~1.7, and <1 ka in climatic zone 3. Our regional synthesis shows at least five inter-regional Himalayan-Tibetan Holocene stages (HTHS) and a Lateglacial stage across the orogen.

v. The spatial distribution of ΔELAs in the orogen during ~15.3–11.8 ka shows locally variable but relatively enhanced monsoonal moisture supply and amplified cooling in climatic zones 1a and 1b (Fig. 10A).

The enhanced ISM during the Early Holocene at ~11.5–9.5 ka may also result in relatively extensive glacier advances in climatic zone 1a (Fig. 10), whereas higher net temperature increase between the Lateglacial and Early Holocene advances in climatic zone 2b may be responsible for its comparatively subdued response during the Early Holocene relative to climatic zone 2a.

The subsequent glacier advances during ~8.8–7.7 ka suggest wet-cold climate in climatic zone 1a, enhanced cooling in the climatic zone 3, and extreme aridity in climatic zone 1b (Fig. 10). During the Mid-Holocene at ~7.0–3.2 ka the regional glacier advances were forced by intensified cooling in climatic zone 3 (Fig. 10). The significant modeled net temperature increases in climatic zones 1a and 1b, from Early to Mid-Holocene, however, suggests extreme aridity in these regions.

The overall cold-dry climate is detected in ΔELAs and modeled temperature in the (tentative) Late Holocene regional glacier advances in the orogen during ~2.3–1.0 ka. Between the last 1.0 and 0.2 ka, we suggest possible cold-dry climate in climatic zone 1a, and cold-wet climate in climatic zone 2a (Fig. 10). The net temperature increase in the last 1 ka is remarkably identical (~0.8 °C) in all the zones of the orogen.

vi. Overall, ^{10}Be, ΔELAs and ΔT show a major regional shift in the relative strength of the prevailing climate systems in the orogen during the Mid- and Late Holocene transition. Generally, enhanced monsoonal humidity is likely replaced by relative cooling and aridity driven by forcing due to North Atlantic climate change teleconnected by mid-latitude westerlies. Northerly sub-polar-type glaciers in the orogen are more affected during this latter part of Mid- and the early part of the Late Holocene than the southerly temperate glaciers in the orogen. We, therefore, reinforce the concept of long-term orbitally influenced Holocene glaciation in the Himalayan-Tibetan orogen, and that changes in strength/influence of summer monsoon and mid-latitude westerlies determine the amplitude of short-term Holocene glacier advances in different regions of the orogen.

Acknowledgments

We thank Professor Yeong B. Seong and David J. Evans for

reviewing our work and providing constructive comments to improve the quality of the manuscript. The current project was funded by the SEED grant of PRIME laboratory, Purdue University, United States to AMS measure ^{10}Be samples. SS, LAO and ENO thank the Department of Geology at the University of Cincinnati, United States for fieldwork support. SS acknowledges support from the Geological Society of America for Graduate Student Research Grant and the Graduate Student Governance Association of the University of Cincinnati for Research Fellowship to conduct fieldwork. Sincere thanks Jawaharlal Nehru University, India for organizational support during part of the fieldwork. Statistical computation is done using the supercomputer facility of the Ohio Supercomputer Center (OSC, 1987; https://www.osc.edu/). SS also thanks to Dr. Patrick Applegate for his constructive comments on the liner flow model and Dr. Jason Dortch for providing the MATLAB script for the Probability-based (Kernal density fit) Cosmogenic Age Analysis Tool (P-CAAT).

Appendix A. Supplementary data

Supplementary data to this article can be found online at https://doi.org/10.1016/j.quascirev.2019.07.021.

References

Abramowski, D., 2004. Exposure Dating of Erratic Boulders in the Reconstruction of the Late Pleistocene Glaciation History of Mountainous Regions, with Examples from Nepal and Central Asia. Dissertation, University of Bayreuth, Bayreuth, p. 185.

Abramowski, U., Bergau, A., Seebach, D., Zech, R., Glaser, B., Sosin, P., Kubik, P.W., Zech, W., 2006. Pleistocene glaciations of Central Asia: results from ^{10}Be surface exposure ages of erratic boulders from the Pamir (Tajikistan), and the Alay–Turkestan range (Kyrgyzstan). Quat. Sci. Rev. 25, 1080–1096.

Anderson, L.S., Roe, G.H., Anderson, R.S., 2014. The effects of interannual climate variability on the moraine record. Geology 42, 55–58.

Applegate, P.J., Urban, N.M., Laabs, B.J.C., Keller, K., Alley, R.B., 2010. Modelling the statistical distributions of cosmogenic exposure dates from moraines. Geosci. Model Dev. 3, 293–307.

Applegate, P.J., Urban, N.M., Keller, K., Lowell, T.V., Laabs, B.J.C., Kelly, M.A., Alley, R.B., 2012. Improved moraine age interpretations through explicit matching of geomorphic process models to cosmogenic nuclide measurements from single landforms. Quat. Res. 77, 293–304.

Azam, M.F., Wagnon, P., Vincent, C., Ramanathan, A., Favier, V., Mandal, A., Pottakkal, J.G., 2014. Processes governing the mass balance of Chhota Shigri Glacier (western Himalaya, India) assessed by point-scale surface energy balance measurements. Cryosphere 8, 2195–2217.

Azharuddin, S., Govil, P., Singh, A.D., Mishra, R., Agrawal, S., Tiwari, A.K., Kumar, K., 2017. Monsoon-influenced variations in productivity and lithogenic flux along offshore Saurashtra, NE Arabian Sea during the Holocene and Younger Dryas: a multi-proxy approach. Palaeogeogr. Palaeoclimatol. Palaeoecol. 483, 136–146.

Bahuguna, I.M., Rathore, B.P., Brahmbhatt, R., Sharma, M., Dhar, S., Randhawa, S.S., Kumar, K., Romshoo, S., Shah, R.D., Ganjoo, R.K., Ajai, 2014. Are the Himalayan glaciers retreating? Curr. Sci. 106, 1008–1013.

Balco, G., Shuster, D.L., 2009. ^{26}Al–^{10}Be–^{21}Ne burial dating. Earth Planet. Sci. Lett. 286, 570–575.

Balco, G., Stone, J.O., Lifton, N.A., Dunai, T.J., 2008. A complete and easily accessible means of calculating surface exposure ages or erosion rates from ^{10}Be and ^{26}Al measurements. Quat. Geochronol. 3, 174–195.

Barker, T., 2007. Climate change 2007: an assessment of the intergovernmental panel on climate change. Change Synth. Rep. 446, 12–17.

Barnard, P.L., Owen, L.A., Finkel, R.C., 2004a. Style and timing of glacial and paraglacial sedimentation in a monsoon-influenced high Himalayan environment, the upper Bhagirathi Valley, Garhwal Himalaya. Sediment. Geol. 165, 199–221.

Barnard, P.L., Owen, L.A., Sharma, M.C., Finkel, R.C., 2004b. Late quaternary (Holocene) landscape evolution of a monsoon-influenced high Himalayan valley, Gori Ganga, Nanda Devi, NE Garhwal. Geomorphology 61, 91–110.

Barnard, P.L., Owen, L.A., Finkel, R.C., 2006. Quaternary fans and terraces in the Khumbu Himal south of Mount Everest: their characteristics, age and formation. J. Geol. Soc. Lond. 163, 383–399.

Barr, I.D., Lovell, H., 2014. A review of topographic controls on moraine distribution. Geomorphology 226, 44–64.

Benn, D.I., Evans, D.J.A., 2010. Glaciers and Glaciation, second ed. Routledge, p. 817.

Benn, D.I., Owen, L.A., 1998. The role of the Indian summer monsoon and the mid-latitude westerlies in Himalayan glaciation: review and speculative discussion. J. Geol. Soc. Lond. 155, 353–363.

Benn, D.I., Owen, L.A., 2002. Himalayan glacial sedimentary environments: a framework for reconstructing and dating the former extent of glaciers in high mountains, 98, 3–25.

Benn, D.I., Owen, L.A., Osmaston, H.A., Seltzer, G.O., Porter, S.C., Mark, B., 2005. Reconstruction of equilibrium-line altitudes for tropical and sub-tropical glaciers. Quat. Int. 138–139, 8–21.

Berger, A.L., 1978. Long-term variations of caloric insolation from the Earth's orbital elements. Quat. Res. 9, 139–167.

Berkelhammer, M., Sinha, A., Stott, L., Cheng, H., Pausata, F.S.R., Yoshimura, K., 2012. An abrupt shift in the Indian monsoon 4, 000 years ago an abrupt shift in the Indian monsoon 4000 Years ago. In: Giosan, L., et al. (Eds.), Climates, Landscapes, and Civilizations, Geophys. Monogr. Ser., vol. 198. AGU, Washington, D. C., pp. 75–87. https://doi.org/10.1029/2012GM001207_(88H)

Bhambri, R., Bolch, T., Chaujar, R.K., Kulshreshtha, S.C., 2011. Glacier changes in the Garhwal Himalaya, India, from 1968 to 2006 based on remote sensing. J. Glaciol. 57, 543–556.

Bhambri, R., Hewitt, K., Kawishwar, P., Pratap, B., 2017. Surge-type and surge-modified glaciers in the Karakoram. Sci. Rep. 7, 1–14.

Bhargava, O.N., 2008. An updated introduction to the Spiti geology. J. Palaeontol. Soc. India 53, 113–129.

Bisht, P., Nawaz Ali, S., Rana, N., Singh, S., Sundriyal, Y.P., Bagri, D.S., Juyal, N., 2017. Pattern of Holocene glaciation in the monsoon-dominated Kosa valley, central Himalaya, Uttarakhand, India. Geomorphology 284, 130–141.

Blomdin, R., Stroeven, A.P., Harbor, J.M., Lifton, N.A., Heyman, J., Gribenski, N., Petrakov, D.A., Caffee, M.W., Ivanov, M.N., Hättestrand, C., Rogozhina, I., Usubaliev, R., 2016. Evaluating the timing of former glacier expansions in the Tian Shan: a key step towards robust spatial correlations. Quat. Sci. Rev. 153, 78–96.

Bolch, T., Kulkarni, A., Kaab, A., Huggel, C., Paul, F., Cogley, J.G., Frey, H., Kargel, J.S., Fujita, K., Scheel, M., Bajracharya, S., Stoffel, M., 2012. The state and fate of Himalayan glaciers. Science 80 (336), 310–314.

Bookhagen, B., Burbank, D.W., 2006. Topography, relief, and TRMM-derived rainfall variations along the Himalaya. Geophys. Res. Lett. 33, L08405.

Borchers, B., Marrero, S., Balco, G., Caffee, M., Goehring, B., Lifton, N., Nishiizumi, K., Phillips, F., Schaefer, J., Stone, J., 2016. Geological calibration of spallation production rates in the CRONUS-Earth project. Quat. Geochronol. 31, 188–198.

Brun, F., Berthier, E., Wagnon, P., Kääb, A., Treichler, D., 2017. A spatially resolved estimate of High Mountain Asia glacier mass balances from 2000 to 2016. Nat. Geosci. 10, 668–673.

Burbank, D.W., Bookhagen, B., Gabet, E.J., Putkonen, J., 2012. Modern climate and erosion in the Himalaya. Compt. Rendus Geosci. 344, 610–626.

Carr, S.J., Lukas, S., Mills, S.C., 2010. Glacier reconstruction and mass-balance modelling as a geomorphic and palaeoclimatic tool. Earth Surf. Process. Landforms 35, 1103–1115.

Chand, P., Sharma, M.C., Bhambri, R., Sangewar, C.V., Juyal, N., 2017. Reconstructing the pattern of the Bara Shigri glacier fluctuation since the end of the Little ice age, Chandra valley, north-western Himalaya. Prog. Phys. Geogr. 41, 643–675.

Chiang, J.C.H., Lee, S.Y., Putnam, A.E., Wang, X., 2014. South Pacific Split Jet, ITCZ shifts, and atmospheric North-South linkages during abrupt climate changes of the last glacial period. Earth Planet. Sci. Lett. 406, 233–246.

Çiner, A., Sarıkaya, M.A., Yıldırım, C., 2017. Misleading old age on a young landform? The dilemma of cosmogenic inheritance in surface exposure dating: moraines vs. rock glaciers. Quat. Geochronol. 42, 76–88.

Clark, P.U., Dyke, A.S., Shakun, J.D., Carlson, A.E., Clark, J., Wohlfarth, B., Mitrovica, J.X., Hostetler, S.W., McCabe, A.M., 2009. The last glacial maximum. Science 325, 710–714.

Clift, P.D., Carter, A., Giosan, L., Durcan, J., Duller, G.A.T., Macklin, M.G., Alizai, A., Tabrez, A.R., Danish, M., VanLaningham, S., Fuller, D.Q., 2012. U-Pb zircon dating evidence for a Pleistocene Sarasvati river and capture of the Yamuna river. Geology 40, 211–214.

Cogley, J.G., Kargel, J.S., Kaser, G., van der Veen, C.J., 2010. Tracking the source of glacier misinformation. Science 327, 522.

Cohen, J., Saito, K., Entekhabi, D., 2001. The role of the Siberian high in northern hemisphere climate variability. Geophys. Res. Lett. 28, 299–302.

Damm, B., 2006. Late Quaternary glacier advances in the upper catchment area of the Indus river (Ladakh and western Tibet). Quat. Int. 154–155, 87–99.

Demske, D., Tarasov, P.E., Wünnemann, B., Riedel, F., 2009. Late glacial and Holocene vegetation , Indian monsoon and westerly circulation in the Trans-Himalaya recorded in the lacustrine pollen sequence from Tso Kar. Palaeogeogr. Palaeoclimatol. Palaeoecol. 279, 172–185.

Denton, G.H., Broecker, W.S., 2008. Wobbly ocean conveyor circulation during the Holocene? Quat. Sci. Rev. 27, 1939–1950.

Deplazes, G., Lückge, A., Stuut, J.B.W., Pätzold, J., Kuhlmann, H., Husson, D., Fant, M., Haug, G.H., 2014. Weakening and strengthening of the Indian monsoon during Heinrich events and Dansgaard-Oeschger oscillations. Paleoceanography 29, 99–114.

Derbyshire, E., Shi, Y., Li, J., Zheng, B., Li, S., Wang, J., 1991. Quaternary glaciation of Tibet: the geological evidence. Quat. Sci. Rev. 10, 485–510.

Deswal, S., Sharma, M.C., Saini, R., Chand, P., Juyal, N., Singh, I., Srivastava, P., Ajai, Bahuguna, I.M., 2017. Late Holocene glacier dynamics in the Miyar basin, Lahaul Himalaya, India. Geosciences 7, 1–23.

Dong, J., Wang, Y., Cheng, H., Hardt, B., Edwards, R.L., Kong, X., Wu, J., Chen, S., Liu, D., Jiang, X., Zhao, K., 2010. A high-resolution stalagmite record of the Holocene East Asian monsoon from Mt Shennongjia, central China. Holocene 20, 257–264.

Dortch, J.M., Owen, L.A., Caffee, M.W., 2013. Timing and climatic drivers for glaciation across semi-arid western Himalayan–Tibetan orogen. Quat. Sci. Rev. 78,

188–208.
Dühnforth, M., Anderson, R.S., Ward, D., Stock, G.M., 2010. Bedrock fracture control of glacial erosion processes and rates. Geology 38, 423–426.
Dunai, T.J., 2010. Cosmogenic Nuclides: Principles, Concepts and Applications in the Earth Surface Sciences. Cambridge Univ. Press, Cambridge.
Duncan, C., Masek, J., Fielding, E., 2003. How steep are the Himalaya? Characteristics and implications of along-strike topographic variations. Geology 31, 75–78.
Dykoski, C.A., Edwards, R.L., Cheng, H., Yuan, D., Cai, Y., Zhang, M., Lin, Y., Qing, J., An, Z., Revenaugh, J., 2005. A high-resolution, absolute-dated Holocene and deglacial Asian monsoon record from Dongge Cave, China. Earth Planet. Sci. Lett. 233, 71–86.
Eaves, S.R., Mackintosh, A.N., Anderson, B.M., Doughty, A.M., Townsend, D.B., Conway, C.E., Winckler, G., Schaefer, J.M., Leonard, G.S., Calvert, A.T., 2016. The last glacial maximum in the central north island, New Zealand: palaeoclimate inferences from glacier modelling. Clim. Past 12, 943–960.
Eugster, P., Scherler, D., Thiede, R.C., Codilean, A.T., Strecker, M.R., 2016. Rapid last glacial maximum deglaciation in the Indian Himalaya coeval with mid-latitude glaciers: new insights from ^{10}Be-dating of ice-polished bedrock surfaces in the Chandra Valley, NW Himalaya. Geophys. Res. Lett. 43, 1589–1597.
Evans, D.J.A., 2003. Glacial Landsystems. Arnold, London, p. 532.
Farinotti, D., Huss, M., Fürst, J.J., Landmann, J., Machguth, H., Maussion, F., Pandit, A., 2019. A consensus estimate for the ice thickness distribution of all glaciers on Earth. Nat. Geosci. https://doi.org/10.1038/s41561-019-0300-3.
Fielding, E., Isacks, B., Barazangi, M., Duncan, C., 1994. How flat is Tibet? Geology 22, 163–167.
Finkel, R.C., Owen, L.A., Barnard, P.L., Caffee, M.W., 2003. Beryllium-10 dating of Mount Everest moraines indicates a strong monsoon influence and glacial synchroneity throughout the Himalaya. Geology 31, 561–564.
Fleitmann, D., Burns, S.J., Mudelsee, M., Neff, U., Kramers, J., Mangini, A., Matter, A., 2003. Holocene forcing of the Indian monsoon recorded in a stalagmite from southern Oman. Science 80 (300), 1737–1739.
Fleitmann, D., Burns, S.J., Mangini, A., Mudelsee, M., Kramers, J., Villa, I., Neff, U., Al-Subbary, A.A., Buettner, A., Hippler, D., Matter, A., 2007. Holocene ITCZ and Indian monsoon dynamics recorded in stalagmites from Oman and Yemen (Socotra). Quat. Sci. Rev. 26, 170–188.
Galbraith, R., Roberts, R., Laslett, G., Yoshida, H., Olley, J., 1999. Optical dating of single and multiple grains of quartz from Jinmium rock shelter, northern Australia: Part I, experimental design and statistical models. Archaeometry 41, 339–364.
Gasse, F., Fontes, J.C., Campo, E. Van, Wei, K., 1996. Holocene environmental changes in Bangong Co basin (western Tibet). Part 4 Discuss. Conclus. 120, 79–92.
Gayer, E., Lavé, J., Pik, R., France-Lanord, C., 2006. Monsoonal forcing of Holocene glacier fluctuations in Ganesh Himal (Central Nepal) constrained by cosmogenic ^{3}He exposure ages of garnets. Earth Planet. Sci. Lett. 252, 275–288.
Gibbons, A.B., Megeath, J.D., Pierce, K.L., 1984. Probability of moraine survival in a succession of glacial advances. Geology 12, 327–330.
Gibson, M.J., Glasser, N.F., Quincey, D.J., Mayer, C., Rowan, A.V., Irvine-Fynn, T.D.L., 2017. Temporal variations in supraglacial debris distribution on Baltoro Glacier, Karakoram between 2001 and 2012. Geomorphology 295, 572–585.
Gosse, J.C., 2005. The contributions of cosmogenic nuclides to unraveling alpine paleo-glacier histories. In: Huber, U.M., et al. (Eds.), Global Change and Mountain Regions, An Overview of Current Knowledge: Advances in Global Change Research, vol. 23. Springer, Dordrecht, pp. 39–50.
Goswami, B.N., Madhusoodanan, M.S., Neema, C.P., Sengupta, D., 2006. A physical mechanism for North Atlantic SST influence on the Indian summer monsoon. Geophys. Res. Lett. 33, 1–4. https://doi.org/10.1029/2005GL024803.
Guérin, G., Combès, B., Lahaye, C., Thomsen, K.J., Tribolo, C., Urbanova, P., Guibert, P., Mercier, N., Valladas, H., 2015. Testing the accuracy of a Bayesian central-dose model for single-grain OSL, using known-age samples. Radiat. Meas. 81, 62–70.
Harcourt, A.F., 2010. Geographical society, B. B. and publishing. On the Himalayan valleys: Kooloo, Lahoul, and Spiti. J. R. Geogr. Soc. 41 (1871), 245–257.
He, S., Gao, Y., Li, F., Wang, H., He, Y., 2017. Impact of Arctic oscillation on the east Asian climate: a review. Earth Sci. Rev. 164, 48–62.
Hedrick, K. a., Seong, Y.B., Owen, L.A., Caffee, M.W., Dietsch, C., 2011. Towards defining the transition in style and timing of Quaternary glaciation between the monsoon-influenced Greater Himalaya and the semi-arid Transhimalaya of Northern India. Quat. Int. 236, 21–33.
Heimsath, A.M., McGlynn, R., 2008. Quantifying periglacial erosion in the Nepal high Himalaya. Geomorphology 97, 5–23.
Herzschuh, U., Winter, K., Wünnemann, B., Li, S., 2006. A general cooling trend on the central Tibetan Plateau throughout the Holocene recorded by the Lake Zigetang pollen spectra. Quat. Int. 154–155, 113–121.
Heyman, J., 2014. Paleoglaciation of the Tibetan plateau and surrounding mountains based on exposure ages and ELA depression estimates. Quat. Sci. Rev. 91, 30–41.
Heyman, J., Applegate, P.J., Blomdin, R., Gribenski, N., Harbor, J.M., Stroeven, A.P., 2016. Boulder height - exposure age relationships from a global glacial ^{10}Be compilation. Quat. Geochronol. 34, 1–11.
Hu, C., Henderson, G.M., Huang, J., Xie, S., Sun, Y., Johnson, K.R., 2008. Quantification of Holocene Asian monsoon rainfall from spatially separated cave records. Earth Planet. Sci. Lett. 266, 221–232.
Huang, L., Zhu, L., Wang, J., Ju, J., Wang, Y., Zhang, J., Yang, R., 2016. Glacial activity reflected in a continuous lacustrine record since the early Holocene from the proglacial Laigu Lake on the southeastern Tibetan Plateau. Palaeogeogr. Palaeoclimatol. Palaeoecol. 456, 37–45.
Hudson, A.M., Olsen, J.W., Quade, J., Lei, G., Huth, T.E., Zhang, H., 2016. A regional record of expanded Holocene wetlands and prehistoric human occupation from paleowetland deposits of the western Yarlung Tsangpo valley, southern Tibetan Plateau. Quat. Res. (United States) 86, 13–33.
Hughes, P.D., 2010. Geomorphology and Quaternary stratigraphy: the roles of morpho-, litho-, and allostratigraphy. Geomorphology 123, 189–199.
Hughes, P.D., Gibbard, P.L., 2015. A stratigraphical basis for the last glacial maximum (LGM). Quat. Int. 383, 174–185.
Hughes, P.D., Gibbard, P.L., Woodward, J., 2005. Quaternary Glacial Records in Mountain Regions : A Formal Stratigraphical Approach Quaternary Glacial Records in Mountain Regions : A Formal Stratigraphical Approach.
Huth, T., Hudson, A.M., Quade, J., Guoliang, L., Hucai, Z., 2015. Constraints on paleoclimate from 11.5 to 5.0 ka from shoreline dating and hydrologic budget modelling of Baqan Tso, southwestern Tibetan Plateau. Quat. Res. (United States) 83, 80–93.
IPCC, 2014. Climate Change 2013, the Fifth Assessment Report, p. 169.
Ivanochko, T.S., Ganeshram, R.S., Brummer, G.J.A., Ganssen, G., Jung, S.J.A., Moreton, S.G., Kroon, D., 2005. Variations in tropical convection as an amplifier of global climate change at the millennial scale. Earth Planet. Sci. Lett. 235, 302–314.
Ivy-Ochs, S., Kerschner, H., Schlüchter, C., 2007. Cosmogenic nuclides and the dating of Lateglacial and Early Holocene glacier variations: the Alpine perspective. Quat. Int. 164–165, 53–63.
Jennerjahn, T.C., Ittekkot, V., Arz, H.W., Behling, H., Pätzold, J., Wefer, G., 2004. Asynchronous terrestrial and marine signals of climate change during Heinrich events asynchronous terrestrial and marine signals of climate change during Heinrich events. Science 80, 2236–2239.
Ji, J., Shen, J., Balsam, W., Chen, J., Liu, L., Liu, X., 2005a. Asian monsoon oscillations in the northeastern Qinghai-Tibet Plateau since the late glacial as interpreted from visible reflectance of Qinghai Lake sediments. Earth Planet. Sci. Lett. 233, 61–70.
Ji, S., Xingqi, L., Sumin, W., Matsumoto, R., 2005b. Palaeoclimatic changes in the Qinghai Lake area during the last 18,000 years. Quat. Int. 136, 131–140.
Jin, L., Schneider, B., Park, W., Latif, M., Khon, V., Zhang, X., 2014. The spatial-temporal patterns of Asian summer monsoon precipitation in response to Holocene insolation change: a model-data synthesis. Quat. Sci. Rev. 85, 47–62.
Kakade, S., Kulkarni, A., 2017. Association between Arctic circulation and Indian summer monsoon rainfall. J. Climatol. Weather Forecast 5, 2–5.
Kaplan, M.R., Schaefer, J.M., Denton, G.H., Doughty, A.M., Barrell, D.J.A., Chinn, T.J.H., Putnam, A.E., Andersen, B.G., Mackintosh, A., Finkel, R.C., Schwartz, R., Anderson, B., 2013. The anatomy of long-term warming since 15 ka in New Zealand based on net glacier snowline rise. Geology 41, 887–890.
Kirkbride, M.P., Brazier, V., 1998. A critical evaluation of the use of glacier chronologies in climatic reconstruction, with reference to New Zealand. In: Owen, I.A. (Ed.), Mountain Glaciations, Quaternary Proceedings, vol. 6. Wiley, Chichester, U.K., pp. 55–64
Kirkbride, M.P., Winkler, S., 2012. Correlation of Late Quaternary moraines: impact of climate variability, glacier response, and chronological resolution. Quat. Sci. Rev. 46, 1–29.
Klok, E.J., Oerlemans, J., 2003. Deriving historical equilibrium-line altitudes from a glacier length record by linear inverse modelling. Holocene 13, 343–351.
Kohl, C.P., Nishiizumi, K., 1992. Chemical isolation of quartz for measurement of in-situ-produced cosmogenic nuclides. Geochem. Cosmochim. Acta 56, 3583–3587.
Kong, P., Na, C., Fink, D., Zhao, X., Xiao, W., 2009. Moraine dam related to late Quaternary glaciation in the Yulong Mountains, southwest China, and impacts on the Jinsha River. Quat. Sci. Rev. 28, 3224–3235.
Koppes, M., Gillespie, A.R., Burke, R.M., Thompson, S.C., Stone, J., 2008. Late quaternary glaciation in the Kyrgyz tien Shan. Quat. Sci. Rev. 27, 846–866.
Kramer, A., Herzschuh, U., Mischke, S., Zhang, C., 2010a. Holocene treeline shifts and monsoon variability in the Hengduan Mountains (southeastern Tibetan Plateau), implications from palynological investigations. Palaeogeogr. Palaeoclimatol. Palaeoecol. 286, 23–41.
Kramer, A., Herzschuh, U., Mischke, S., Zhang, C., 2010b. Late glacial vegetation and climate oscillations on the southeastern Tibetan Plateau inferred from the Lake Naleng pollen profile. Quat. Res. 73, 324–335.
Kumar, G., Joshi, A., Mathur, V.K., 1987. Redlichid trilobites from the tal Formation. Lesser Himalaya. India. Curr. Sci. 56, 659–663.
Lal, D., 1991. Cosmic ray labeling of erosion surfaces: in situ nuclide production rates and erosion models. Earth Planet. Sci. Lett. 104, 424–439.
Lasserre, C., Gaudemer, Y., Tapponnier, P., Mériaux, A.-S., Van der Woerd, J., Daoyang, y., Ryerson, F.J., Finkel, R.C., Caffee, M.W., 2002. Fast late Pleistocene slip rate on the Leng long ling segment of the Haiyuan fault, qinghai, China. J. Geophys. Res. 107. ETG 4-1–ETG 4-15.
Lea, D.W., Pak, D.K., Peterson, L.C., Hughen, K.A., 2003. Synchroneity of tropical and high-latitude Atlantic temperatures over the last glacial termination. Science 80 (301), 1361–1364.
Lee, S.Y., Seong, Y.B., Owen, L.A., Murari, M.K., Lim, H.S., Yoon, H. Il, Yoo, K.-C., 2014. Late Quaternary glaciation in the Nun-Kun massif, northwestern India. Boreas 43, 67–89.
Leipe, C., Demske, D., Tarasov, P.E., 2014. A Holocene pollen record from the northwestern Himalayan lake Tso Moriri: implications for palaeoclimatic and archaeological research. Quat. Int. 348, 93–112.
Li, Y., Wang, N., Zhou, X., Zhang, C., Wang, Y., 2014. Synchronous or asynchronous Holocene Indian and East Asian summer monsoon evolution: a synthesis on

Holocene Asian summer monsoon simulations, records and modern monsoon indices. Glob. Planet. Chang. 116, 30–40.
Li, J., Ehlers, T.A., Werner, M., Mutz, S.G., Steger, C., Paeth, H., 2017. Late Quaternary climate, precipitation δ18O, and Indian monsoon variations over the Tibetan Plateau. Earth Planet. Sci. Lett. 457, 412–422.
Liang, F., Brook, G.A., Kotlia, B.S., Railsback, L.B., Hardt, B., Cheng, H., Edwards, R.L., Kandasamy, S., 2015. Panigarh cave stalagmite evidence of climate change in the Indian Central Himalaya since AD 1256: monsoon breaks and winter southern jet depressions. Quat. Sci. Rev. 124, 145–161.
Lifton, N., Sato, T., Dunai, T.J., 2014. Scaling in situ cosmogenic nuclide production rates using analytical approximations to atmospheric cosmic-ray fluxes. Earth Planet. Sci. Lett. 386, 149–160.
Liu, K., Thompson, L.G., 1998. A pollen record of Holocene climatic changes from the Dunde ice cap, Qinghai-Tibetan Plateau. Geology 1986, 135–138.
Lukas, S., Graf, A., Coray, S., Schlüchter, C., 2012. Genesis, stability and preservation potential of large lateral moraines of Alpine valley glaciers - towards a unifying theory based on Findelengletscher, Switzerland. Quat. Sci. Rev. 38, 27–48.
Lund, D.C., Lynch-Stieglitz, J., Curry, W.B., 2006. Gulf Stream Density Structure and Transport during the Past Millennium, vol. 444, pp. 601–604.
Mahmood, A., 2016. Statistical Methods in Geographical Studies. Rajesh Publications, New Delhi, p. 88.
Marcott, S.A., Clark, P.U., Shakun, J.D., Brook, E.J., Davis, P.T., Caffee, M.W., 2019. ^{10}Be age constraints on latest Pleistocene and Holocene cirque glaciation across the western United States. npj Clim. Atmos. Sci. 5, 1–7.
Martin, L.C.P., Blard, P.H., Balco, G., Lavé, J., Delunel, R., Lifton, N., Laurent, V., 2017. The CREp program and the ICE-D production rate calibration database: a fully parameterizable and updated online tool to compute cosmic-ray exposure ages. Quat. Geochronol. 38, 25–49.
Matero, I.S.O., Gregoire, L.J., Ivanovic, R.F., Tindall, J.C., Haywood, A.M., 2017. The 8.2 ka cooling event caused by Laurentide ice saddle collapse. Earth Planet. Sci. Lett. 473, 205–214.
Mischke, S., Zhang, C., 2010. Holocene cold events on the Tibetan Plateau. Glob. Planet. Chang. 72, 155–163.
Mix, A.C., Bard, E., Schneider, R., 2001. Environmental processes of the ice age: land, oceans, glaciers (EPILOG). Quat. Sci. Rev. 20, 627–657.
Mölg, T., Maussion, F., Scherer, D., 2013. Mid-latitude westerlies as a driver of glacier variability in monsoonal High Asia. Nat. Clim. Chang. 4, 68–73.
Mölg, T., Maussion, F., Scherer, D., 2014. Mid-latitude westerlies as a driver of glacier variability in monsoonal High Asia. Nat. Clim. Chang. 4, 68–73.
Moran, A.P., Kerschner, H., Ochs, S.I., 2015. Redating the moraines in the Kromer valley (Silvretta mountains) – new evidence for an early Holocene glacier advance. Holocene 26, 655–664.
Moran, A.P., Ivy-Ochs, S., Schuh, M., Christl, M., Kerschner, H., 2016. Evidence of central Alpine glacier advances during the Younger Dryas–early Holocene transition period. Boreas 45, 398–410.
Murari, M.K., Owen, L.A., Dortch, J.M., Caffee, M.W., Dietsch, C., Fuchs, M., Haneberg, W.C., Sharma, M.C., Townsend-Small, A., 2014. Timing and climatic drivers for glaciation across monsoon-influenced regions of the Himalayan–Tibetan orogen. Quat. Sci. Rev. 88, 159–182.
Nesje, A., Dahl, S.O., 1992. Equilibrium-line altitude depressions of reconstructed Younger Dyras and Holocene glaciers in Fosdalen, inner Nordfjord, western Norway. Nor. Geol. Tidsskr. 72, 209–216.
New, M., Lister, D., Hulme, M., Makin, I., 2002. A high-resolution data set of surface climate over global land areas. Clim. Res. 21, 1–25.
Nishiizumi, K., Finkel, R.C., Caffee, M.W., Southon, J.R., Kohl, C.P., Arnold, J.R., Olinger, C.T., Poths, J., Klein, J., 1994. Cosmogenic production of ^{10}Be and ^{26}Al on the surface of the Earth and underground. In: Eighth International Conference on Geochronology, Cosmochronology and Isotope Geochemistry, vol. 1107. U.S. Geol. Surv. Circular, Berkeley, California, p. 234.
Oerlemans, J., 1997. Climate sensitivity of Franz Josef glacier, New Zealand, as revealed by numerical modelling. Arct. Alp. Res. 29, 233–239.
Oerlemans, J., 2001. Glaciers and Climate Change. Swets and Zeitlinger, Lisse, Netherlands, p. 160.
Oerlemans, J., 2005. Extracting a climate signal from 169 glacier records. Science 308, 675–677.
Oerlemans, J., Anderson, B., Hubbard, A., Huybrechts, P., Jóhannesson, T., Knap, W.H., Schmeits, M., Stroeven, A.P., van de Wal, R.S.W., Wallinga, J., Zuo, Z., 1998. Modelling the response of glaciers to climate warming. Clim. Dyn. 14, 267–274.
Ohio Supercomputer Center, 1987. Ohio Supercomputer Center. Ohio Supercomputer Center, Columbus OH. http://osc.edu/ark:/19495/f5s1ph73.
Orr, E.N., Owen, L.A., Murari, M.K., Saha, S., Caffee, M.W., 2017a. The timing and extent of Quaternary glaciation of Stok, northern Zanskar Range, Transhimalaya, of northern India. Geomorphology 284, 142–151.
Orr, E., Owen, L.A., Saha, S., 2017b. Determining the Rates and Drivers of Headwall Erosion within Glaciated Catchments in the NW Himalaya, EP33F. Presented at 2017 Fall Meeting. AGU, New Orleans, LA.
Orr, E.N., Owen, L.A., Saha, S., Caffee, M.W., Murari, M.K., 2018. Quaternary glaciation of the Lato massif, Zanskar range of the NW Himalaya. Quat. Sci. Rev. 183, 140–156.
Osmaston, H., 1994. The geology, geomorphology and Quaternary history of Zangskar. In: Crook, J., Osmaston, H. (Eds.), Himalayan Buddhist Villages. University of Bristol Press, UK, pp. 1–36.
Osmaston, H., 2005. Estimates of glacier equilibrium line altitudes by the area x altitude, the area x altitude balance ratio and the area x altitude balance index methods and their validation. Quat. Int. 138–139, 22–31.
Owen, L.A., 2018. Earth surface processes and landscape evolution in the Himalaya: a framework for sustainable development and geohazard mitigation. Geol. Soc. Spec. Publ. 462, 169–188.
Owen, L.A., Benn, D.I., 2005. Equilibrium-line Altitudes of the Last Glacial Maximum for the Himalaya and Tibet : an Assessment and Evaluation of Results, vol. 139, pp. 55–78.
Owen, L.A., Derbyshire, E., 1989. The Karakoram glacial depositional system. Zeitschrift f€ur Geomorphologie N.F. Suppl. 76, 33–73.
Owen, L.A., Dortch, J.M., 2014. Nature and timing of Quaternary glaciation in the Himalayan–Tibetan orogen. Quat. Sci. Rev. 88, 14–54.
Owen, L.A., Derbyshire, E., Richardson, S., Benn, D.I., Evans, D.J.A., Mitchell, W.A., 1996. The quaternary glacial history of the Lahul Himalaya, northern India, 11, 25–42.
Owen, L.A., Bailey, R.M., Rhodes, E.J., Mitchell, W.A., Coxon, P., 1997. Style and timing of glaciation in the Lahul Himalaya, northern India: a framework for reconstructing late Quaternary palaeoclimatic change in the western Himalayas. J. Quat. Sci. 12, 83–109.
Owen, L.A., Gualtieri, L., Finkel, R.C., Caffee, M.W., Benn, D.I., Sharma, M.C., 2001. Cosmogenic radionuclide dating of glacial landforms in the Lahul Himalaya, northern India: defining the timing of Late Quaternary glaciation. J. Quat. Sci. 16, 555–563.
Owen, L.A., Finkel, R.C., Caffee, M.W., Gualtieri, L., 2002. Timing of multiple late Quaternary glaciations in the Hunza Valley, Karakoram Mountains, northern Pakistan: defined by cosmogenic radionuclide dating of moraines. Bull. Geol. Soc. Am. 114, 593–604.
Owen, L.A., Finkel, R.C., Haizhou, M., Spencer, J.Q., Derbyshire, E., Barnard, P.L., Caffee, M.W., 2003a. Timing and style of late quaternary glaciation in northeastern Tibet. Bull. Geol. Soc. Am. 115, 1356–1364.
Owen, L.A., Finkel, R.C., Minnich, R.A., Perez, A.E., 2003b. Extreme southwestern margin of late Quaternary glaciation in North America: timing and controls. Geology 31, 729–732.
Owen, L.A., Finkel, R.C., Barnard, P.L., Haizhou, M., Asahi, K., Caffee, M.W., Derbyshire, E., 2005. Climatic and topographic controls on the style and timing of Late Quaternary glaciation throughout Tibet and the Himalaya defined by ^{10}Be cosmogenic radionuclide surface exposure dating. Quat. Sci. Rev. 24, 1391–1411.
Owen, L.A., Finkel, R.C., Haizhou, M., Barnard, P.L., 2006. Late Quaternary landscape evolution in the Kunlun Mountains and Qaidam Basin, Northern Tibet: a framework for examining the links between glaciation, lake level changes and alluvial fan formation. Quat. Int. 154–155, 73–86.
Owen, L.A., Robinson, R., Benn, D.I., Finkel, R.C., Davis, N.K., Yi, C., Putkonen, J., Li, D., Murray, A.S., 2009. Quaternary glaciation of mount everest. Quat. Sci. Rev. 28, 1412–1433.
Owen, L.A., Yi, C., Finkel, R.C., Davis, N.K., 2010. Quaternary glaciation of Gurla Mandhata (Naimon'anyi). Quat. Sci. Rev. 29, 1817–1830.
O'Hara, S.L., Briner, J.P., Kelley, S.E., 2017. A ^{10}Be chronology of early Holocene local glacier moraines in central West Greenland. Boreas 46, 655–666.
Pellitero, R., Rea, B.R., Spagnolo, M., Bakke, J., Ivy-Ochs, S., Frew, C.R., Hughes, P., Ribolini, A., Lukas, S., Renssen, H., 2016. GlaRe, a GIS tool to reconstruct the 3D surface of palaeoglaciers. Comput. Geosci. 94, 77–85.
Phadtare, N.R., 2000. Sharp decrease in summer monsoon strength 4000-3500 cal yr B.P. in the central Higher Himalaya of India based on pollen evidence from alpine peat. Quat. Res. 53, 122–129.
Pratt-Sitaula, B., 2005. Glaciers, Climate, and Topography in the Nepalese Himalaya. Ph.D. thesis. University of California, Santa Barbara.
Pratt-Sitaula, B., Burbank, D.W., Heimsath, A.M., Humphrey, N.F., Oskin, M., Putkonen, J., 2011. Topographic control of asynchronous glacial advances: A case study from Annapurna, Nepal. Geophys. Res. Lett. 38, 1–6.
Putkonen, J., Connolly, J., Orloff, T., 2008. Landscape evolution degrades the geologic signature of past glaciations. Geomorphology 97, 208–217.
Putnam, A.E., Schaefer, J.M., Denton, G.H., Barrell, D.J.A., Andersen, B.G., Koffman, T.N.B., Rowan, A.V., Finkel, R.C., Rood, D.H., Schwartz, R., Vandergoes, M.J., Plummer, M.A., Brocklehurst, S.H., Kelley, S.E., Ladig, K.L., 2013a. Warming and glacier recession in the Rakaia valley, Southern Alps of New Zealand, during Heinrich Stadial 1. Earth Planet. Sci. Lett. 382, 98–110.
Putnam, A.E., Schaefer, J.M., Denton, G.H., Barrell, D.J.A., Birkel, S.D., Andersen, B.G., Kaplan, M.R., Finkel, R.C., Schwartz, R., Doughty, A.M., 2013b. The Last Glacial Maximum at 44°S documented by a ^{10}Be moraine chronology at Lake Ohau, Southern Alps of New Zealand. Quat. Sci. Rev. 62, 114–141.
R Core Team, 2018. R : A Language and Environment for Statistical Computing, ISBN 3-900051-07-0. Vienna, Austria.
Raina, V.K., Shehmani, Sangewar, C.V., 2015. Glacier Snout Monitoring in the Himalayas. Geological Society of India, Bengaluru, pp. 227–251.
Rajeevan, M., Sridhar, L., 2008. Inter-annual relationship between Atlantic sea surface temperature anomalies and Indian summer monsoon. Geophys. Res. Lett. 35, 1–7.
Ramanathan, A.L., 2011. Status Report on Chhota Shigri Glacier (Himachal Pradesh) Status Report on Chhota Shigri Glacier (Himachal Pradesh). Sci. Eng. Res. Counc. Dep. Sci. Technol. Gov. India 1–89.
Rawat, S., Gupta, A.K., Sangode, S.J., Srivastava, P., Nainwal, H.C., 2015a. Late Pleistocene-Holocene vegetation and Indian summer monsoon record from the Lahaul, Northwest Himalaya, India. Quat. Sci. Rev. 114, 167–181.
Rawat, S., Gupta, A.K., Srivastava, P., Sangode, S.J., Nainwal, H.C., 2015b. A 13,000 year record of environmental magnetic variations in the lake and peat deposits from the Chandra valley, Lahaul: Implications to Holocene monsoonal

variability in the NW Himalaya. Palaeogeogr. Palaeoclimatol. Palaeoecol. 440, 116–127.
Rawat, B.S., Purohit, K.K., 1988. Geology of the area around Chhota Shigri glacier, Lahul and Spiti district, (H.P.). In: Technical Report on Multi-Disciplinary Glacier Expedition to Chhota Shigri, vol. 2. Department of Science and Technology, pp. 152–157.
RGI Consortium, 2017. Randolph Glacier Inventory (RGI) – A Dataset of Global Glacier Outlines: Version 6.0. Tech. Report, Glob. L. Ice Meas. From Space, Boulder, Color. USA.
Roe, G.H., 2011. What do glaciers tell us about climate variability and climate change? J. Glaciol. 57, 567–578.
Roe, G.H., Baker, M.B., 2014. Glacier response to climate perturbations : an accurate linear geometric model. J. Glaciol. 60, 670–684.
Röhringer, I., Zech, R., Abramowski, U., Sosin, P., Aldahan, A., Kubik, P.W., Zöller, L., Zech, W., 2012. The late Pleistocene glaciation in the Bogchigir Valleys (Pamir, Tajikistan) based on ^{10}Be surface exposure dating. Quat. Res. 78, 590–597.
Romesburg, C., 2004. Cluster Analysis for Researchers. North Carolina, p. 330.
Röthlisberger, F., Geyh, M.A., 1985a. Gletscherschwankungen der letzten 10.000 Jahre e Ein Verleich zwischen Nordund Südhemisphare (Alpen, Himalaya, Alaska, Südamerika, Neuseeland). Verlag Sauerländer, Aarau.
Röthlisberger, F., Geyh, M., 1985b. Glacier variations in Himalayas and Karakoram. Z. Gletsch. Glazialgeol. 21, 237–249.
Rounce, D.R., Quincey, D.J., McKinney, D.C., 2015. Debris-covered energy balance model for Imja-Lhotse Shar Glacier in the Everest region of Nepal. Cryosphere Discuss. 9, 3503–3540.
Rowan, A.V., Quincey, D.J., Gibson, M.J., Glasser, M.J., Westoby, M.J., Irvine-Fynn, T.D.L., Porter, P.R., Hambrey, M.J., 2018. The sustainability of water resouces in High Mountain Asia in the context of recent and future glacier change. Geol. Soc. Lond. Spcl. Publ. 462, 189–204.
Rupper, S., Roe, G., 2008. Glacier Changes and Regional Climate: A Mass and Energy Balance Approach. J. Clim. 21, 5384–5401.
Rupper, S., Roe, G., Gillespie, A., 2009. Spatial patterns of Holocene glacier advance and retreat in Central Asia. Quat. Res. 72, 337–346.
Sagredo, E.A., Lowell, T.V., 2012. Climatology of Andean glaciers: A framework to understand glacier response to climate change. Glob. Planet. Chang. 86–87, 101–109.
Saha, S., Owen, L. A., Orr, E. N., Caffee, M. W., in review. Systematically Inherited Cosmogenic ^{10}Be in Late Holocene Moraine Boulders in the Bhagirathi Catchment of the Garhwal Himalaya, Northern India. (Earth Surface Processes and Landforms).
Saha, S., Sharma, M.C., Murari, M.K., Owen, L.A., Caffee, M.W., 2016. Geomorphology, sedimentology and minimum exposure ages of streamlined subglacial landforms in the NW Himalaya, India. Boreas 45, 177–202.
Saha, S., Owen, L.A., Orr, E.N., Caffee, M.W., 2018. Timing and nature of Holocene glacier advances at the northwestern end of the Himalayan-Tibetan orogen. Quat. Sci. Rev. 187, 177–202.
Saini, R., Sharma, M.C., Deswal, S., Barr, I.D., Kumar, P., 2016. Glacio-archaeological evidence of warmer climate during the Little Ice Age in the Miyar basin, Lahul Himalaya, India. Clim. Past Discuss. 1–24.
Scäfer, J.M., Tschudi, S., Zhao, Z., Wu, X., Ivy-ochs, S., Wieler, R., Baur, H., Kubik, P.W., Schlu, C., 2002. The limited influence of glaciations in Tibet on global climate over the past 170 000 yr. Earth Planet. Sci. Lett. 194, 287–297.
Schaefer, J.M., Oberholzer, P., Zhao, Z., Ivy-Ochs, S., Wieler, R., Baur, H., Kubik, P.W., Schlüchter, C., 2008. Cosmogenic beryllium-10 and neon-21 dating of late Pleistocene glaciations in Nyalam, monsoonal Himalayas. Quat. Sci. Rev. 27, 295–311.
Scherler, D., Egholm, 2017. Debris supply to mountain glaciers and how it effects their sensitivity to climate change–A case study from the Chhota Shigri Glacier, India. In: Presented at 2017 Fall Meeting. AGU, New Orleans, LA, 206444.
Scherler, D., Bookhagen, B., Strecker, M.R., von Blanckenburg, F., Rood, D., 2010. Timing and extent of late Quaternary glaciation in the western Himalaya constrained by ^{10}Be moraine dating in Garhwal, India. Quat. Sci. Rev. 29, 815–831.
Schimmelpfennig, I., Schaefer, J.M., Akçar, N., Ivy-Ochs, S., Finkel, R.C., Schlüchter, C., 2012. Holocene glacier culminations in the Western Alps and their hemispheric relevance. Geology 40, 891–894.
Schimmelpfennig, I., Schaefer, J.M., Akçar, N., Koffman, T., Ivy-Ochs, S., Schwartz, R., Finkel, R.C., Zimmerman, S., Schlüchter, C., 2014. A chronology of Holocene and Little Ice Age glacier culminations of the Steingletscher, Central Alps, Switzerland, based on high-sensitivity beryllium-10 moraine dating. Earth Planet. Sci. Lett. 393, 220–230.
Schindelwig, I., Akçar, N., Kubik, P.W., Schlüchter, C., 2012. Lateglacial and early Holocene dynamics of adjacent valley glaciers in the Western Swiss Alps. J. Quat. Sci. 27, 114–124.
Schmeits, M.J., Oerlemans, J., 1997. Simulation of the historical variations in length of Unterer Grindelwaldgletscher, Switzerland. J. Glaciol. 43, 152–164.
Seaby, R., Henderson, P., 2014. Community Analysis Package 5.0: Searching for Structure in Community Data. PISCES Conserv. Ltd., Engl., p. 186
Searle, A.M.P., Parrish, R.R., Hodges, K.V., Hurford, A., Ayres, M.W., Searle, M.P., Parrish, R.R., Hodges, K.V., Hurford, A., Ayres, M.W., Whitehouse, M.J., 1997. Shisha Pangma Leucogranite, South Tibetan Himalaya: Field Relations, Geochemistry, Age, Origin, and Emplacement. J. Geol. 105, 295–318.
Seong, Y.B., Owen, L.A., Bishop, M.P., Bush, A., Clendon, P., Copland, L., Finkel, R., Kamp, U., Shroder, J.F., 2007. Quaternary glacial history of the Central Karakoram. Quat. Sci. Rev. 26, 3384–3405.
Seong, Y.B., Owen, L.A., Yi, C., Finkel, R.C., 2009. Quaternary glaciation of Muztag Ata and Kongur Shan: Evidence for glacier response to rapid climate changes throughout the Late Glacial and Holocene in westernmost Tibet. Geol. Soc. Am. Bull. 121, 348–365.
Severinghaus, J.P., Beaudette, R., Headly, M.A., Taylor, K., Brook, E.J., 2009. The Terrestrial Biosphere 1431–1434.
Shangzhe, Z., Jie, W., Liubing, X., Xiaoli, W., Colgan, P.M., Mickelson, D.M., 2010. Glacial advances in southeastern Tibet during late Quaternary and their implications for climatic changes. Quat. Int. 218, 58–66.
Sharma, P., Bourgeois, M., Elmore, D., Granger, D., Lipschutz, M.E., Ma, X., Miller, T., Mueller, K., Rickey, F., Simms, P., Vogt, S., 2000. PRIME lab AMS performance, upgrades and research applications. Nucl. Instrum. Methods Phys. Res. Sect. B-Beam Interact. Mater. Atoms 172, 112–123.
Sharma, S., Chand, P., Bisht, P., Shukla, A.D., Bartarya, S.K., Sundriyal, Y.P., Juyal, N., 2016. Factors responsible for driving the glaciation in the Sarchu Plain, eastern Zanskar Himalaya, during the late Quaternary. J. Quat. Sci. 31, 495–511.
Shi, X., Kirby, E., Furlong, K.P., Meng, K., Robinson, R., Lu, H., Wang, E., 2017. Rapid and punctuated Late Holocene recession of Siling Co, central Tibet. Quat. Sci. Rev. 172, 15–31.
Shroder, J.F., Bishop, M.P., Copland, L., Sloan, V.F., 2000. Debris-covered glaciers and rock glaciers in the Nanga Parbat Himalaya, Pakistan. Geogr. Ann. Ser. A Phys. Geogr. 82, 17–31.
Singh, D.S., Dubey, C.A., Kumar, D., Vishawakarma, B., Singh, A.K., Tripathi, A., Gautam, P.K., Bali, R., Agarwal, K.K., Sharma, R., 2019. Monsoon variability and major climatic events between 25 and 0.05 ka BP using sedimentary parameters in the Gangotri Glacier region, Garhwal Himalaya, India. Quat. Int. 507, 148–155.
Solomina, O.N., Bradley, R.S., Hodgson, D.A., Ivy-Ochs, S., Jomelli, V., Mackintosh, A.N., Nesje, A., Owen, L.A., Wanner, H., Wiles, G.C., Young, N.E., 2015. Holocene glacier fluctuations. Quat. Sci. Rev. 111, 9–34.
Solomina, O.N., Bradley, R.S., Jomelli, V., Geirsdottir, A., Kaufman, D.S., Koch, J., McKay, N.P., Masiokas, M., Miller, G., Nesje, A., Nicolussi, K., Owen, L.A., Putnam, A.E., Wanner, H., Wiles, G., Yang, B., 2016. Glacier fluctuations during the past 2000 years. Quat. Sci. Rev. 149, 61–90.
Srivastava, D., 2012. Status Report on Gangotri Glacier, Science and Engineering Research Board, Department of Science and Technology, New Delhi. Himal. Glaciol. Tech. Rep. 1–102.
Srivastava, P., Agnihotri, R., Sharma, D., Meena, N., Sundriyal, Y.P., Saxena, A., Bhushan, R., Sawlani, R., Banerji, U.S., Sharma, C., Bisht, P., Rana, N., Jayangondaperumal, R., 2017. 8000-year monsoonal record from Himalaya revealing reinforcement of tropical and global climate systems since mid-Holocene. Sci. Rep. 7, 1–10.
Steck, A., 2003. Geology of the NW Indian Himalaya. Eclogae Geol. Helv. 96. 147-U13.
Stone, J.O., 2000. Air pressure and cosmogenic isotope production. J. Geophys. Res. 105, 23753–23759.
Stuiver, M., Reimer, P.J., Reimer, R.W., 2018. CALIB 7.1 [WWW program] at. accessed 2018-10-20. http://calib.org.
Sugden, D.E., John, B.S., 1976. Glaciers and Landscape. A Geomorphological Approach. Edward Arnold, London.
Taylor, J.R., 1997. An Introduction to Error Analysis, second ed. University Science Books, Sausalito, Calif.
Thomas, E.K., Huang, Y., Clemens, S.C., Colman, S.M., Morrill, C., Wegener, P., Zhao, J., 2016. Changes in dominant moisture sources and the consequences for hydroclimate on the northeastern Tibetan Plateau during the past 32 kyr. Quat. Sci. Rev. 131, 157–167.
Thompson, L.G., Tao, T., Davis, M.E., Henderson, A., Mosley-Thompson, E., Lin, P.N., Beer, J., Synal, H.A., Cole-Dai, J., Bolzan, J.F., 1997. Tropical Climate Instability: The Last Glacial Cycle from a Qinghai-Tibetan Ice Core. Science 80 (276), 1821–1825.
Tschudi, S., Schäfer, J.M., Zhao, Z., Wu, X., Ivy-Ochs, S., Kubik, P.W., Schlüchter, C., 2003. Glacial advances in Tibet during the Younger Dryas? Evidence from cosmogenic ^{10}Be, ^{26}Al, and ^{21}Ne. J. Asian Earth Sci. 22, 301–306.
Van der Bilt, W.G.M., Bakke, J., Vasskog, K., D'Andrea, W.J., Bradley, R.S., Ólafsdóttir, S., 2015. Reconstruction of glacier variability from lake sediments reveals dynamic Holocene climate in Svalbard. Quat. Sci. Rev. 126, 201–218.
Vance, D., Harris, N., 1999. Timing of prograde metamorphism in the Zanskar Himalaya. Geology 27, 395–398.
Vaux Jr., H.J., Balk, D., Cook, E.R., Gleick, P., Lau, W.K.-M., Levy, M., Malone, E.L., Mcdonald, R., Shindell, D., Thompson, L.G., Wescoat, J.L., Williams, M.W., 2012. Himalayan Glaciers Climate Change, Water Resources, and Water Security. National Academy of Sciences, Washington, DC, p. 165.
Walker, H., Pascoe, E.N., 1907. Notes on certain glaciers in Lahaul. Rec. Geol. Surv. India 35, 139–147.
Walker, M.J.C., Berkelhammer, M., Björck, S., Cwynar, L.C., Fisher, D.A., Long, A.J., Lowe, J.J., Newnham, R.M., Rasmussen, S.O., Weiss, H., 2012. Formal subdivision of the Holocene Series/Epoch: A Discussion Paper by a Working Group of INTIMATE (Integration of ice-core, marine and terrestrial records) and the Subcommission on Quaternary Stratigraphy (International Commission on Stratigraphy). J. Quat. Sci. 27, 649–659.
Wang, B., Wu, R., Lau, K.-M., 2001. Interannual Variability of the Asian Summer Monsoon : Contrasts between the Indian and the Western North Pacific–East Asian Monsoons*. J. Clim. 14, 4073–4090.
Wang, X., Auler, A.S., Edwards, R.L., Cheng, H., Cristalli, P.S., Smart, P.L., Richards, D.A., Shen, C.-C., 2004. Wet periods in northeastern Brazil over the past 210 kyr linked to distant climate anomalies. Nature 432, 740–743.

Wang, Y., Cheng, H., Edwards, R.L., He, Y., Kong, X., An, Z., Wu, J., Kelly, M.J., Dykoski, C.A., Li, X., 2005. The Holocene Asian Monsoon . Links Solar Changes N. Atl. Clim. 854–858.
Wang, J., Kassab, C., Harbor, J.M., Caffee, M.W., Cui, H., Zhang, G., 2013. Cosmogenic nuclide constraints on late Quaternary glacial chronology on the Dalijia Shan, northeastern Tibetan Plateau. Quat. Res. 79, 439–451.
Ward, D.J., Anderson, R.S., 2011. The use of ablation-dominated medial moraines as samplers for ^{10}Be-derived erosion rates of glacier valley walls, Kichatna Mountains, AK. Earth Surf. Process. Landforms 36, 495–512.
Wünnemann, B., Demske, D., Tarasov, P., Kotlia, B.S., Reinhardt, C., Bloemendal, J., Diekmann, B., Hartmann, K., Krois, J., Riedel, F., Arya, N., 2010. Hydrological evolution during the last 15 kyr in the Tso Kar lake basin (Ladakh, India), derived from geomorphological, sedimentological and palynological records. Quat. Sci. Rev. 29, 1138–1155.
Xu, X., Yi, C., 2014. Little Ice Age on the Tibetan Plateau and its bordering mountains: Evidence from moraine chronologies. Glob. Planet. Chang. 116, 41–53.
Yan, Q., Owen, L.A., Wang, H., Zhang, Z., 2018. Climate constraints on glaciation over high-mountain Asia during the last glacial maximum. Geophys. Res. Lett. 45, 9024–9033.
Yancheva, G., Nowaczyk, N.R., Mingram, J., Dulski, P., Schettler, G., Liu, J., Sigman, D.M., Peterson, L.C., Haug, G.H., 2007. Influence of the intertropical convergence zone on the East Asian monsoon, 445, 3–6.
Yang, B., Bräuning, A., Liu, J., Davis, M.E., Yajun, S., 2009a. Temperature changes on the Tibetan Plateau during the past 600 years inferred from ice cores and tree rings. Glob. Planet. Chang. 69, 71–78.
Yang, B., Kang, X., Liu, J., Bräuning, A., Qin, C., 2009b. Annual temperature history in southwest Tibet during the last 400 years recorded by tree rings. Int. J. Climatol. 30, 962–971.
Yanhong, W., Lücke, A., Zhangdong, J., Sumin, W., Schleser, G.H., Battarbee, R.W., Weilan, X., 2006. Holocene climate development on the central Tibetan Plateau: A sedimentary record from Cuoe Lake. Palaeogeogr. Palaeoclimatol. Palaeoecol. 234, 328–340.
Yao, T., Thompson, L., Yang, W., Yu, W., Gao, Y., Guo, X., Yang, X., Duan, K., Zhao, H., Xu, B., Pu, J., Lu, A., Xiang, Y., Kattel, D.B., Joswiak, D., 2012. Different glacier status with atmospheric circulations in Tibetan Plateau and surroundings. Nat. Clim. Chang. 2, 663–667.
Young, N.E., Briner, J.P., Rood, D.H., Finkel, R.C., 2012. Glacier extent during the Younger Dryas and 8.2-ka event on Baffin Island, Arctic Canada. Science (80) 337, 1330–1333.
Yu, Y., Yang, T., Li, J., Liu, J., An, C., Liu, X., Fan, Z., Lu, Z., Li, Y., Su, X., 2006. Millennial-scale Holocene climate variability in the NW China drylands and links to the tropical Pacific and the North Atlantic. Palaeogeogr. Palaeoclimatol. Palaeoecol. 233, 149–162.
Zech, R., 2012. A late Pleistocene glacial chronology from the Kitschi-Kurumdu Valley, Tien Shan (Kyrgyzstan), based on ^{10}Be surface exposure dating. Quat. Res. 77, 281–288.
Zech, R., Zech, M., Kubik, P.W., Kharki, K., Zech, W., 2009. Deglaciation and landscape history around Annapurna, Nepal, based on ^{10}Be surface exposure dating. Quat. Sci. Rev. 28, 1106–1118.
Zhu, L., Zhen, X., Wang, J., Lü, H., Xie, M., Kitagawa, H., Possnert, G., 2009. A ~30,000-year record of environmental changes inferred from Lake Chen Co, Southern Tibet. J. Paleolimnol. 42, 343–358.
Zhu, H., Xu, P., Shao, X., Luo, H., 2013. Little Ice Age glacier fluctuations reconstructed for the southeastern Tibetan Plateau using tree rings. Quat. Int. 283, 134–138.
Zuming, L.A.I., Maohuan, H., 1989. A numerical classification of glaciers in China by means of glaciological indices at the equilibrium line. Snow Cover Glacier Var. (Proceedings Balt. Symp. Maryland) 103–111.